

**RECOVERY AND RECRYSTALLIZATION KINETICS OF
CONTINUOUS AND INGOT CAST AA5754**

BY

SUJAY SARKAR

Bachelor of Engineering, Bengal Engineering College (Deemed University),

Howrah, India, 1998.

A THESIS SUBMITTED IN PARTIAL FULFILLMENT OF THE
REQUIREMENTS FOR THE DEGREE OF MASTER OF APPLIED SCIENCE

IN

THE FACULTY OF GRADUATE STUDIES
(DEPARTMENT OF METALS AND MATERIALS ENGINEERING)

We accept this thesis as confirming to the required standard

THE UNIVERSITY OF BRITISH COLUMBIA

OCTOBER, 2003

© Sujay Sarkar, 2003

In presenting this thesis in partial fulfilment of the requirements for an advanced degree at the University of British Columbia, I agree that the Library shall make it freely available for reference and study. I further agree that permission for extensive copying of this thesis for scholarly purposes may be granted by the head of my department or by his or her representatives. It is understood that copying or publication of this thesis for financial gain shall not be allowed without my written permission.

Department of METALS AND MATERIALS ENGINEERING

The University of British Columbia
Vancouver, Canada

Date OCT 14th, 2003

Abstract

The influence of processing route (continuous casting versus ingot casting) on the recovery and recrystallization behaviour during isothermal annealing of cold rolled AA5754 was examined. Industrially produced continuous and ingot cast AA5754 material was supplied by Alcan and a series of annealing tests were conducted in a salt bath at temperatures ranging from 200°C to 375°C for various lengths of times. Recovery and recrystallization kinetics were examined by analyzing the change in the mechanical properties of the material as a function of time and temperature. Differences in the recrystallized microstructure for both the continuous and ingot cast AA5754 were also examined in terms of recrystallized grain size and recrystallized texture.

The results of the present study indicate that the ingot cast AA5754 exhibits a faster recovery and recrystallization behaviour compared to the continuous cast material. The absence of the homogenization treatment in the continuous cast AA5754, has been identified as the critical difference in the processing. The homogenization step effects the evolution and distribution of the dispersoid precipitates and associated change in the solid solution content, which thereby influences the softening kinetics of the continuous cast material. The present study also provides a comprehensive characterization of final recrystallized microstructure for continuous and ingot cast AA5754.

Table of Contents

Abstract	II
List of Tables	V
List of Figures	VII
List of Symbols	XI
Acknowledgements	XII
1. Introduction	1
1.1 Characteristics of Twin-Belt Caster	4
1.2 Continuous Casting Compared to Ingot Casting	5
1.3 Al-Mg Alloys	7
1.4 Motivation of Research	8
2. Literature Review	10
2.1 Introduction	10
2.2 Processing	11
2.2.1 Casting	11
2.2.2 Effect of Homogenization	16
2.2.3 Hot Rolling	17
2.3 Recovery and Recrystallization	18
2.3.1 Recovery in Al-Mg Alloys	18
2.3.1.1 General Observation	18
2.3.1.2 Effect of Processing	22
2.3.2 Recrystallization in Al-Mg Alloys	22
2.3.2.1 General Observation	22
2.3.2.2 Effect of Processing	29
2.4 Texture	32
2.4.1 Recrystallization Texture in Al-Mg Alloys	33
2.4.1.1 General Observation	33
2.4.1.2 Effect of Processing	37
3. Experimental	40
3.1 Introduction	40
3.2 Starting Material	40
3.2.1 Processing History	41
3.3 Isothermal Annealing	42

3.4 Characterization of Annealed Materials	46
3.4.1 Tensile Measurements	46
3.4.2 Quantitative Optical Metallography	46
3.4.3 Resistivity Measurements	48
3.4.4 Composition of Second-phase particle	50
3.4.5 Comparative Texture measurements	51
4. Results (Continuous Cast vs. Ingot Cast)	55
4.1 Initial Material	55
4.2 Cold Rolled Material	57
4.2.1 Recovery at Room Temperature	59
4.3 Isothermal Annealing- Mechanical Testing	61
4.3.1 Comparison of Softening Kinetics	61
4.3.1.1 Effect of Direct Cold Rolling	70
4.4 Characterization of Fully Recrystallized Material	72
4.4.1 Mechanical Properties	72
4.4.2 Grain Size Analysis	73
4.4.3 Texture Analysis	76
4.5 Summary	82
5. Effect of Homogenization – Results and Discussion	84
5.1 Changes in Resistivity	85
5.2 Homogenized As-cast Material	86
5.3 Characterization of Cold Rolled Material	87
5.3.1 Second-Phase Particles Distribution	88
5.4 Isothermal Annealing	91
5.4.1 Comparative Recovery Kinetics	91
5.4.2 Comparative Recrystallization Kinetics	93
5.4.3 Discussion of Recovery and Recrystallization	96
5.5 Characterization of Recrystallized Material	98
5.6 Texture Analysis	99
5.7 Summary	103
6. Summary and Conclusions	104
6.1 Future Works	107
References	109
Appendix A	114
Appendix B	115
Appendix C	116

List of Tables

Table 1.1.	Nominal composition of the AA5754 alloys (in wt%).	8
Table 3.1.	Chemical composition of AA5754 provided by Alcan (in wt%).	41
Table 3.2	Thermal processing route for continuous and ingot cast AA5754.	42
Table 3.3	Anodizing method used for AA5754.	47
Table 3.4	Condition for electropolishing of AA5754.	51
Table 3.5	Condition for electropolishing of AA5754.	53
Table 4.1	Average grain size and yield stress of continuous and ingot cast AA5754.	57
Table 4.2	Average as rolled yield stress of continuous and ingot cast AA5754.	59
Table 4.3	Room temperature recovery for ingot cast AA5754.	61
Table 4.4	The flow stress at which recrystallization was observed to begin and the final recrystallized yield stress for the continuous and ingot cast material with 40% and 80% cold reduction.	64
Table 4.5	Average recrystallized yield stress of continuous and ingot cast AA5754 after various level of cold deformation.	72
Table 4.6	Average grain size of recrystallized continuous and ingot cast AA5754.	75
Table 4.7	Measured volume fraction of texture components (in %) for both the ingot cast and continuous cast AA5754 after 40% and 80% cold deformation and annealing at 325°C using an EBSD system.	82
Table 5.1	Comparative as-cast grain size along with as-rolled yield stress (80% direct cold rolled) for continuous cast AA5754 before and after homogenization.	88

Table 5.2	Comparative recrystallized grain size along with recrystallized yield stress for recrystallized 80% cold rolled continuous and ingot cast AA5754.	99
Table 5.3	Measured volume fraction of texture components (in %) for both the ingot cast and continuous cast AA5754 after 80% cold deformation and annealing at 325°C using an EBSD system.	103

List of Figures

Figure 1.1	Historical change in material consumption in an average car.	2
Figure 1.2	The twin-belt caster.	5
Figure 1.3	Comparison of continuous cast and ingot cast processing routes to produce Al-Mg alloys.	9
Figure 2.1	Effect of Fe on grain structure of continuous as-cast AA5754.	13
Figure 2.2	Micrographs of second phase particles.	15
Figure 2.3	Schematic diagram describing recovery and recrystallization process in deformed material.	19
Figure 2.4	Partial annealing curve for a series of binary Al-Mg alloys cold rolled to 70% and annealed for 2 hours at annealing temperature.	20
Figure 2.5	Typical recrystallization kinetics during isothermal annealing.	24
Figure 2.6	Fraction recrystallized plotted against annealing temperature for Al-Mg alloys with various Mg content.	26
Figure 2.7	The interaction between recrystallization and precipitation.	27
Figure 2.8	Basic layout of the components of a typical EBSD system.	34
Figure 3.1	Schematic of the tensile sample.	43
Figure 3.2	Schematic of a metallography specimen taken from the rolled strip.	44
Figure 3.3	Heating profile at 300°C for tensile specimens.	45
Figure 3.4	As-cast specimen for resistivity measurement.	49
Figure 3.5	Schematic of a SAM specimen taken from rolled strip.	50
Figure 3.6	Schematic of texture measurement sample taken from continuous cast material.	53
Figure 4.1	As-cast AA5754 microstructure showing location near the surface and at the centerline.	56

Figure 4.2	Micrographs of hot band structure for continuous and ingot cast material.	57
Figure 4.3	Microstructure for continuous cold rolled continuous cast material at different cold reductions.	58
Figure 4.4	Logarithmic time decay of yield stress at room temperature for continuous cast AA5754.	60
Figure 4.5	Recovery kinetics for continuous cast AA5754 for two levels of cold rolling (40% and 80%).	62
Figure 4.6	Comparative isothermal recovery kinetics of continuous and ingot cast AA5754.	63
Figure 4.7	Isothermal softening kinetics of 80% cold rolled continuous cast AA5754.	64
Figure 4.8	Microstructure evolution of 80% cold rolled continuous cast material during annealing at 300°C at various times.	66
Figure 4.9	Validation of isothermal recrystallization kinetics for 80% cold rolled continuous cast AA5754 at 300°C derived from mechanical testing by quantitative metallography results.	67
Figure 4.10	Isothermal recrystallization kinetics of 80% cold rolled continuous cast AA5754.	68
Figure 4.11	Comparative isothermal recrystallization kinetics of 80% cold rolled and 40% cold rolled continuous and ingot cast AA5754.	69
Figure 4.12	Comparative isothermal recovery kinetics of 80% directly cold rolled continuous cast AA5754 and 80% cold rolled continuous and ingot cast AA5754 at 200°C.	70
Figure 4.13	Comparative isothermal recrystallization kinetics of 80% directly cold rolled continuous cast AA5754 and 80% cold rolled continuous and ingot cast AA5754 at 300°C.	71
Figure 4.14	Microstructure of recrystallized 40% cold rolled and recrystallized 80% cold rolled continuous cast AA5754.	74
Figure 4.15	Microstructure of recrystallized 80% directly cold rolled continuous cast and recrystallized 80% cold rolled ingot cast AA5754.	74

Figure 4.16	Graph shows the relation between yield stresses vs. recrystallized grain size based on Hall-Petch Equation.	76
Figure 4.17	Texture component map of recrystallized 40% cold rolled continuous cast and recrystallized 40% cold rolled ingot cast AA5754.	78
Figure 4.18	Orientation Distribution Function (ODF) of recrystallized 40% cold rolled continuous cast AA5754 and recrystallized 40% cold rolled ingot cast AA5754.	79
Figure 4.19	Texture component map of recrystallized 80% directly cold rolled continuous cast AA5754 and recrystallized 80% cold rolled ingot cast AA5754. Texture components are shown in different colours.	80
Figure 4.20	Orientation Distribution Function (ODF) of recrystallized 80% directly cold rolled continuous cast AA5754 and recrystallized 80% cold rolled ingot cast AA5754.	81
Figure 5.1	Change in resistivity value of as-cast continuous cast AA5754 during homogenization at 500°C and 530°C.	85
Figure 5.2	Microstructure of the continuous as-cast AA5754 in the unetched condition before homogenization and after homogenization.	87
Figure 5.3	Presence of second-phase particles in 80% direct cold rolled continuous cast material from homogenized as-cast AA5754.	89
Figure 5.4	SAM result for constituent particle in homogenized 80% directly cold rolled continuous cast material.	90
Figure 5.5	SAM result for Mg ₂ Si particle in non-homogenized 80% directly cold rolled continuous cast material.	90
Figure 5.6	Isothermal recovery kinetics for 80% directly cold rolled continuous cast AA5754 annealed at 200°C.	92
Figure 5.7	Comparative isothermal recovery kinetics of 80% direct cold rolled continuous cast materials and 80% cold rolled continuous and ingot cast material at 200°C.	92
Figure 5.8	Isothermal recrystallization kinetics for 80% directly cold rolled continuous cast AA5754 at 300°C.	93

Figure 5.9	Comparative isothermal recrystallization kinetics for 80% direct cold rolled continuous cast materials and 80% cold rolled continuous and ingot cast material at 300°C.	94
Figure 5.10	Resistivity curve for continuous cast materials at 300°C.	95
Figure 5.11	Microstructure of recrystallized 80% directly cold rolled continuous cast AA5754 rolled from homogenized as-cast material.	98
Figure 5.12	Texture component map of recrystallized 80% direct cold rolled continuous cast AA5754 from non-homogenized as-cast material and recrystallized 80% direct cold rolled continuous cast material from homogenized as-cast material.	101
Figure 5.13	Orientation Distribution Function (ODF) of recrystallized 80% directly cold rolled continuous cast AA5754 from non-homogenized as-cast and recrystallized 80% cold rolled ingot cast AA5754 from homogenized as-cast material.	102

List of Symbols

$\sigma_{Re.}$	Yield stress in fully recovered state
$\sigma_{Rx.}$	Yield stress in the fully recrystallized state
σ_t	Yield stress measured at different time interval, used in Equation 4.1
σ_Y	Yield stress used in Equation 4.2
σ_0	Frictional stress
D	Average grain size
K	Hall-Petch constant, used in Equation 4.2
ρ	Measured resistivity of the material
$\rho(T)$	Intrinsic resistivity
α	Matthiessen's constant or specific resistivity
C_I	Concentration of the solute

Acknowledgements

There are a number of people who helped to make this project a success. Firstly, I would like to thank my advisors: Professor Mary A. Wells and Professor Warren Poole for supervising my research and providing me the support and encouragement throughout my studies. I am also grateful to Professor Matthias Militzer and Professor Chad Sinclair for their valuable suggestions regarding various aspects of this project.

I wish to thank Alcan International Ltd. for providing the material and specifically want to thank Dr. David Lloyd, Dr. Mark Gallerneault and Mr. Ed Luce of (Kingston Research and Development Centre, Alcan) for sharing their great expertise regarding aluminum alloys processing. I wish to thank Natural Sciences and Engineering Council of Canada for funding this project.

I like to extend a special thank-you to many people in the Department of Metals and Materials Engineering, at UBC. In particular, special thanks to Dr. Phil Wang, Mr. Ross Mcleod, Mr. Carl Ng, Mr. David Torok, Mr. Serge Milaire, Mr. Gary Lockhart and Ms. Mary Mager for assisting me in preparing my samples and helping me performing my experiments. I would like to acknowledge my friends Johnson Go, Babak Raeisenia, Rajat Bathla, Hany Ahmed, and Taryn Biggs for their valuable discussions and suggestions.

Finally, this work would not have been completed without the continuous encouragement and support from my family and friends.

1. Introduction

Recently, the demands for improved fuel efficiency of automobiles have increased due to the issues such as global warming, pollution and overall damage inflicted on the environment. As a result, environmental issues directly related to the performance and operation of automobiles, are under extreme scrutiny [Miller et al., 2000; Hayashi and Nakagawa, 1994]. Specifically the need to improve energy efficiency in order to address the issue of global warming is a major concern. On the other hand, the demands for improved impact safety performance and increased standard features have added weight to the cars [Katsukura, 2001]. One method to address these conflicting issues is the use of lighter weight materials in automobile structures. The characteristic properties of aluminum alloys, such as, low density (2.7g/cm^3), good formability, good corrosion resistance, and recyclability make it a potential candidate to replace heavier materials such as, steel (density 7.8g/cm^3), in automotive applications.

The entry of aluminum alloys into the automotive industry has been quite remarkable and the extent of their use is growing as shown in Figure 1.1 [Miller et al., 2000, Carle and Blount, 1999]. In fact, several global players in the automotive industry, such as, Audi, General Motors, Honda, Ford and Chrysler are currently producing aluminum intensive vehicles [Katsukura, 2001; Miller et al., 2000]. Among the different aluminum alloys used by the North American automotive industry, non-heat-treatable aluminum alloys, such as AA5754 and AA5182 are generally used for internal body panels, where-

as heat-treatable alloys such as AA2036 and AA6111 are generally considered for exterior body panels [Burgers et al., 1995; Miller et al., 2000].

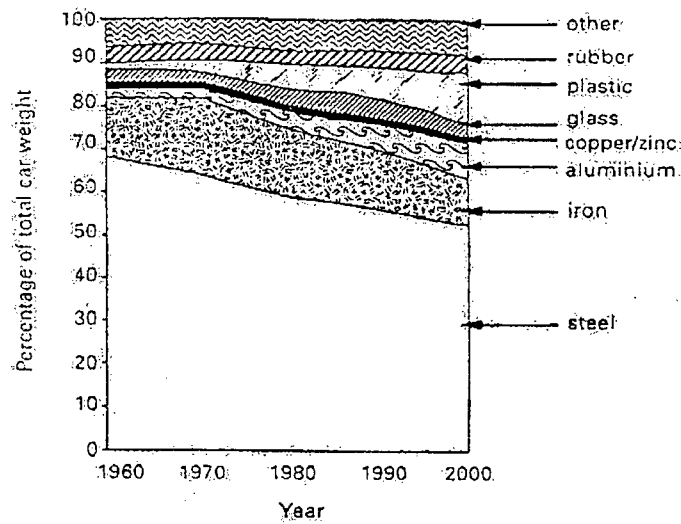


Figure 1.1 - Historical change in material consumption in an average car [Miller et al., 2000].

In terms of the widespread use of aluminum in automobiles, it is critical to maintain the same cost and performance as cars in which steel is the dominant material. Currently, one of the main barriers faced by the aluminum industry in automotive sheet applications is reducing the cost of fabrication such that the cost of a sheet of aluminum is at par with steel [Carle and Blount, 1999]. Currently aluminum sheets cost 4 to 5 times more as compared to the final cost of steel sheets on a per pound basis [Karlík et al., 2002]. The main reason behind the huge cost difference is related to processing the aluminum from the liquid stage to the final sheet form. Traditionally, conversion of aluminum from liquid to the end product has been accomplished using a Direct Chill (DC) semi-continuous casting process which produces large rolling ingots which are

then processed into sheet through a number of manufacturing steps. These range from homogenization to hot and cold rolling and final heat treatment [Friedman and Sherman, 1998]. In order for the aluminum industry to substantially reduce the cost of sheet production, it is necessary to focus their efforts towards alternative less expensive processing technologies, such as near-net-shape casting. Continuous casting is one type of near-net-shape casting technology which is able to cast sheets to a much smaller thickness than the DC or ingot casting process (i.e., 10-20mm strip thickness in continuous casting vs. 400-500mm ingot thickness in ingot casting). In contrast to the ingot casting process, continuous casting of aluminum eliminates the cost intensive intermediary stages of homogenization (or pre-heat treatment) and potentially hot rolling. This not only reduces the fabrication cost of the as-cast material to final sheet form, but also reduces the size of a continuous cast mill to one-sixth that of traditional DC cast and ingot rolling mills based on volume. This decreases both the capital costs associated with a new plant start-up as well as operational costs such as maintenance and labour [Pennington, 1993]. In addition, the ingot casting operation is semi-continuous in nature, with the casting process having to be restarted for each new ingot produced. In continuous casting however the process does not need to be continually restarted hence the yield loss would be expected to be lower.

Currently, many types of continuous casting technologies are being used by the aluminum industry for commercial production of aluminum alloys, including: twin-roll casting [Haga et al., 2001], wheel-belt casting [Altenpohl, 1998;], Hunter-Douglas casting [Altenpohl, 1998;], and Hazelett twin-belt casting [Petry, 1986]. Among the

continuous casting processes, the Hazelett twin-belt caster and twin-roll caster have generated a great deal of interest because of their high productivities, superior product quality and versatility [Haga et al., 2003; Girard, 2002] and make them a real potential for use by the aluminum industry for automotive sheet alloys.

1.1 Characteristics of Twin-Belt Caster

As shown in Figure 1.2, the Hazelett twin-belt caster is generally used for the production of wide strips [Petry, 1986; Girard, 2002]. In this process, liquid aluminum comes out of the furnace into a tundish, creating a dam of molten metal as a source for the casting process. Molten metal then feeds to the moving mould (or belt) made of copper through ceramic nozzles at a slight angle. The fully or partially solidified strip exits the caster into downstream pinch rolls [Petry and Szczypiorski, 1987, Petry, 1986]. The strip is then either cut to the desired length or coiled for further processing.

The ceramic nozzles used in this process are generally segmented into several pieces to eliminate dimensional inaccuracy due to thermal distortion. The opening of the nozzles is controlled to manage the metal velocity and the associated turbulence of the molten metal in the mould [Girard, 2002].

The most important part of the twin belt continuous cast process is the combination of the two moving copper or steel belts, which corresponds to the fully moving mould. The belts require an efficient cooling system and hence cold water cooling is applied to the back of the belts. A ceramic-based permanent coating is generally applied to the belts to

prevent rust from occurring as well as moderating the heat transfer. The space between the belts is closed at each edge by metallic side dams, which move at the same velocity. These side dams, made of non-conductive material are provided for homogeneous heat transfer across the moving mould and prevent the liquid metal from coming out of the mould [Petry, 1986].

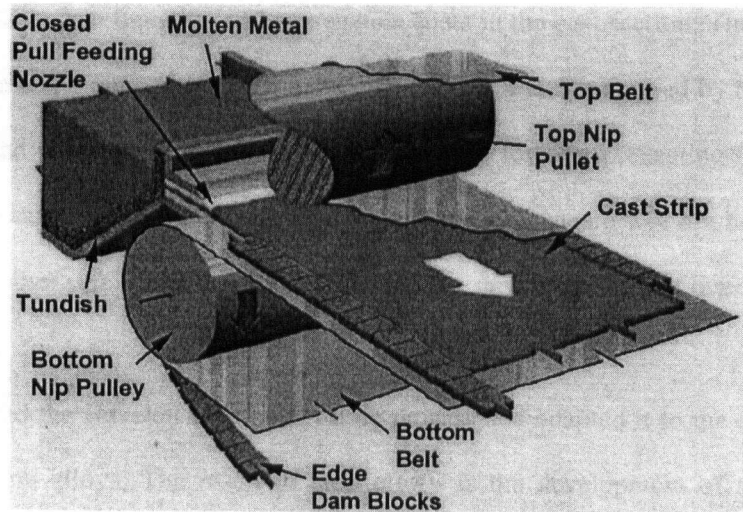


Figure 1.2 - The twin-belt caster [Girard, 2002].

1.2 Continuous Casting Compared to Ingot Casting

The main advantage of continuous casting is the lower production cost involved with processing of the material from casting to the final product. The thickness of the as-cast product from continuous casting is typically in the range of 10 to 20mm, which is quite close to the final gauge thickness of aluminum sheets (1 to 3mm) [Girard, 2002]. The reduction in thickness from casting to final product may be as little as 60% for continuous casting products, whilst for ingot casting, values of about 99% minimum deformation are typical [Gallerneault and Lloyd, 2002]. In fact, strips produced from

continuous casting can be potentially taken for direct cold reduction, which corresponds to a huge economical benefit for the company, as it avoids the costly hot rolling process.

To date, the continuous casting process has only been successfully used for certain aluminum alloys as compared to ingot casting. The reason for this is the cooling rate difference between ingot and continuous casting. The cooling rate during continuous casting is around 100°C/s (for twin-belt casting, twin roll casting adopts a cooling rate of 1000°C/s) compared to much slower cooling rates experienced during ingot casting (2°C/s) [Sanders et al., 1986; Gallerneault and Lloyd, 2002]. Due to the higher cooling rates in continuous casting, solute partitioning can occur in certain aluminum alloys [Gallerneault and Lloyd, 2002]. Specifically twin roll casting, where the solidification rate is significantly higher than other continuous casting processes (like twin-belt casting), is only suitable for low freezing range aluminum alloys (i.e., AA5xxx alloys where the Mg content is $< 1\%$). For large freezing range aluminum alloys, more pronounced solute partitioning occurs during solidification creating defects such as, solute channeling to the cast surface and surface liquation as well as segregation spots on the as-cast surface. As the continuous cast material is not scalped, this kind of as-cast surface defect or any kind of imperfection is retained through to the final gauge, which is unacceptable in terms of sheet quality. Hence the whole process requires superior cleanliness to minimize surface defects in the final material. [Gallerneault and Lloyd, 2002].

In recent years, gradual development in the twin-belt continuous cast process has allowed casting of aluminum alloys up to 3% Mg contents without solute partitioning and good surface finish [Girard, 2002]. These developments include: the use of a ceramic-coated belt to reduce the tendency of strips to stick to the belt during casting, higher casting speeds by positioning the pinch roll after the twin-belt caster, controlled pressure during casting for optimizing the heat transfer rate during solidification and belt prewarming for controlling the solidification rate and minimizing solute partitioning. As a result, much interest has been generated to understand the properties of aluminum alloy sheets with high Mg contents such as AA5754 produced through continuous casting.

1.3 Al-Mg Alloys

Among the non-heat treatable aluminum alloys used in the manufacturing industry, work-hardened 5xxx (Al-Mg alloys) alloys provide the highest level of strength possible without any kind of precipitation hardening [Sanders et al., 1989]. The microstructure of these alloys consists of the Al-Mg matrix, constituent particles, which form during the casting process and dispersoid particles, which precipitate during subsequent processing after casting (i.e., homogenization and rolling). These alloys attain their strength through work hardening, solid solution hardening and grain size strengthening; though work hardening remains the primary strengthening mechanism [Sanders et al., 1986]. From a property perspective, 5xxx alloys have good formability, good spot weldability and good corrosion resistance. On the other hand, it shows relatively low strength compared to heat treatable alloys and a tendency towards

Lüdering, which is detrimental for outer autobody applications. These properties make some 5xxx alloys suitable for structural applications, where high surface quality is not important [Burger et al., 1995]. Hence, some of the 5xxx aluminum alloys have been targeted for use as inner body panels for automobiles. These include: AA5754, AA5182, AA5030 and AA5032, with AA5754 being the most common alloy used by the North American automotive industry for inner body panels [Miller et al., 2000]. Table 1.1 shows the nominal composition of AA5754.

Table 1.1 - Nominal composition of the AA5754 alloys (in wt. percent).

Alloying elements	Mg	Mn	Si	Fe	Al
AA5754	2.6-3.6	≤.5	≤.4	≤.4	Rest

1.4 Motivation of Research

Development of final microstructure and hence final product properties of a product are based on the composition of the material as well as processing operations experienced by the material. Figure 1.3 shows the processing routes involved in the continuous and ingot casting of Al-Mg alloys. In general, the process route used for continuous cast Al-Mg alloys is similar to that of the ingot cast process route. However, there are some obvious differences between these two process routes including: the solidification rate experienced during casting (much higher in continuous casting), absence of the homogenization stage in continuous casting and the amount of hot and cold deformation applied to the material after casting (total amount of deformation is significantly lower for a material produced via continuous casting).

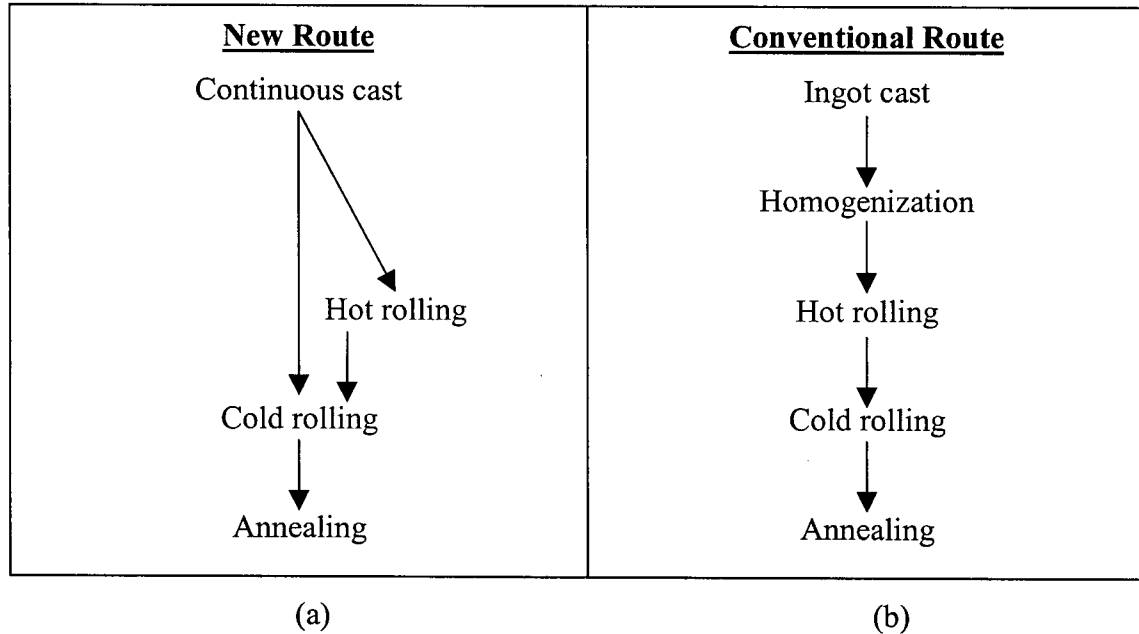


Figure 1.3 - Comparison of continuous cast and ingot cast processing routes to produce Al-Mg alloys.

As a result, the goal of the research is to understand the effect of processing route on the microstructure evolution during the continuous annealing process after cold rolling. The annealing operation, which consists of two fundamental processes, namely recovery and recrystallization, determines the final microstructure and properties of the end sheet product and hence is critical in terms of the final product properties. The material selected for study is AA5754, an important Al-Mg alloy used for structural applications in the automotive industry.

2. Literature Review

2.1 Introduction

In commercial production of AA5754 alloys, the final properties of the alloy are determined both by the composition of the material, as well as the processing it experiences. The final microstructure can be characterized in terms of the dislocation density within the grains, the grain size, shape and crystallographic orientation as well as the volume fraction and size distribution of second-phase particles. The annealing operation, which is often the final heat treatment process experienced by aluminum sheets, influences both the microstructure evolution and final mechanical properties of the material. During the annealing operation, two important softening mechanisms occur, recovery and recrystallization. The material properties after the annealing operation depend on the extent to which these two mechanisms occur.

To date, research has been conducted to understand the annealing behaviour of Al-Mg aluminum sheet alloys such as AA5754 that have been produced either via the continuous cast route or ingot cast route. However few studies have focused on a comparison of the recovery and recrystallization behaviour during annealing and final microstructure of continuous and ingot cast Al-Mg alloys. Recently, some studies carried out University of Kentucky [1997-2003] have provided some information regarding the influence of the process route (i.e., continuous casting versus ingot casting) on the microstructure evolution in Al-Mg alloys. The aim of this chapter is to provide a comparative review about the influence of prior processing route of cold

rolled sheets on the microstructure development during an annealing heat treatment Al-Mg aluminum alloys through both experimental observation and analysis. The initial part of the literature review will focus on the commercial processing routes available to produce cold rolled aluminum sheet

2.2 Processing

2.2.1 Casting

Casting is the initial stage of material preparation and has tremendous influence on the microstructure development in subsequent processing operations. In general two kinds of casting processes are adopted by the aluminum industry. The more conventional casting process used by the aluminum industry is ingot casting, where large ingots (400-500mm) are produced with a cross-section suitable for further fabrication processing like rolling, extrusion and forging. But during the last decade a considerable amount of interest has been invested towards an alternate processing route of aluminum casting from economic point of view. This newly developed alternate casting process is known as continuous or strip casting where liquid aluminum is cast in finer thickness (around 10 to 20mm) with higher solidification rate [Granger, 1989; Girard, 2002].

Casting determines the initial grain size and shape, cell size, and constituent type and distribution [Sanders et al., 1989; Granger, 1989]. The goal of this section is to provide a general discussion about the effect of the continuous and ingot casting process on the

as-cast microstructural features, focusing predominantly on the grain size, shape and second-phase particle size and distribution.

One of the most striking differences in the microstructure of aluminum alloys cast via continuous cast and ingot cast routes is the grain size. The average as-cast grain size for continuously cast material is reported to be approximately 65-70 μm at the centre, and 40-50 μm near the surface [Girard, 2002]. On the other hand, the average grain size reported for ingot cast material is much larger and can vary from 50-500 μm [Granger, 1989]. The difference in as-cast grain size can be directly attributed to the differences in solidification rate experienced during each casting process. During the continuous casting process the cooling rates are much higher compared to the ingot casting process ($\sim 100/1000^\circ\text{C}/\text{sec}$ vs. $\sim 1-2^\circ\text{C}/\text{sec}$) [Sanders et al., 1986; Gallerneault and Lloyd, 2002]. Both ingot and continuous cast Al-Mg alloys show dendrite arm (cell structure) within each grain, however the spacing between the arms is finer for continuous cast material [Granger, 1989].

In addition to the solidification rate applied during casting, the composition of the material may play an important role in deciding the average as-cast grain size. A comparative study on low and high Fe continuous as-cast AA5754 indicated that the material containing more Fe had a smaller average grain size as shown in Figure 2.1. [Girard, 2002]. Second phase particles rich in Fe solidify before the equiaxed grains and generally act as nucleation sites. With increasing Fe content, the formation of new grains increases and therefore the overall structure becomes finer.

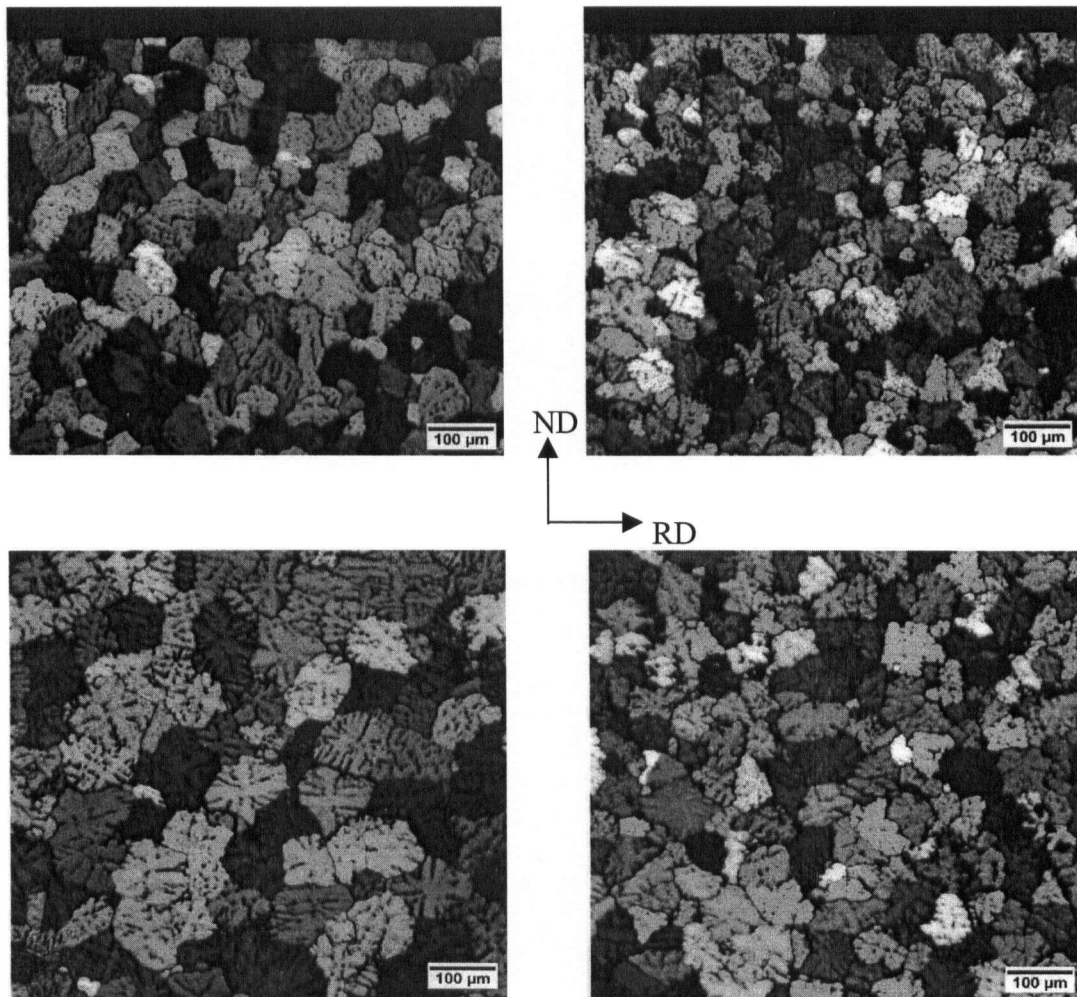


Figure 2.1 - Effect of Fe on grain structure of continuous as-cast AA5754. Left top and left bottom figures are showing surface and centre grain structure for low Fe (.09wt%) AA5754; Right top and right bottom figures show surface and centre grain structure for high Fe (.28wt%) AA5754 [Girard, 2002].

Another important feature during casting operation of Al-Mg alloys is the formation of intermetallic phases, commonly known as constituent particles. The shape, size and distribution of these second-phase particles play a significant role in determining the evolution of microstructure during subsequent processing of the as-cast material. During hot and cold rolling, they can break up into smaller particles and become distributed

throughout the matrix. These constituent particles can then become potential nucleation sites for recrystallization [Sanders et al., 1986, 1989; Humphreys and Hatherly, 1995]. Research in Alcoa [Stumpf, 1965-1971] showed that most common constituent particles reported in Al-Mg alloys consist of Al and Fe, since the solid solubility limit of Fe in aluminum is relatively low i.e. 0.05wt% at the eutectic temperature. Hence, any additional Fe can precipitate as second phase particles with compositions close to Al_3Fe . Mn can also be involved in the formation of second phase particles, i.e. $Al_6(Fe, Mn)$ [Gandhi, 1999; Girard, 2002]. The presence of Mg and Si in Al-Mg alloys also promotes the formation of Mg_2Si during the casting operation, but not as extensively as in 6000 series. Work by Karlík [Karlík et al., 2002] on continuous and ingot as-cast AA5754 and AA5182 revealed three types of constituent particles: (1) particles containing Al, Fe; (2) particles containing Al, Fe, Mn and Si and (3) to lesser extent, particles consisting of Mg and Si.

Though the composition of the second phase particles is the same for both ingot and continuous cast material, the size and shape of the particles differ depending on the casting process. Due to the high solidification rate, as compared to the ingot casting process, the continuous casting process produces finer constituent particles [Nes et al., 1979; Gallerneault & Lloyd, 2002]. In contrast, during ingot solidification an initial distribution of coarse (often $>100\mu m$) constituent particles is observed [Sanders et al., 1986]. Particles are present mostly in clusters and located mainly at the prior interdendritic regions. Work by Karlík and his coworkers [Karlík et al., 2002] on continuous and ingot cast AA5754 and AA5182 has also shown that the higher

solidification rates during continuous casting produce finer second-phase particles. A similar microstructure study on continuous and ingot cast AA5052 and AA5182 [Slámová et al., 2003] exhibited not only finer constituents in continuous as-cast structure but also higher particle density in continuous cast material as compared to ingot cast material. Figure 2.2 shows the differences in constituent particle size and distribution between continuous cast and ingot cast AA5xx aluminum alloys.

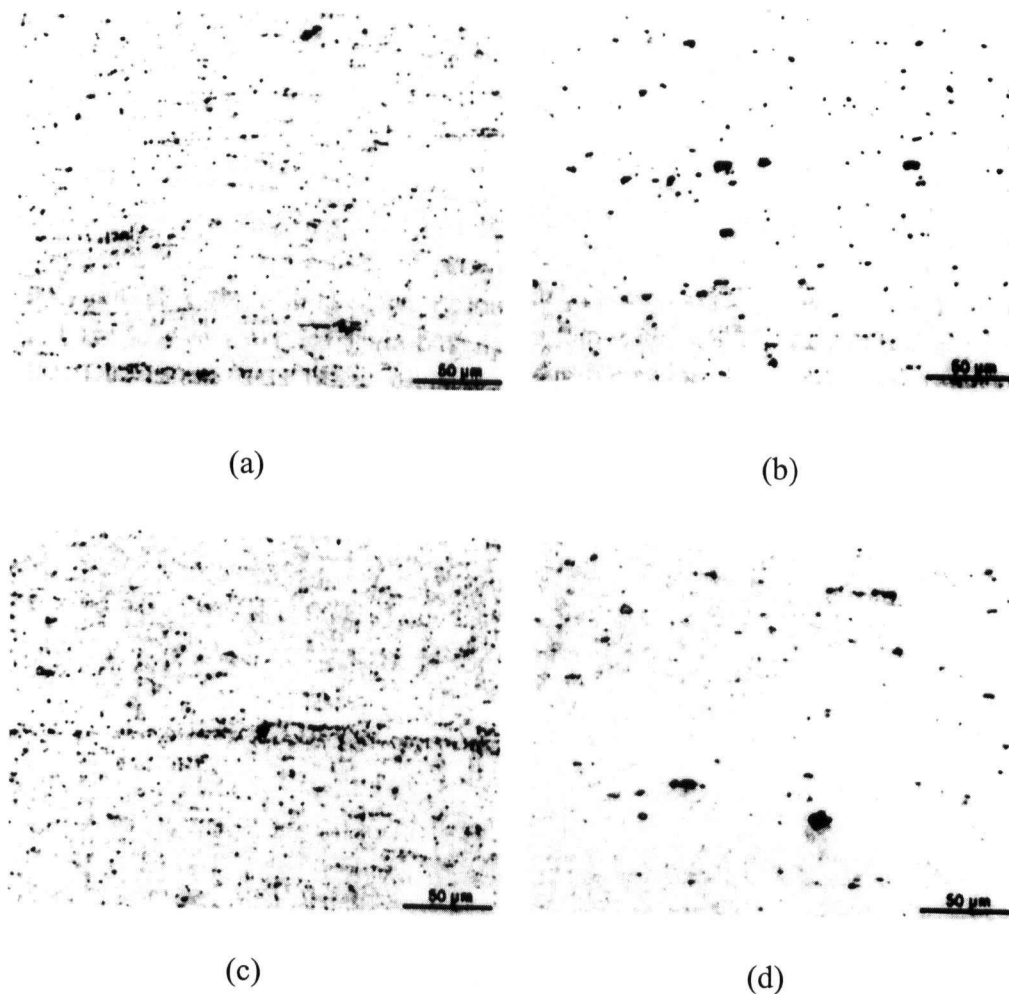


Figure 2.2 – Micrographs of second phase particles: (a) Continuous cast AA5052, (b) Ingot cast AA5052, (c) Continuous cast AA5182, (d) Ingot cast AA5182 [Slámová et al., 2003].

2.2.2 Effect of Homogenization

Homogenization treatment is an important stage that is required to reduce the amount of segregation as well as preheat the material to the hot rolling temperature after ingot casting [Granger, 1989]. In addition to the reduction in microsegregation of some elements (mainly Fe and Mn) in solid solution several other microstructural changes occur during homogenization in the matrix, such as [Gandhi, 1999]:

- precipitation of supersaturated elements as dispersoids,
- dissolution of unstable phases or precipitates, and
- coarsening of stable constituent phases.

The size and density of the constituents and dispersoids are greatly affected by the homogenization treatment applied to the material [Liu et al., 1998; Slámová et al., 2002]. High temperature soaking and long times during the homogenization process can coarsen the constituents and results in a uniform spatial distribution of dispersoids. Further thermomechanical processing will then break up these particles and distribute them along the rolling direction. In contrast, continuous cast material does not typically experience any homogenization treatment and therefore the solid solution remains supersaturated with elements such as Fe and Mn. A study on hot band AA5182 material by Liu [Liu et al., 1998] showed a strong presence of broken constituents and dispersoids in ingot cast material; whilst continuous cast hot band showed little presence of dispersoids along the primary grain boundary. A good review by Azari [Azari et al., 2002] on continuous cast AA5754 revealed the effect of homogenization treatment on the dispersoids distribution in the as-cast material. As-cast material after

homogenization exhibits higher distribution of Mn rich dispersoids compared to non-homogenized material.

2.2.3 Hot Rolling

Hot rolling is the intermediate step between final cold reduction and the initial casting operation. Hot rolling is mainly applied to reduce the thickness of large ingots to lower thickness suitable for cold reduction. This process also breaks up the solidification cell structure as well as constituent and dispersoid particles [Sanders et al., 1986].

A comparative microstructure study on hot rolled continuous and ingot cast Al-Mg alloys carried at University of Kentucky [Liu et al., 1998, Cheng et al., 2002] revealed some interesting results. The research, which was done using continuous and ingot cast hot band AA5182 showed a fully recrystallized grain structure in the ingot cast hot band, whereas continuous cast hot band exhibited no recrystallization and was only recovered. Particle stimulated nucleation (PSN), the large amount of hot deformation (400/500mm cast ingot thickness to around 4-5mm hot band thickness) and high hot rolling temperature (around 350°C - 400°C) were the probable reasons behind the occurrence of full recrystallization in the ingot cast material [Liu et al., 1998; Cheng et al., 2002].

2.3 Recovery and Recrystallization

Heat treatment at elevated temperature during annealing facilitates the material to move into a lower energy configuration from a higher energy state (evolved after deformation) through two fundamental processes, namely recovery and recrystallization. Recovery in general is responsible for partial restoration of cold rolled structure by cell/subgrain formation through dislocation (generated during deformation) annihilation and rearrangement. During recrystallization complete restoration of strain free grains are produced. The microstructure evolution of material during recovery and recrystallization is shown in Figure 2.3.

Numerous studies have been done on recovery and recrystallization of various materials, but the main focus of this section is to present the importance of the two fundamental softening mechanism (recovery and recrystallization) that occur during annealing of Al-Mg aluminum alloys and the characteristic similarities and differences between continuous and ingot cast Al-Mg aluminum alloys.

2.3.1 Recovery in Al-Mg Alloys

2.3.1.1 General Observation

Recovery plays an important part in softening of strain-hardened Al-Mg alloys. During deformation Mg atoms pin dislocation motion due to their high diffusivity in Al [Lloyd, 1980, Burger et al., 1995], hence the rate of dynamic recovery is reduced during cold rolling of Al-Mg alloys. The absence of dynamic recovery not only promotes a higher degree of work hardening, but also produces a higher stored energy for

subsequent static recovery and recrystallization to occur. In fact, experimental evidence has shown that with an increasing amount of Mg in Al, the static recovery potential increases for Al-Mg alloys [Sanders et al., 1989]. Work at Alcoa [Sanders et al., 1989] showed about 50% softening in Al-4.5%Mg alloys due to static recovery before any kind of initiation of recrystallization (Figure 2.4).

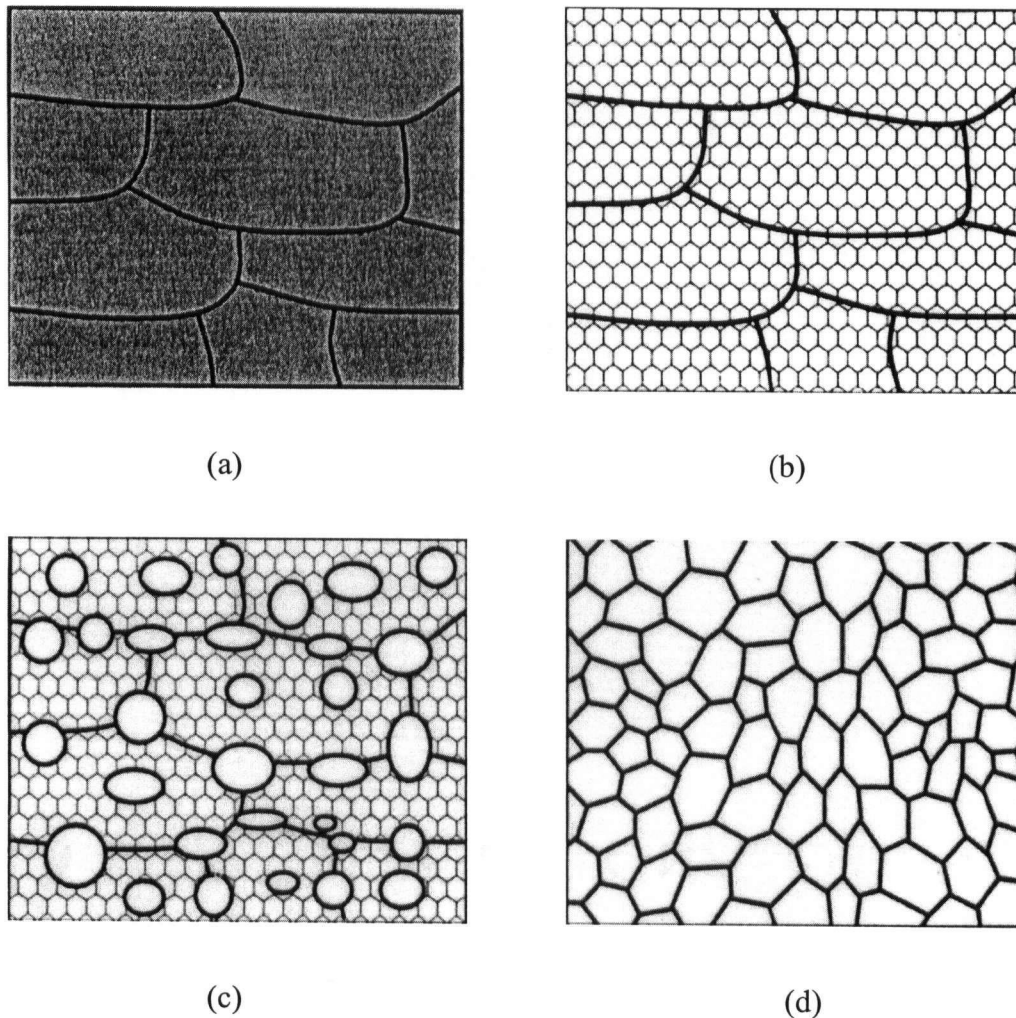


Figure 2.3 – Schematic diagram describing recovery and recrystallization process in deformed material; (a) Deformed state, (b) Recovered state, (c) Partially recrystallized state, (d) Fully recrystallized state [Humphreys & Hatherly, 1995].

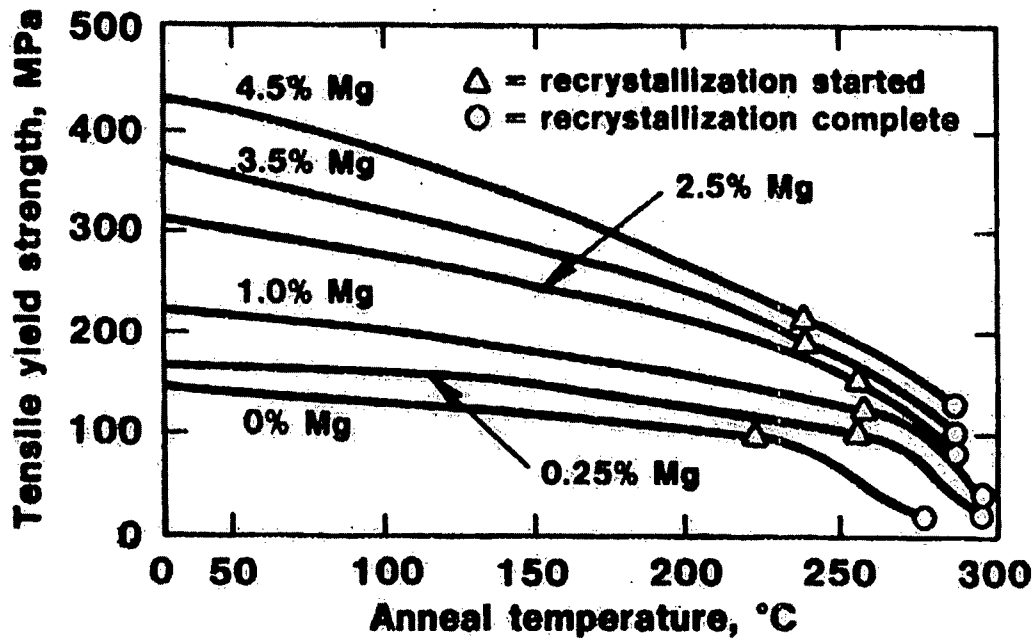


Figure 2.4 – Partial annealing curve for a series of binary Al-Mg alloys cold rolled to 70% and annealed for 2 hours at annealing temperature [Sanders et al., 1989].

Based on the general review on aluminum alloys by Humphreys and Hatherly [Humphreys & Hatherly, 1995], solute atoms and second-phase particles have a tremendous effect on the recovery kinetics of commercial purity aluminum alloys. In general, the solute effect on the recovery behaviour of Al-Mg alloys depends on their solid solubility in aluminum and their effect on the deformation microstructure [Sanders et al., 1989]. A small amount of solute drastically reduces the mobility of cell structure or dislocation substructure and grain boundary. The retarding effect of solute atoms on the growth of dislocation substructures or grain boundaries is known as the solute drag effect. Mg being the main alloying element in the Al-Mg alloys is the most effective solute element in affecting the recovery behaviour of Al-Mg alloys. In addition Mn and Si in solution impedes the recovery during annealing of cold rolled material [Sanders et

al., 1989]. In separate work at Queens' University, the significant solute drag effect of Fe on Al-Mg alloy had been mentioned by Saimoto and his co-workers [Saimoto et al., 2002]. Early work on the presence of Cu and Mg solute atoms on aluminum [Humphreys and Hatherly, 1995] has shown a severe decrease in mobility of the low mobility grain boundary in Al alloys. Generally it is observed that at low boundary velocities, the velocity is inversely proportional to the solute concentration; whereas at higher driving force associated with gradual transition to the high velocity regime, the boundary velocity is independent of solute content [Humphreys & Hatherly, 1995].

Second-phase particles, which are a common feature in Al-Mg alloys, can also have a significant influence during recovery of aluminum alloys [Humphreys & Hatherly, 1995]. Generally, second-phase particles present in the matrix can retard the recovery behaviour of the material by pinning dislocations. A fine dispersion of small particles stabilizes the substructure and impedes the substructure growth necessary for nucleation to occur [Nes and Embury, 1975; Sanders et al., 1989]. The drag pressure on boundary movement by the random distribution of particles is known as Zener pinning pressure [Humphreys and Hatherly, 1995]. This effect is stronger when the interparticle spacing is less than the cell or substructure size.

In some cases, precipitation occurs during the recovery process, usually on the dislocation substructures and low or high angle boundaries. This situation can be detrimental to the recovery kinetics of the material, as the particle distribution does not remain uniform during concurrent precipitation. Such non-uniformly distributed

precipitates exert a strong pinning effect on the boundaries and retard the further softening of the material [Humphreys & Hatherly, 1995].

2.3.1.2 Effect of Processing

As discussed previously, processing variables are largely responsible for the solute supersaturation, presence and distribution of second-phase particles in the Al-Mg alloys, which in turn significantly affect the recovery process of Al-Mg alloys. Unfortunately very little information is available in the literature on the comparative recovery behaviour of continuous and ingot cast Al-Mg alloys. Generally particle-dislocation interaction should be less prominent in continuous cast material as it shows a lower density of dispersoids in the rolled microstructure [Liu et al., 1998]. This should enhance the possibility of strong solute dislocation interaction in the continuous cast material during recovery. In comparison, ingot cast material has a higher density of finer dispersoids, which are responsible for retarding the recovery behaviour of ingot cast Al-Mg alloy. Precipitation during annealing may affect recovery behaviour of the cold rolled continuous cast alloys, as it is observed in Al-Mg and Al-Mn alloys [Koizumi et al., 2000; Tangen et al., 2002], but this mechanism is of importance at elevated temperature annealing (i.e. around 300°C and above).

2.3.2 Recrystallization in Al-Mg Alloys

2.3.2.1 General Observation

Recrystallization is a further restoration process that occurs after recovery in the material. This process is of immense importance for the final mechanical property, grain

size and texture of the material. The basic mechanism of recrystallization involves the formation or nucleation of dislocation free grains and the growth of that grain by consumption of the deformed or recovered structure. Figure 2.5 shows the typical sigmoidal shaped recrystallization kinetics observed during isothermal annealing of a material. There are some factors, which affect the recrystallization process including:

[Doherty et al., 1997]:

- deformation or recovered microstructure
- initial grain size
- presence of solutes
- influence of particles on nucleation and grain growth
- processing parameters, such as annealing temperature, heating rate, cooling rate etc.

The initial stage in the recrystallization process during annealing is the formation of relatively strain free recrystallized nuclei. In general, recrystallized nuclei form in heavily deformed aluminum alloys in four main areas, namely: cube bands, grain boundaries, deformation zones around second-phase particles and occasionally shear bands [Engler, 1998]. All of these sites exhibit the ideal condition (high degree of misorientation and high interfacial energy) for producing high mobility boundaries. For Al-Mg alloys, nucleation has been observed in cube bands, on grain boundaries and shear bands and on new non-deforming particles (particle stimulated nucleation, i.e. PSN) [Azari et al., 2002].

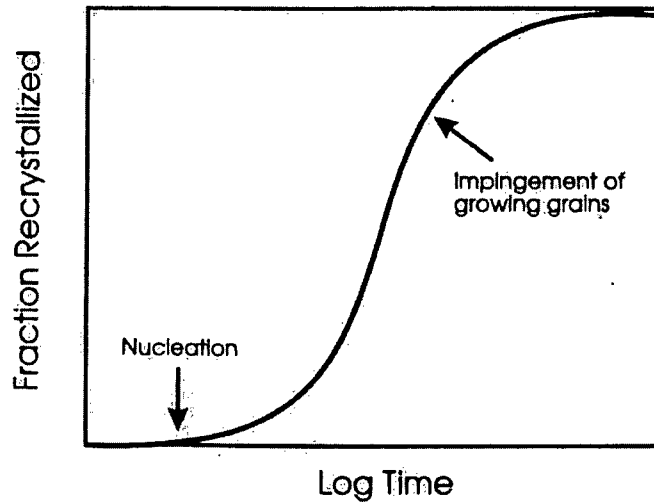


Figure 2.5 – Typical recrystallization kinetics during isothermal annealing [Humphreys & Hatherly, 1995].

Similar to recovery, solute atoms play an important role in the recrystallization kinetics of Al-Mg alloys. Solute drag has significant effect on the onset of recrystallization and on the growth of recrystallized nuclei by retarding the boundary mobility [Bréchet and Purdy, 2003]. Mg being present as the main solute in the Al-Mg alloys has a strong effect on the onset of recrystallization. Studies by Koizumi [Koizumi et al., 2000] showed the effect of Mg on recrystallization kinetics of 95% cold deformed Al-Mg alloys during annealing at various temperatures (between 200°C to 450°C) as shown in Figure 2.6. According to their study, recrystallization kinetics of Al-Mg alloys changes depending on the Mg amount in the alloy. It was found that increasing the Mg content from .5 to 1% slightly retarded the onset of recrystallization, since solute Mg atoms strongly interact with dislocation structures and suppressed recovery. Hence in this low

solute concentration region in the Al-Mg alloys, nucleation rate, growth rate and the rate of recrystallization are reduced with increasing solute content.

On the other hand, it can be seen from the Figure 2.6 that the increases with Mg content more than 1%. At this level, the dominant effect appears to be the role of Mg on the work hardening and thus the stored energy, rather than its effect on the mobility of the high angle grain boundaries [Koizumi et al., 2000]. But the effect of Mg on recrystallization is very much related to the amount of cold deformation experienced by the material. At low deformation level (cold reduction below 50%) the critical value of Mg content changed from 1% to 2% [Perryman, 1955]. Figure 2.6 shows the effect of Mg content on the recrystallization kinetics of Al-Mg alloys.

Second-phase particles have a strong influence on the recrystallization kinetics of Al-Mg alloys. In general Al-Mg alloys exhibit two kinds of second-phase particles. Coarse constituent particles ($>1\mu\text{m}$) accelerate the recrystallization kinetics of Al-Mg alloys by particle stimulated nucleation, but in contrast, the much finer dispersoids significantly retard the recrystallization kinetics of these alloys [Humphreys, 1977; Sanders et al., 1986; Engler et al., 1998]. Deformation zones form around the constituent particles due to deformation incompatibilities at the matrix/particle interface. During annealing, these deformation zones with very high dislocation densities and complete misorientation compared to the surrounding matrix, become the preferred nucleation sites for recrystallization to occur [Sanders et al., 1989; Samajdar et al., 1998].

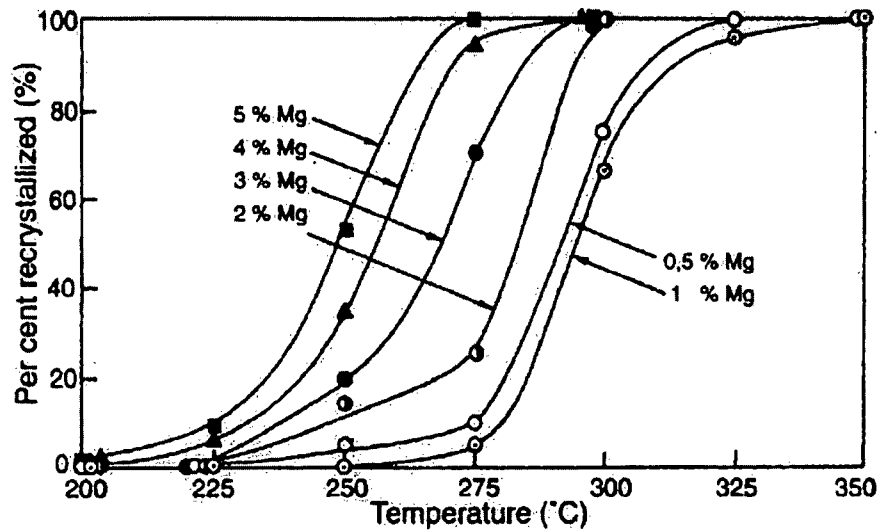


Figure 2.6 – Fraction recrystallized plotted against annealing temperature for Al-Mg alloys with various Mg content. All alloys initially cold rolled to 95% and annealed for 5 min at each temperature [Koizumi et al., 2000].

Dispersoids have the opposite effect on the recrystallization kinetics of Al-Mg alloys [Sanders et al., 1986, 1989]. Dispersoids being present as fine particles within the matrix strongly interact with low angle grain boundaries and thus impede the grain growth. This not only delays the process of nucleation, but also reduces the number of nuclei formed during the initial stages of recrystallization [Nes and Embury, 1975; Chan and Humphreys, 1984]. The pinning of grain boundary movement by fine particles is commonly termed as Zener pinning. The effect of finer particles on recrystallization kinetics may be quite severe if concurrent precipitation occurs during annealing of the material. In this case, particles are unlikely to be distributed uniformly and will precipitates preferentially on the boundaries or the high-energy regions within the matrix. The pinning pressure due to the particles will therefore be greater than for a

uniform particle distribution [Humphreys and Hatherly, 1995]. Tangen and his coworkers studied the effect of concurrent precipitation preceding recrystallization for AA3103 alloys [Tangen et al., 2002]. According to their study on AA3103, various cold rolled materials from different initial condition were taken for annealing at 500°C. Experimental results showed the most delayed onset of recrystallization and slowest recrystallization kinetics for the cold rolled material rolled from non-homogenized as-cast material. Cold rolled material rolled from fully homogenized as-cast material showed the fastest recrystallization behaviour among all the materials taken for experimentation. The variation in recrystallization kinetics is attributed to the amount of concurrent precipitation of Mn rich dispersoids during annealing. Figure 2.7 shows the effect of concurrent precipitation effect on recrystallization of Al alloys.

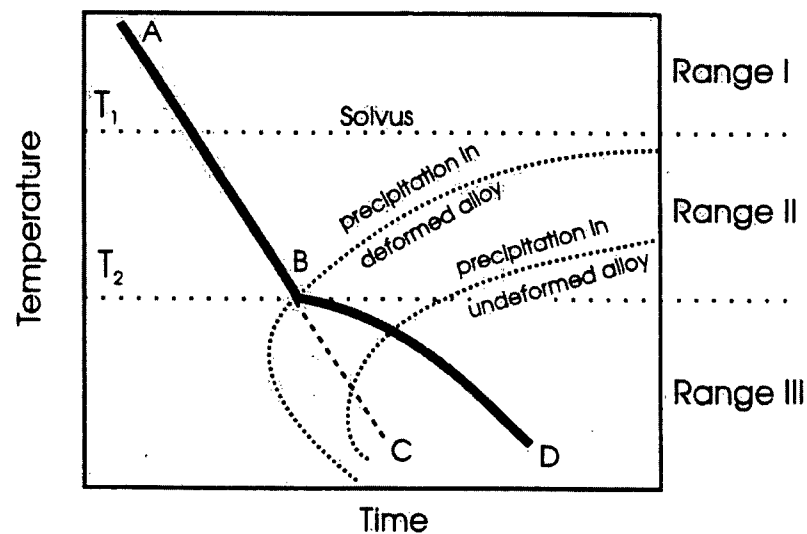


Figure 2.7 – The interaction between recrystallization and precipitation [Humphreys & Hatherly, 1995].

According to Figure 2.7, annealing temperature above T_1 (above solvus temperature) always promotes recrystallization faster than precipitation and hence the recrystallization follows the 'ABC' curve; similar result would be observed if the annealing temperature is above T_2 (corresponds to the temperature for intersection of recrystallization and precipitation in deformed alloy). But annealing at temperature below T_2 , precipitation occurs before recrystallization. In the last case, precipitation occurs preferentially on the low and high angle grain boundaries, hinders the recovery and recrystallization; hence the recrystallization gets delayed and follows the 'ABD' curve.

There is a correlation observed between Mg content and the final recrystallized grain size [Sanders et al., 1986]. Recrystallized grain size decreases in Al-Mg alloys with increasing Mg content in the alloy. Experimental work performed in Alcoa [Sanders et al., 1986] on Al-Mg alloys with various Mg content (approximately 0%-5%) showed a decrease in recrystallized grain size up to a Mg content of 3.5% in Al-Mg alloys. A study on the recrystallization behaviour of Al-Mg alloys by Koizumi and his coworkers [Koizumi et al., 2000] also support the fact that a higher Mg content decreases the recrystallized grain size. The decrease in recrystallized grain size is generally attributed to the increasing presence of shear bands, which increases considerably with increasing presence of Mg. These shear bands act as strong nucleation sites and promote a higher number of recrystallization nuclei.

Though increasing Mg content decreases the final recrystallized grain size, higher Mg content in Al-Mg alloys seems to increase the inhomogeneity in the final recrystallized grain structure. A comparative study on pure Al and Al-5%Mg alloy [Ryum and Embury, 1982] showed that the presence of Mg not only produces high strain hardening, but also creates strong inhomogeneities in the dislocation structure associated with localized lattice rotations and shear bands. As a result, the number and distribution of recrystallization nuclei are markedly inhomogeneous in Al-Mg alloy compared to commercial pure aluminum [Ryum and Embury, 1982]. During subsequent annealing one grain recrystallized much faster compared to neighbouring grains. The resultant microstructure of Al-Mg alloys exhibits finer grain size, but comparative inhomogeneous grain structure distribution compared to pure recrystallized Al microstructure. In addition to compositional effect, the recrystallized grain size also depends greatly on the amount of cold reduction [Go, 2001].

Second-phase particles play an important role in determining the recrystallized grain size. A uniform distribution of constituent particles produce a finer recrystallized grain size due to the higher numbers of effective nucleation sites within the matrix [Doherty and Martin, 1962]. However, the effect of a fine distribution of dispersoid particles on recrystallized grain size is more complex in nature [Sanders et al., 1986].

2.3.2.2 Effect of Processing

Based on the literature for AA5182, recrystallization kinetics of the ingot cast material seems to be faster compared to continuous cast material for the same level of

cold reduction [Liu et al., 1998; Liu et al., 2003]. Work on continuous and ingot cast AA5182, showed that ingot cast AA5182 recrystallizes more easily than continuous cast material for a similar level of cold reduction; the initial material were hot bands for both ingot and continuous cast material [Liu et al., 1998]. Differences in the recrystallization behaviour of continuous and ingot cast material is probably due to the differences in the initial hot band structure of the continuous and ingot cast AA5182 before any kind of cold reduction. The particles and dispersoids characteristics observed in the two hot bands are greatly different. In the ingot cast fully recrystallized hot band, the intermetallic particles are distributed uniformly; the dispersoids are dense and evenly distributed. Conversely, in the continuous cast unrecrystallized hot band, intermetallic particles form a banded type of structure, with only a few dispersoids being distributed along the primary grain boundaries [Liu et al., 1998]. In separate work, experimental evidence on approximately 72% cold rolled continuous cast and ingot cast AA5182 showed different final microstructures after 3 hours of annealing at 232°C, 260°C and 371°C. Similar annealed microstructure for continuous and ingot cast material at 232°C and 371°C, however at 260°C, microstructure of ingot cast material seems to possess higher volume fraction of recrystallized grains compared to continuous cast material [Liu et al., 2003].

Homogenization of the continuous cast material prior to hot rolling affects the recrystallization kinetics. During the homogenization treatment extra solute precipitated from solid solution as fine precipitates and uniformly distributed in the matrix, which is the common phenomena observed in the ingot cast material [Liu et al., 1998]. This

brings a similarity in the as-cast microstructure between continuous and ingot cast material based on the second-phase particle distribution within the matrix. After equal levels of cold reduction from recrystallized hot band, homogenized continuous cast material exhibited similar trends in recrystallization kinetics with ingot cast material during annealing at various temperatures [Liu et al., 1998]. The similar recrystallization kinetics of homogenized continuous cast material and ingot cast material can be directly attributed to the microstructural similarities in the initial as-cast structure, specifically the second-phase particle distribution within the matrix.

Generally recrystallized continuous cast material exhibits finer average grain size compared to ingot cast material [Slámová et al., 2002]. Studies on fully recrystallized ingot and continuous cast AA5182 and AA5052 showed finer grain size for the continuous cast material. However, ingot cast material exhibited more homogeneous distribution of recrystallized grain structure [Slámová et al., 2002]. As mentioned previously, higher solidification rate during continuous casting not only produces finer second-phase particles (constituents), but also larger in number compared to ingot cast material. During annealing these constituents become the potential sites for particle stimulated nucleation (PSN) and hence these higher potential sites for nucleation give rise to finer recrystallized grain structure for continuous cast material [Slámová et al., 2002].

In summary, the recrystallized microstructure in Al-Mg alloys depends greatly on the Mg content [Ryum and Embury, 1982], processing history of the material [Liu et al.,

1998; Slámová et al., 2002] and amount of hot and cold reduction experienced by the material before final annealing [Go, 2001; Girard et al., 2002]. Though experimental studies on continuous and ingot cast AA5052 and AA5182 showed that both material exhibited homogeneous grain structure after fully recrystallization, the continuous cast material produced somewhat elongated recrystallized grains compared to equiaxed grains of ingot cast material [Liu et al., 1998; Slámová et al., 2002]. When a homogenization treatment was applied to the continuous cast material, it changes the solute presence in the as-cast material, specifically by precipitating finer dispersoids within the matrix, which ultimately leads to a uniform recrystallized grain structure [Liu et al., 1998; Tangen et al., 2002].

Finally, cold rolling prior to final annealing produces much finer and homogeneous structure for both continuous and ingot cast material compared to the only application of hot deformation prior to annealing [Go, 2001; Girard et al., 2002]. The final recrystallized grain size becomes finer with increasing amount of cold reduction. Given the same amount of cold reduction, ingot cast material exhibited more homogeneous grain structure, because of the higher amount of prior hot deformation as compared to continuous cast material [Girard et al., 2002].

2.4 Texture

Crystallographic texture or preferred orientation is an important aspect of a microstructure and will affect the material properties like tensile property, formability of the material [Girard, 2002]. Texture analysis can be done on two different measurement

scales. Bulk texture analysis is representative of the macrotexture in a material, and is usually studied either using by X-ray or neutron diffraction techniques. For more detailed texture information on a microscopic level, like the individual orientation of small population of grains; microtexture studies are conducted using techniques such as EBSD or TEM. [Randle, 1992]. The basis for the EBSD technique including calibration and general operation, analysis and interpretation of the Kikuchi diffraction pattern is well described in the books by Randle [Randle and Engler, 2000] and Schwartz [Schwartz et al., 2000]. A basic layout of EBSD setup is given in Figure 2.8. In general, textures of a material can be represented using either pole figures or the orientation distribution functions (ODF's) [Randle and Engler, 2000].

2.4.1 Recrystallization Texture in Al-Mg Alloys

2.4.1.1 General Observation

Evolution of recrystallization texture in Al-Mg is complex issue, however a general understanding can be obtained on the concepts of the nucleation and the growth phenomena. Though, much research have been done to understand this complex issue of texture development during annealing of Al-Mg alloys, many issues related to texture evolution in continuous and ingot cast Al-Mg alloys have not been investigated. Hence the aim of this section is not only to highlight the texture development in the recrystallized Al-Mg alloys after annealing but also provide a comparative review about the recrystallization texture observed in continuous and ingot cast Al-Mg alloys.

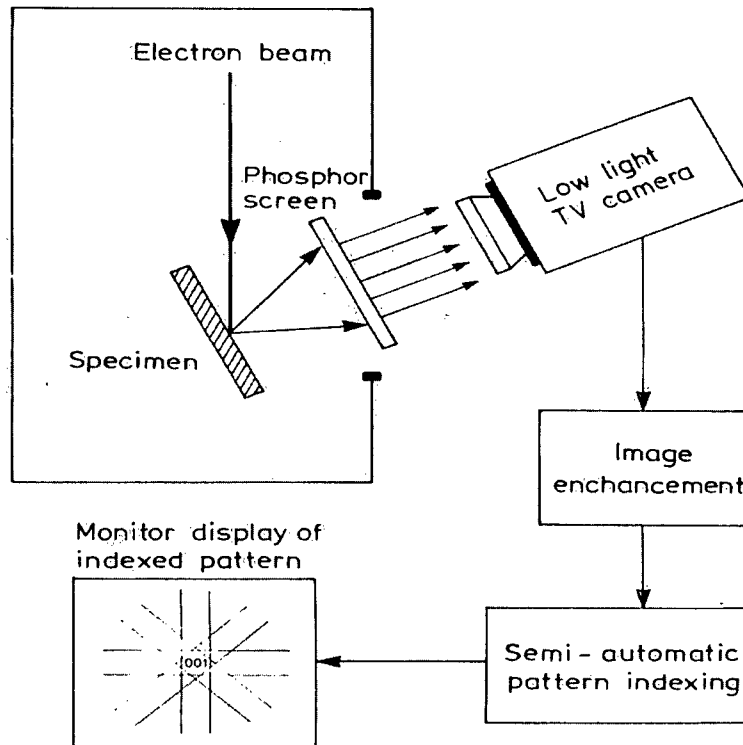


Figure 2.8 – Basic layout of the components of a typical EBSD system [Randle, 1992].

Development of recrystallization texture is normally discussed by two theories [Engler 1998]:

- Oriented nucleation – It is assumed that preferred formation of the recrystallization nuclei of special orientations determines the final recrystallization texture. Nuclei have to be part of the deformed structure.
- Oriented growth – It is assumed that from a broad spectrum of nucleus orientations, those with best growth conditions relative to deformed matrix grow fastest and decide the final recrystallized texture. In Al alloys it is observed that rolling and recrystallization texture has an orientation

relationship of 40° $\langle 111 \rangle$ and hence it is normally assumed that nucleus formed in rolling texture will prefer to grow at that preferred orientation [Lücke et al., 1974; Gottstein et al., 1992].

In general, evolution of recrystallization texture solely based on either of these two theories is not satisfactory and hence a combination of these two theories needs to be considered in order to rationalize the final recrystallized texture [Jensen, 1995; Engler, 1998].

In Al-Mg alloys, it is observed that the resulting recrystallization texture generally have a strong Cube ($\{001\}\langle 100 \rangle$) presence [Azari et al., 2002]. When shear bands dominate as the nucleation sites the resulting recrystallization texture is Goss ($\{011\}\langle 100 \rangle$), Q ($\{013\}\langle 2\bar{3}1 \rangle$) and P ($\{011\}\langle 122 \rangle$) with a weak deformation texture like Brass ($\{011\}\langle 211 \rangle$) and Cu ($\{112\}\langle 111 \rangle$). Normally it is observed that P and to a lesser extent Q and Goss possess an orientation relation of 40° $\langle 111 \rangle$ with the deformation texture component Cu [Lücke et al., 1990]. The recrystallized texture becomes random if particle stimulated nucleation (PSN) plays an important role during recrystallization. Nuclei formed within the deformation zone around the particles typically have a random orientation relative to the surrounding matrix [Sanders et al., 1986, Azari et al., 2002]. Mg content has a significant influence in the final recrystallized texture [Koizumi et al., 1997; Endou and Inagaki, 2002]. Al-Mg alloys with Mg content up to 3% promote Cube texture in the alloy. By inhibiting dynamic recovery, Mg increases the driving force for recrystallization and hence the effect of PSN and shear bands on nucleation is less

effective. The presence of Mg more than 3% and higher cold reduction increases the presence of shear bands, which is favourable for the development of new texture components such as, P and Q at the expense of Cube texture. That is why, recrystallized AA5182 shows weaker Cube texture compared to AA5754, consistent with the higher Mg content of AA5182 compared to AA5754 i.e. 4% vs. 3% respectively [Cheng et al., 2002]. In addition, recrystallized Al-Mg alloys exhibits a moderate presence of R texture component, which is considered as transition from deformed texture S ($\{123\}\langle 634\rangle$) during recrystallization; it normally decreases with increasing Mg content [Girard, 2002].

The presence of second-phase particles can also have a strong influence on the final recrystallized texture. Randomly oriented cell structure formed within the deformation zones present around the particles grows preferably in favourable orientations, like along $40^\circ \langle 111\rangle$ relationship to the matrix. As random nuclei compete with cube nuclei during recrystallization, an increase in the constituent's volume percentage would reduce the presence of Cube texture component.

Finally, annealing temperature can have a strong influence on recrystallization texture in Al-Mg alloys [Saitou et al., 2001; Endou and Inagaki, 2002; Cheng and Morris, 2002]. Low temperature annealing (between 300°C to 350°C) shows a strong presence of Cube and S texture and to some extent the presence of R ($\{124\}\langle 211\rangle$) texture. At high temperature annealing ($>450^\circ\text{C}$), with higher Mg content ($>2\%$), recrystallization texture exhibits texture components like P and Q, which develop at the expense of Cube

texture. Euler angles and Miller indices of the important texture components are presented in the Appendix A.

2.4.1.2 Effect of Processing

Some studies have been done on the comparative recrystallized texture for continuous and ingot cast Al-Mg alloys in recent years. Though recrystallized texture observed for continuous and ingot cast Al-Mg alloys tend to be random in nature, some small differences in the recrystallized texture were reported by Liu and his coworkers [Liu et al., 1998; Liu et al., 1999; Liu et al., 2002; Liu et al., 2003].

Ingot cast hot band exhibited strong presence of recrystallized texture, like Cube, Goss and R texture components, because of the recrystallized hot rolled microstructure observed in ingot cast hot band; whereas continuous cast hot band showed comparative strong presence of rolling texture components, with Brass, Cu and S as major texture component [Liu et al., 1999; Liu et al., 2002] due to its unrecrystallized grain structure. High temperature annealing of the continuous cast hot band produced fully recrystallized material associated with recrystallized texture similar to the ingot cast hot band.

Although after cold rolling, the rolling texture is stronger for continuous cast Al-Mg alloys compared to ingot cast material, the recrystallization texture in the continuous cast material is weaker as compared to ingot cast material [Slámová et al., 2003; Liu et al., 2003]. Cube texture component is higher in ingot cast material compared to

continuous cast material [Slámová et al., 2003]. Texture analysis on continuous cast AA5754 by Azari and his coworkers [Azari et al., 2002], showed that recrystallized continuous cast AA5754 from lower cold reduction (50% cold rolled) exhibited strong rolling texture component, but as the initial cold deformation level increased (>75%-90% cold rolled) the overall recrystallization texture became random in nature. Further increase in cold reduction up to 95%-97%, recrystallized texture showed strong presence of Cube texture component [Azari et al., 2002]. This change in recrystallized texture has been attributed to the continuous competition between the operation of cube nuclei and its' growth associated with impeding action of fine dispersoids. At higher deformation level, due to larger driving force the cube grain breaks the barrier of finer particles.

Homogenization treatment in continuous cast material changes the recrystallization texture of the material [Azari et al., 2002] by changing the initial microstructure features prior to cold working of the as-cast material. Work by Samajdar [Samajdar et al., 1998] on recrystallized AA5182 material from initial homogenized as-cast material showed both Cube and some new recrystallized texture components like P, CH and H. The effect of homogenization on the recrystallized texture of continuous cast AA5754 is also reviewed by Azari [Azari et al., 2002]. His work showed that the homogenization stage changed the recrystallized texture of higher cold deformed continuous cast AA5754 material (deformation of about 90%-97%) by exhibiting more random texture components (CH, H, Q etc.), rather than Cube texture; where-as material without homogenization produced more Cube and C_{ND} texture in the final recrystallized texture.

The development of new texture components is explained by two different arguments. In one case it is thought to be the effect of PSN with random orientation and in other way the situation is analyzed by the growth of new grains in some preferred directions.

3. Experimental

3.1 Introduction

The objective of this research was to compare the effect of processing route on the microstructure evolution and material behaviour during annealing of AA5754 sheets. The material was processed using the traditional ingot cast (IC) route as well as the newer continuous cast (CC) route. The study on the softening kinetics of the ingot cast AA5754 was carried out by Go [Go, 2001] and hence this section will outline only the experimental portion related to the continuous cast AA5754.

A number of different techniques were used during the course of this study to quantify the microstructure evolution and material behaviour during the annealing process. These techniques ranged from tensile measurements to evaluate the strength of the material, to optical metallography and Electron Backscattered Diffraction (EBSD) to assess the microstructure evolution, to resistivity measurements to study the change in solute content during homogenization to Scanning Auger Measurements (SAM) to investigate the particles in the material.

3.2 Starting Material

The experimental work was undertaken on a continuous-cast commercial quality aluminum sheet alloy, AA5754. The material was obtained from Alcan International Limited's Kingston Research and Development Centre (KRDC) located in Kingston,

Ontario. The AA5754 material received from KRDC was processed using the lab-scale continuous caster and rolling facilities available at their facility.

The chemical composition of the continuous cast AA5754 alloy supplied by Alcan is shown in Table 3.1. Since the main goal of this investigation was to compare the influence of processing route (ingot cast versus continuous cast) on the properties of AA5754, the composition of the both these materials is shown in Table 3.1.

Table 3.1 - Chemical composition of AA5754 provided by Alcan (in wt%).

AA5754	Mg.	Mn.	Fe.	Si.	Al.
Ingot cast	3.07	.24	.17	.057	~ balance
Continuous cast	3.11	.20	.16	.090	~ balance

3.2.1 Processing History

The continuous cast material was produced at the KRDC, Alcan. After casting, two different processes were applied to the as-cast strip. In one case, the as-cast strip was hot rolled to a reduction of 70% at around 300°C. The hot band strip was then recrystallized in a salt-bath (60% potassium nitrate + 40% sodium nitrate) at 500°C for 30mins. and cold rolled by 40% and 80%. In addition, some of the as-cast material was directly cold rolled by an amount of 80%-90% using the KRDC rolling facilities. Although not anticipated at the start of the research, some of the as-cast material was processed at the University of British Columbia (UBC) so that the influence of a homogenization treatment prior to cold rolling could be assessed. The homogenization treatment was done on the as-cast material at 500°C for 24 hrs. in a high temperature salt

bath (60% potassium nitrate + 40% sodium nitrate) and the material was then directly cold rolled by 80% to achieve similar processing history as that previous material. Table 3.2 summarizes the different thermal, mechanical treatments performed on the as-cast material as compared to the ingot cast material.

Table 3.2 - Thermal processing route for continuous and ingot cast AA5754 (value in bracket is the value of material thickness). Material highlighted in bold is the starting material for the cold reduction.

Continuous Cast	Continuous Cast	Continuous Cast	Ingot Cast
↓	↓	↓	↓
Hot Rolling (70%)	↓	Homogenization at 500°C for 24 hrs.	Homogenization at 550°C for 24 hrs.
↓	↓	↓	↓
Recrystallized at 500°C for 30mins	↓	↓	Hot Rolling (99.4%)
↓	↓	↓	↓
Cold Rolling (40% and 80%)	Direct Cold Rolling (80%)	Direct Cold Rolling (80%)	Cold Rolling (40% and 80%)

3.3 Isothermal Annealing

A series of annealing experiments were conducted to study the isothermal recovery and recrystallization behaviour of the cold rolled material and compare the results with that of the ingot cast material. Rectangular strips of 104.0 x 19.0mm were

cut along the longitudinal direction (parallel to the rolling direction) of the sheets and tensile specimens with 40mm gauge length were punched out from rectangular strips using a manual die. Figure 3.1 shows a schematic of the tensile specimens used for each test. In addition specimens with dimensions of 20.0 x 15.0 mm were taken from the edge area of cold rolled sheets for optical metallography as shown in Figure 3.2. These samples were immersed into salt baths (60% potassium nitrate + 40% sodium nitrate) for annealing experiments at various temperatures ranging from 200°C to 375°C. The Omega CN9000A auto-tune temperature controller monitored the temperature in the salt baths. The salt bath temperature was also checked periodically using a type-K thermocouple inserted into the bath and it indicated that difference between the temperature controller and thermocouple reading was in the order of $\pm 3^{\circ}\text{C}$. The holding time in the salt bath was varied from 30seconds to 15hours. The holding times reported only include the soak time at temperature and not the heating-time required to get to the soak temperature. At the end of each experiment, samples were taken out from the salt bath, quenched and then marked accordingly using an electronic engraver.

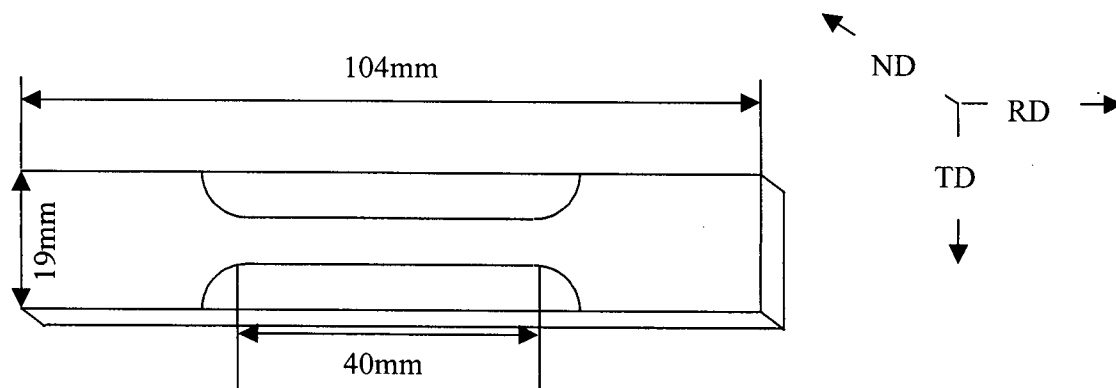


Figure 3.1 - Schematic of the tensile sample.

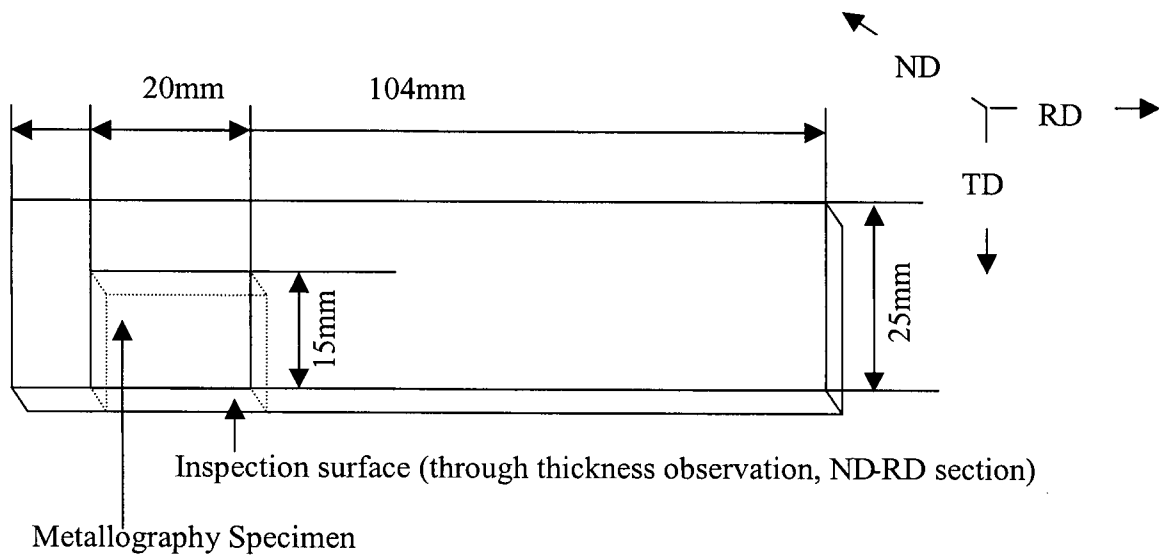
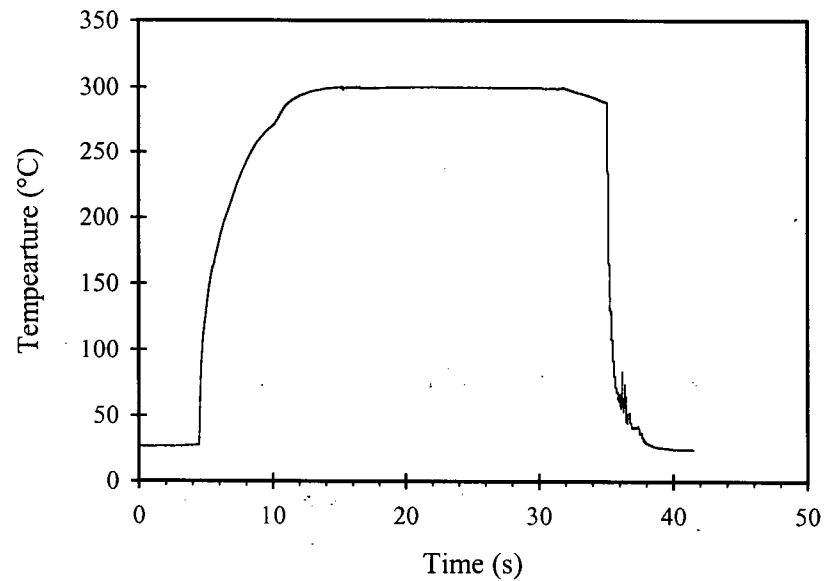


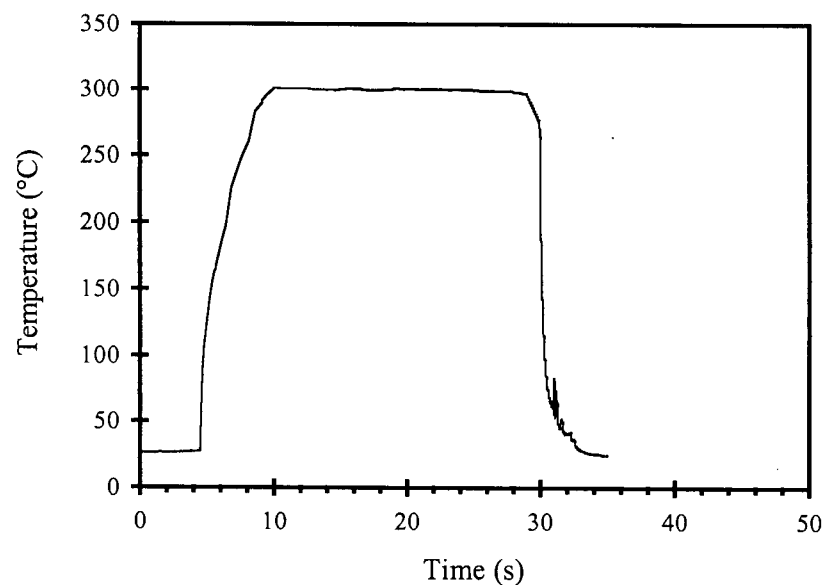
Figure 3.2 – Schematic of a metallography specimen taken from the rolled strip.

The time required to heat a sample to its soak temperature varied with sample thickness and was determined using samples instrumented with thermocouples. To determine the thermal history of the thick samples (40% cold rolled samples or 80% directly cold rolled sample), the instrumented samples were constructed by inserting a thermocouple into the center of a initial hot rolled sample and then cold rolling the sample by approximately 40%. A specimen with dimensions similar to the tensile specimen (Figure 3.3) was cut from the rolled material and immersed into the salt bath at a particular temperature. Figure 3.3 shows the time-temperature plot for the thick sample at salt bath temperature 300°C. As can be seen that the sample took around 12s to reach the soak temperature. Although, the heat-up time varied with the soak temperature, a value of 12s was assumed to be a reasonable heating time for these samples. For the thin samples (80% cold rolled samples from hot rolled material), the thermocouple was

welded to the sample and immersed into the salt bath. The thinner sample took around 10s on average to reach the desired temperature as shown in Figure 3.3.



(a) Thick sample



(b) Thin sample

Figure 3.3 - Heating profile at 300°C for (a) thick sample (80% directly cold rolled sample from as-cast material) and (b) thin sample (80% cold rolled sample from hot rolled material).

3.4 Characterization of Annealed Materials

3.4.1 Tensile Measurements

The softening behaviour of the annealed samples was quantified by measuring the change in the mechanical properties namely the yield strength as a function of annealing time and temperature. Tensile tests were performed using the MTS 8500R tensile machine located at UBC. A schematic of the tensile specimen used during testing is shown in Figure 3.1. A 40mm gauge length extensometer was attached to the tensile sample and used to measure the elongation of the sample during deformation. A constant strain rate of 0.002/s was used for each test. Engineering and true stress strain curves were then developed using the load-elongation data from each test. The yield strength for each sample was derived from the engineering stress-strain curves based on the 0.2% standard proof stress method.

3.4.2 Quantitative Optical Metallography

Optical metallography was done to determine the initial (as deformed) and final (fully recrystallized) microstructure for each of the samples. These microstructures were then compared with those from AA5754, which had been ingot cast. In addition, some quantitative metallography were done to determine the fraction recrystallized in each specimen during a heat treatment cycle so that these results could be compared with the predictions of fraction recrystallization based on mechanical property measurements. Specimens were mounted so that the microstructure in the ND-RD plane could be examined. This was done by cold mounting the specimens in an acrylic resin and then grinding and polishing the samples. The samples were then anodized using a

Barker's solution (Table 3.3). Initial grinding was done with silicon carbide with a grit size starting at 80 and ending at 1200. After grinding, polishing was done using a Buehler Phoenix 4000 automatic polisher with 6 μ m and 1 μ m diamond solutions. Final polishing was done using the 0.05 μ m colloidal silica. Between each polishing step the samples were cleaned using an ultrasonic bath and then washed with soap and rinsed with denatured ethanol. After final polishing, all specimens were anodized using Barker's solution for different times to reveal the microstructure. After anodizing a Nikon EPIPHOT 300 series inverted microscope equipped with a digital camera and cross-polarizer was used to take the pictures of the microstructure. All the pictures were taken at the quarter thickness position for each sample so that a direct comparison could be made between the samples and any differences through the thickness of the sample in terms of grain size could be avoided.

Table 3.3 - Anodizing method used for AA5754.

Material	Anodizing solution	Anodizing condition
AA5754	Barker's reagent: 1.5% HBF ₄ solution (48wt% solution) in distilled water.	Pure Al as anode & specimen as cathode, 30V DC for 1.5-2 mins.

The main purpose of the quantitative optical metallography was to compare the recrystallized grain size of the continuous cast AA5754 to the ingot cast material under different deformation and heat treatment conditions. The grain size was measured according to the ASTM E112-88 standard (Jeffries' method). For this method, grain sizes were calculated from micrographs taken at 355x magnification such that each micrograph contained at least 250 grains. According to the Jeffries method the total

number of grains is considered to consist of the total number of whole grains inside the area of the micrograph plus half of the total number of grains, which intersect with the perimeter of the micrograph. The average area of each grain was then determined by dividing the total area of the micrograph by the total number of grains in the micrograph. The grain size (average diameter of a single grain) was then calculated based on an equivalent area method.

Fraction recrystallized at various stages during annealing was estimated according to the ASTM E562-89 standard point counting method. According to this method, a clear plastic test grid with a regular array of test points was placed on the micrograph. The ratio between the numbers of test points falling within the recrystallized grains and the total number of the plastic grid test points, provided an estimate of the fraction recrystallized. In the present study, 4 micrographs from different locations were taken at approximately 1000x and a square grid of 144 test points was used to find the volume fraction of recrystallized grains for each sample. A minimum of 24 fields was measured (6fields/micrograph) for each sample under investigation.

3.4.3 Resistivity Measurements

Resistivity measurements were done to assess the precipitation of dispersoids during annealing and homogenization treatment of the continuous cast material in the as-cast condition. These measurements were done using a Verimet M4900C conductivity meter. The meter was used under 'COMP' mode (this mode helps to neglect the effect of any temperature changes of the sample during conductivity

measurement); to measure the conductivity of the as-cast material at the quarter line thickness. Resistivity values were then calculated from the measured conductivity values as shown in Appendix B.

The sample size used for this work was around 2"×2" and the thickness of the sample was approx. 7.5mm, so that edge and thickness effects could be avoided. The measurement was made on the TD-CD (CD: casting direction) plane and the measurement was carried out at the quarter thickness of the as-cast material. The same material was then homogenized in a salt-bath at 500°C for 30hrs. During the heat treatment, the conductivity of the sample was measured at different times to determine how the conductivity and hence the resistivity of the sample was changing as a function of the homogenization process. Figure 3.4 shows the resistivity sample used for resistivity measurements.

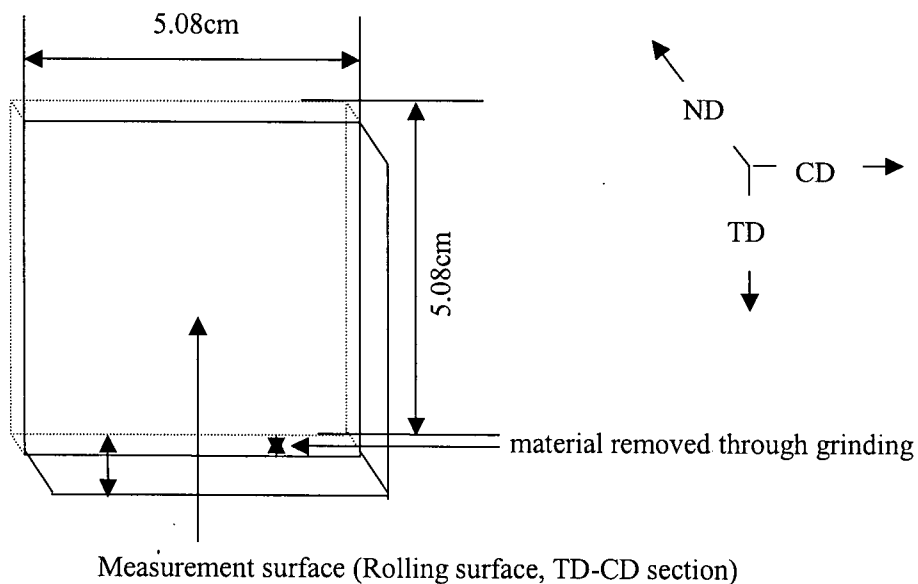


Figure 3.4 – As-cast specimen for resistivity measurement.

3.4.4 Composition of Second-phase particle

Samples were prepared for Scanning Auger Microprobe (SAM) analysis to study the composition of the second phase particles. Samples for this analysis were taken from both ingot and continuous cast cold rolled sheets that had been rolled 80%, with the continuous cast material directly cold rolled after casting. As shown in Figure 3.5 samples were taken with the following typical dimensions: height 3mm, length 10mm and width material thickness. Each sample was then mounted and polished to 1 μ m diamond. Final polishing was done by electropolishing at subzero temperature (-20°C) to preferentially reveal the various particles present in the aluminum matrix. Table 3.4 shows the composition and condition of the electropolishing used for the SAM samples. Similar to the anodizing treatment, pure aluminum was used as the cathode, and the specimens were used as the anode during electropolishing. After electropolishing, the samples were washed in ethanol.

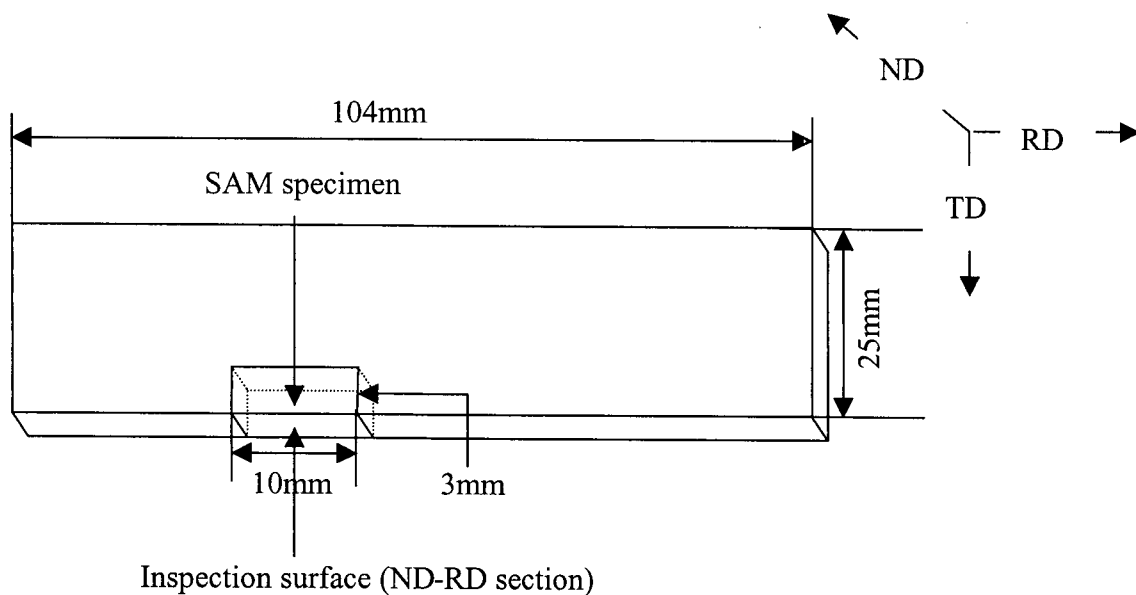


Figure 3.5 – Schematic of a SAM specimen taken from rolled strip.

Initially, Scanning Electron Microscope equipped with Energy Dispersive X-ray Spectrometry (SEM-EDX) was used to study the composition of the second phase particles in the samples. EDX analysis would cover a diameter of 5-7 μ m. In the material, the dispersoid particle size was in the order of one micron; hence EDX analysis would not be able to just analyze the particle composition and would include the matrix composition as well. Hence after polishing, each sample was put into the SAM analysis chamber at a vacuum of approx. 1.5×10^{-9} mbar for Auger analysis. SAM was chosen for the second-phase particle analysis, as it is suitable for surface analysis (surface depth of 5-8nm) with an electron probe diameter less than 20nm. This creates an ideal method to analyze second-phase particles less than 1 μ m typical of dispersoids in aluminum. The composition of various sizes of second-phase particles (ranging from 100nm to 1 μ m) was studied using SAM.

Table 3.4 - Condition for electropolishing of AA5754.

Material	Electrolyte	Base Bath	Electropolishing Condition
AA5754	10gm potassium iodide (KI) + 500ml methanol	Base bath: 1000ml denatured ethanol + liquid nitrogen	Voltage: 20V Current Density: .25A/cm ² Time: 2mins.

3.4.5 Comparative Texture measurements

Texture measurement was done for both ingot and continuous cast material in the fully recrystallized condition for a variety of deformation conditions. All the samples were annealed at 350°C for two hours to ensure full recrystallization. Materials selected for texture analysis were as follows:

- 1) Ingot cast- 40% cold rolled and fully recrystallized.
- 2) Ingot cast- 80% cold rolled and fully recrystallized.
- 3) Continuous cast- 40% cold rolled (from hot rolled material) and fully recrystallized.
- 4) Continuous cast- 80% directly cold rolled (from non-homogenized as-cast material) and fully recrystallized.
- 5) Continuous cast- 80% directly cold rolled (from homogenized as-cast material) and fully recrystallized.

All the materials were cut into small pieces (20mm×15mm) and the samples were polished using silica grinding paper, 6 μ and 1 μ diamond polisher. Figure 3.6 shows a picture of a specimen for texture measurement indicating the surface of texture measurement with respect to RD. Electropolishing was applied to improve the pattern quality for this Al-Mg alloy using the Perryman and Blade method [Girard, 2002] with the samples being electropolished at sub-zero temperatures (-15-20°C). During electropolishing, the sample was used as the anode, whereas pure aluminum strip was used as the cathode. Table 3.5 gives the composition and condition used for electropolishing of samples.

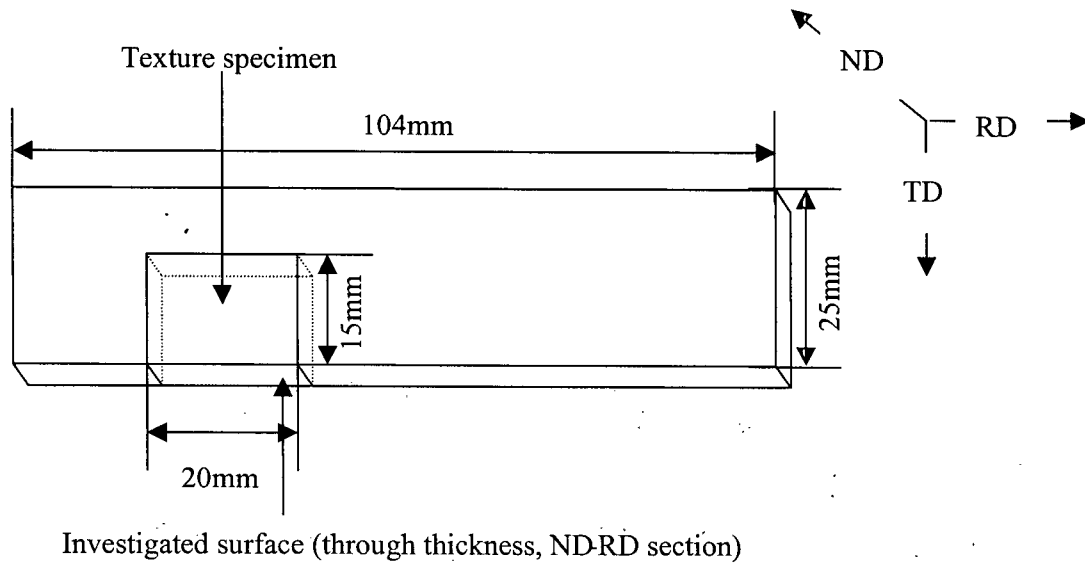


Figure 3.6 – Schematic of texture measurement sample taken from continuous cast material.

Table 3.5 - Condition for electropolishing of AA5754.

Material	Electrolyte	Base Bath	Electropolishing Condition
AA5754	100ml perchloric acid + 500ml ethanol (absolute)	Base bath: 1000ml denatured ethanol + liquid nitrogen	Voltage: 10V Current Density: .2A/cm ² Time: 2-2.30mins.

After electropolishing, each sample was put into a Hitachi made S-570 SEM attached to the EBSD system. Each sample was put into the SEM chamber at a vacuum level of 1.5×10^{-5} milibar and a working distance of 23mm was kept as the default. The tilt angle was maintained at 70° and the accelerating voltage and probe current were 20KV respectively. These values were chosen to maintain a balance between good spatial resolution and the proportion of backscattered electron to absorbed electrons. EBSD software, supplied by HKL technology was used for data acquisition and processing.

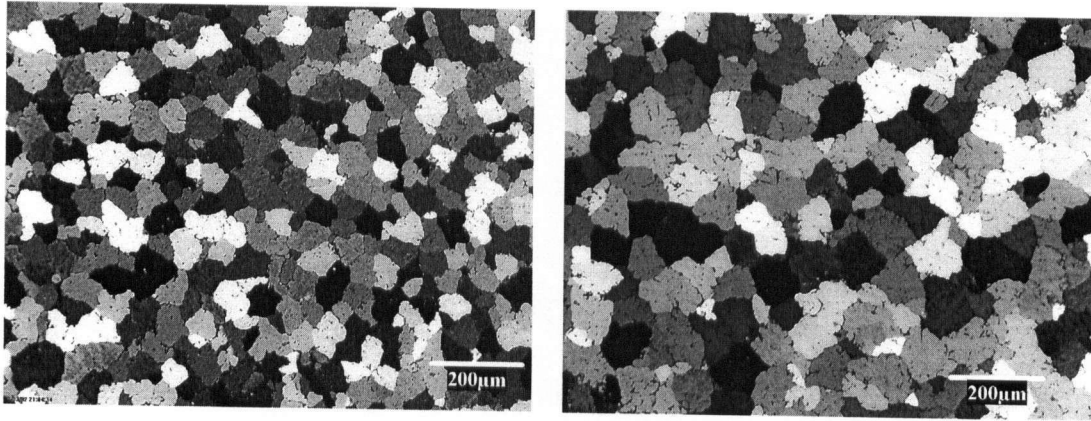
Each sample was taken for at least 7-8 EBSD runs and a total of approx. 200,000 data, at least 7,500 grains, were investigated for the post processing texture analysis. A step size of 2-3 μ m and minimum misorientation angle of 12° between two grains (a value between 10° -15° is generally considered as the misorientation angle between two high angle grain boundaries) was considered for the calculation of grains.

4. Results (Continuous Cast vs. Ingot Cast)

This chapter summarizes the experimental results obtained in this study on continuous cast AA5754 and compares the findings with that of ingot cast AA5754. Starting with the characterization of the initial material, this chapter outlines the measured recovery and recrystallization kinetics of continuous cast cold rolled AA5754 during annealing and the associated microstructure evolution and compares the softening behaviour to similarly cold rolled AA5754 that was produced via ingot casting. Experimental results related to the initial and final mechanical properties of the continuous cast material, recrystallized grain size, and recrystallized textures are also described in this section.

4.1 Initial Material

Characterization of the initial material is necessary for better understanding of the material behaviour during subsequent processing. Continuous as-cast material received from KRDC, Alcan and hot rolled material rolled from as-cast material are the initial materials used for all the experimentation carried out on the continuous cast material. Figure 4.1 shows the grain structure of as-cast material on casting direction-normal direction (CD-ND) section. Throughout the thickness of the as-cast material the grain size is equiaxed as shown in Figure 4.1. However, the average grain size changes significantly from surface to centre, i.e. $50\mu\text{m}$ versus $70\mu\text{m}$. H. N. Azari [Azari et al., 2002] has reported similar microstructural features with finer grains nearer the slab surface in continuous as-cast material.



(a)

(b)

Figures 4.1 – As-cast AA5754 microstructure showing location (a) near the surface and (b) at the centerline.

Hot band produced at KRDC from the as-cast structure was not recrystallized as shown in Figure 4.2. Figure 4.2(a) shows the micrograph of hot rolled material taken at the quarter thickness of \sim ND-RD section. The grains are elongated along the rolling direction with an aspect ratio of \sim 6-7. Heat-treatment of this material at 500°C for 30mins yields a fully recrystallized material with equiaxed grains from the surface to the centre. Figure 4.2(b) shows the quarter thickness micrograph of continuous cast recrystallized hot rolled material. A similar grain structure is observed in the ingot cast hot band. Figure 4.2(c) shows the typical grain structure of ingot cast hot band at the quarter thickness position of a ND-RD section. Both the recrystallized hot band materials exhibited gradual change in grain size from surface to centre; surface grain remains finer compared to centre grains. Table 4.1 provides the average grain sizes measured at the quarter thickness of as-cast, hot rolled continuous and ingot cast materials along with their corresponding yield stresses. As shown, little difference is

observed in the average grain size and yield stress of the fully recrystallized hot rolled material produced by continuous and ingot cast routes.

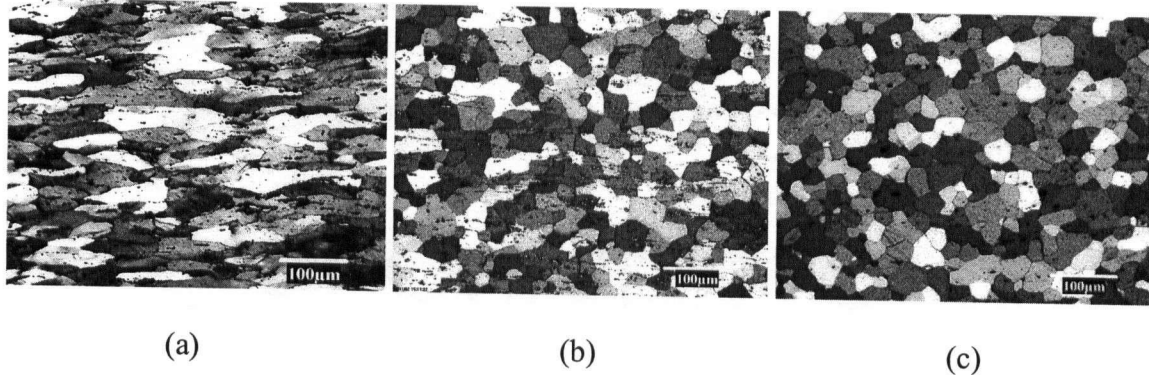


Figure 4.2 – Micrographs of hot band structure showing (a) as hot rolled continuously cast material, (b) continuously cast material hot rolled and then recrystallized at 500°C for 30 minutes and (c) ingot cast material fully recrystallized after hot rolling.

Tables 4.1 - Average grain size and yield stress of continuous and ingot cast AA5754. Error associated with the grain size and yield stress measurement was $\pm 1 \mu\text{m}$ and $\pm 5 \text{MPa}$ respectively.

Characteristics	Continuous cast AA5754			Ingot cast AA5754
	As-cast material	Hot rolled material		Hot rolled material
		Unrecrystallized	Recrystallized	
Grain size (μm)	60	-	29	30
Yield stress (MPa)	-	180	86	90

4.2 Cold Rolled Material

All of the materials examined in this study were cold rolled prior to annealing. The continuous cast materials were cold rolled to 40% and 80% and the softening kinetics were compared with the experimental results measured for the ingot cast

materials. Figure 4.3 shows a typical through thickness micrograph taken at the quarter thickness of 40% and 80% cold rolled continuous cast materials that were deformed from fully recrystallized hot rolled material. As can be seen, Figure 4.3(a) shows mostly elongated grains with some grains being less deformed than others. As expected for a higher cold reduction, Figure 4.3(b) shows heavily deformed grains.

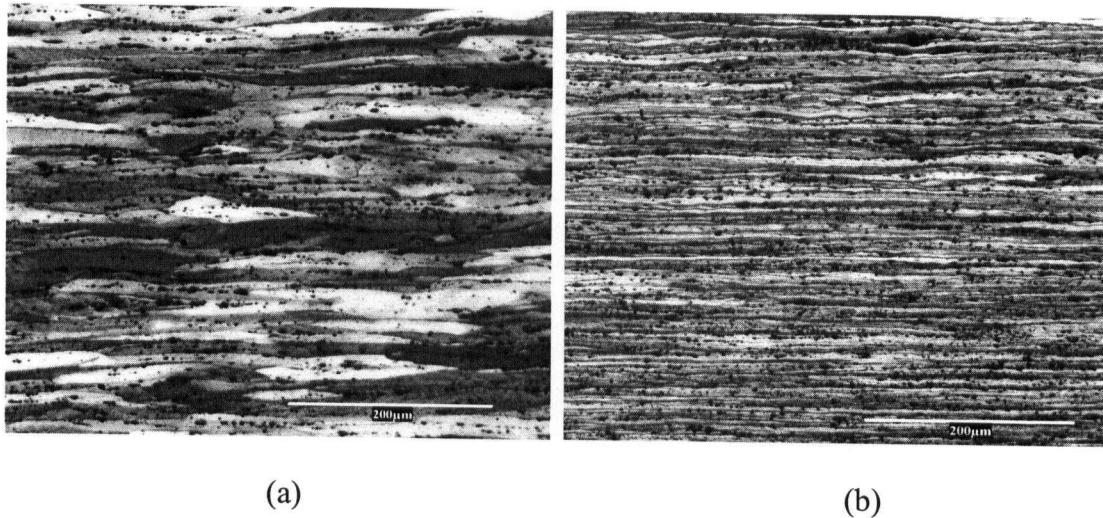


Figure 4.3 – Microstructure at the quarter thickness position for continuously cast material cold rolled from fully recrystallized hot band for (a) 40% cold rolling and (b) 80% cold rolling.

In addition to cold rolling from the hot rolled structure, continuous as-cast material was directly cold rolled by 80% and 90% to study the effect of direct cold rolling on the softening kinetics of the continuous cast material. Table 4.2 gives the comparative as rolled yield stresses for continuous cast material rolled under the different conditions. The as-rolled yield stress of the ingot cast material under different levels of cold reduction is provided for comparative purposes.

Table 4.2 – Average as-rolled yield stress of continuous and ingot cast AA5754. Material mentioned in the first column in bracket is the starting material for cold rolling. Error associated with the yield stress measurement was $\pm 5\text{MPa}$.

Material (starting material)	40% CR (MPa)	60% CR (MPa)	80% CR (MPa)	90% CR (MPa)
Ingot cast (Rx. HR)	288	312	343	-
Continuous cast (Rx. HR)	285	316	335	351
Continuous cast (UnRx. HR)	299	323	357	-
Continuous cast (as-cast)	-	-	352	370

* HR: Hot rolled; CR: Cold rolled; Rx.: Recrystallized; UnRx.: Unrecrystallized.

It is evident from Table 4.2, that the work hardening behaviour is quite similar for both continuous and ingot cast material. As shown, the variation in the as-rolled yield stress is within 5% for the continuous and ingot cast material under the same level of cold reduction. Table 4.2 also indicates that the continuously cast material cold deformed from the unrecrystallized hot rolled material does not significantly change the final as-rolled yield stress.

4.2.1 Recovery at Room Temperature

An interesting result regarding continuous cast material is the observation of room temperature recovery of the cold rolled material. The extent of room temperature recovery was measured for 40% cold rolled and 60% cold rolled continuous cast material. Tensile results were then measured over a period of nine months with the first specimen being measured 30 minutes after cold reduction was completed. Figure 4.4 shows the extent of room temperature recovery of the continuous cast material. As

shown the change in the as-rolled yield stress over the total time period is around 10%. The initial drop in yield stress was quite sharp; whereas the yield stresses measured after 4months and 9months of cold rolling shows little variation. Room temperature recovery has also been observed in other commercial Al-Mg and Al-Mg-Mn alloys [Nes, 1995; Sanders et al., 1989; Cheng et al., 2001].

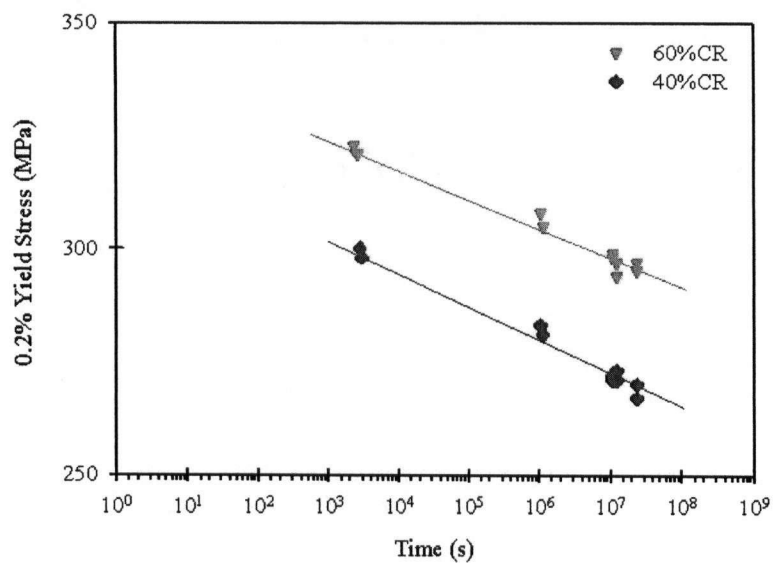


Figure 4.4 - Logarithmic time decay of yield stress at room temperature for continuous cast AA5754.

Similar results for room temperature recovery have been observed for ingot cast AA5754. Table 4.3 enlisted the variation in yield stress measured within 30mins and after around 1 year of cold rolling for ingot cast material for 40%, 60% and 80% cold deformation. Though for each reduction, there is a sharp drop in the as-rolled yield stress, there is no particular trend observed for these results.

Table 4.3 – Room temperature recovery for ingot cast AA5754.

Measuring time after cold rolling	40%CR (MPa)	60%CR (MPa)	80%CR (MPa)
Within 30mins.	288	312	343
After 1 year	245	298	316

4.3 Isothermal Annealing- Mechanical Testing

Isothermal annealing was done to study the recovery and recrystallization kinetics of continuous cast material at various temperatures ranging from 200°C to 375°C. Due to the room temperature recovery behaviour exhibited by the continuous cast materials after cold rolling, all the annealing experiments were done within 10-15 minutes after cold rolling. The annealed specimens were then tensile tested within 10-15 minutes after annealing as well. The results of the recovery and recrystallization kinetics for AA5754 that were produced via continuous casting and ingot casting were then compared.

4.3.1 Comparison of Softening Kinetics

The first part of this section investigates the role of casting process on the annealing behaviour of the material after cold deformation when the starting material for cold reduction was recrystallized hot rolled material. The major difference in the hot rolling practice for the two materials is that the ingot cast material underwent a much larger amount of hot reduction (99.5%) as compared to the continuous cast material (70%). In both materials, the final hot rolled strength is similar as shown in Table 4.1. Figure 4.5 shows the softening kinetics of the continuous cast material as measured by

the change in the yield stress over time at 200°C and 225°C. No recrystallized grains were detected in these materials by optical microscopy even after 2 hours and 30 minutes of annealing at 200°C and 250°C. Therefore the softening of the materials is attributed to the effect of recovery at these temperatures. Figure 4.5 shows that, as expected at higher temperatures, the recovery kinetics are faster, regardless of the amount of cold work experienced by the continuously cast material. Figure 4.6 shows the difference in recovery kinetics between continuous and ingot cast material for 40% cold rolling and 80% cold rolling at 200°C. Considering the as rolled yield stress of continuous and ingot cast materials are the same as shown in Table 4.2, it is clear that the ingot cast material exhibited faster recovery kinetics compared to that of continuous cast material for both 40% and 80% cold rolling.

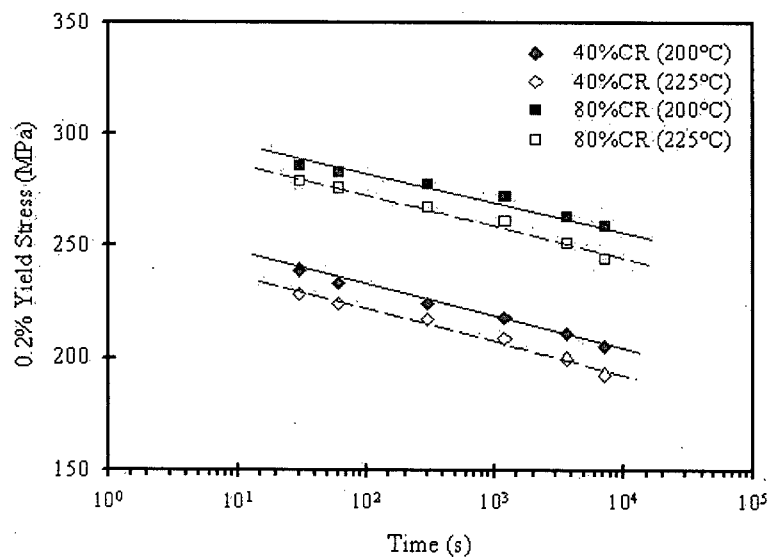


Figure 4.5 - Recovery kinetics for continuous cast AA5754 for two levels of cold rolling (40% and 80%) for material annealed at two different temperatures.

Starting material for cold rolling was recrystallized hot rolled AA5754.

Note: Starting material fully recrystallized hot band.

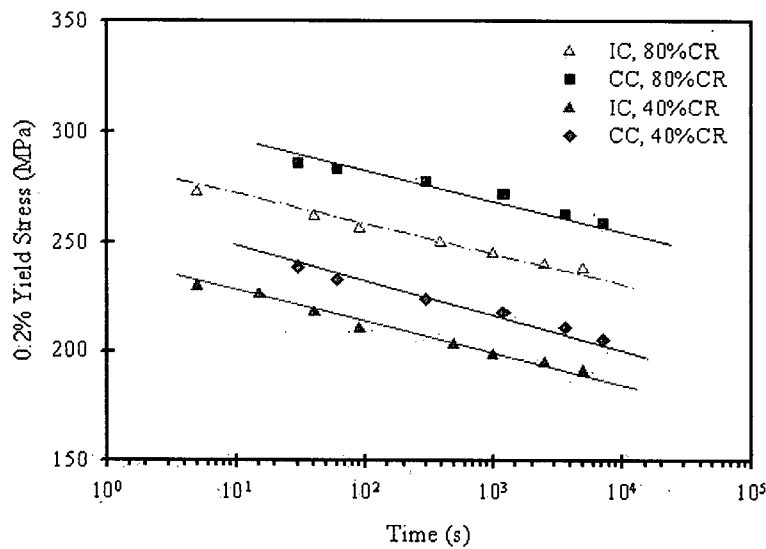


Figure 4.6 - Comparative isothermal recovery kinetics of continuous and ingot cast AA5754 at 200°C for 40% and 80% cold deformation.

Note: Starting material fully recrystallized hot band.

* IC: Ingot cast; CC: Continuous cast

As shown in Figure 4.7, when the isothermal annealing temperature is increased to 275°C, 300°C, 325°C and 375°C a large change in the softening curve can be observed. Optical metallography confirmed that the sharp drop in the yield stress observed at these temperatures was due to the recrystallization process. From the experimental data, it was determined that the recrystallization start yield stress was approximately 227MPa for all the temperatures. A parallel study on 40% cold rolled material revealed that for this level of cold work the recrystallization start yield stress was approximately 173MPa and remained constant regardless of the annealing temperature. Table 4.4 shows the recrystallization start and finish yield stress determined from the experimental results for 40% and 80% cold rolled continuous and ingot cast materials during annealing.

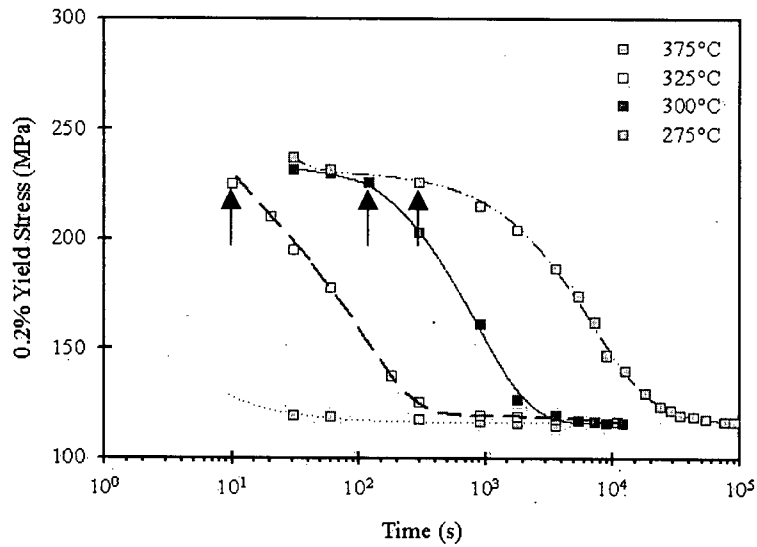


Figure 4.7 - Isothermal softening kinetics of 80% cold rolled continuous cast AA5754. Arrows indicate recrystallization start temperature verified by optical metallography.

Note: Starting material fully recrystallized hot band.

Table 4.4 – The flow stress at which recrystallization was observed to begin and the final recrystallized yield stress for the continuous and ingot cast material with 40% and 80% cold reduction.

Temperature (°C)	Continuous cast material		Ingot cast material	
	40%CR	80%CR	40%CR	80%CR
Rx. start	173	227	170	219
Rx. finish	106	117	94	112

Using the recrystallization begin (fully recovered yield stress) and finish yield stress presented in Table 4.4, the fraction recrystallized could then be estimated based on Equation 4.1. The simple assumption considered here is that the softening due to the recovery is negligible once the recrystallization has started during the annealing process.

$$\text{Fraction Rx.} = \frac{\sigma_{Rc} - \sigma_{\tau}}{\sigma_{Rc} - \sigma_{Rx.}} \quad \text{Eq. (4.1)}$$

Where, σ_{Rc} is the yield stress of the material in the fully recovered state, $\sigma_{Rx.}$ is the yield stress in the fully recrystallized state and σ_{τ} is the yield stress at different time interval of the material during annealing ranging from σ_{Rc} to $\sigma_{Rx.}$

The decrease in the yield stress during annealing as shown in Figure 4.7, and associated with the recrystallization process, can be characterized by the microstructure evolution from a deformed material to a fully recrystallized material. Unlike the process of recovery, the process of nucleation and growth of new grains during recrystallization can be observed using optical metallography. Figure 4.8 shows the microstructure evolution of an 80% cold rolled continuous cast material during annealing at 300°C. All micrographs were taken at high magnification (1000X) and at the quarter thickness of the samples to optically examine the recrystallization process in this alloy.

Fraction recrystallized calculated from experimental softening data was then verified by quantitative metallography at 300°C. Quantification of fraction recrystallization was done using the ASTM E562-89 standard point counting method at the quarter thickness location of each sample at various stages during the annealing experiment at 300°C. As shown in Figure 4.9, recrystallization kinetics obtained using optical metallographic techniques show good agreement with recrystallization kinetics determined using mechanical test data. Comparison between mechanical testing results and quantitative optical metallography data regarding calculation of fraction recrystallization kinetics for

40% cold rolled material and 80% directly cold rolled material are presented in Appendix C.

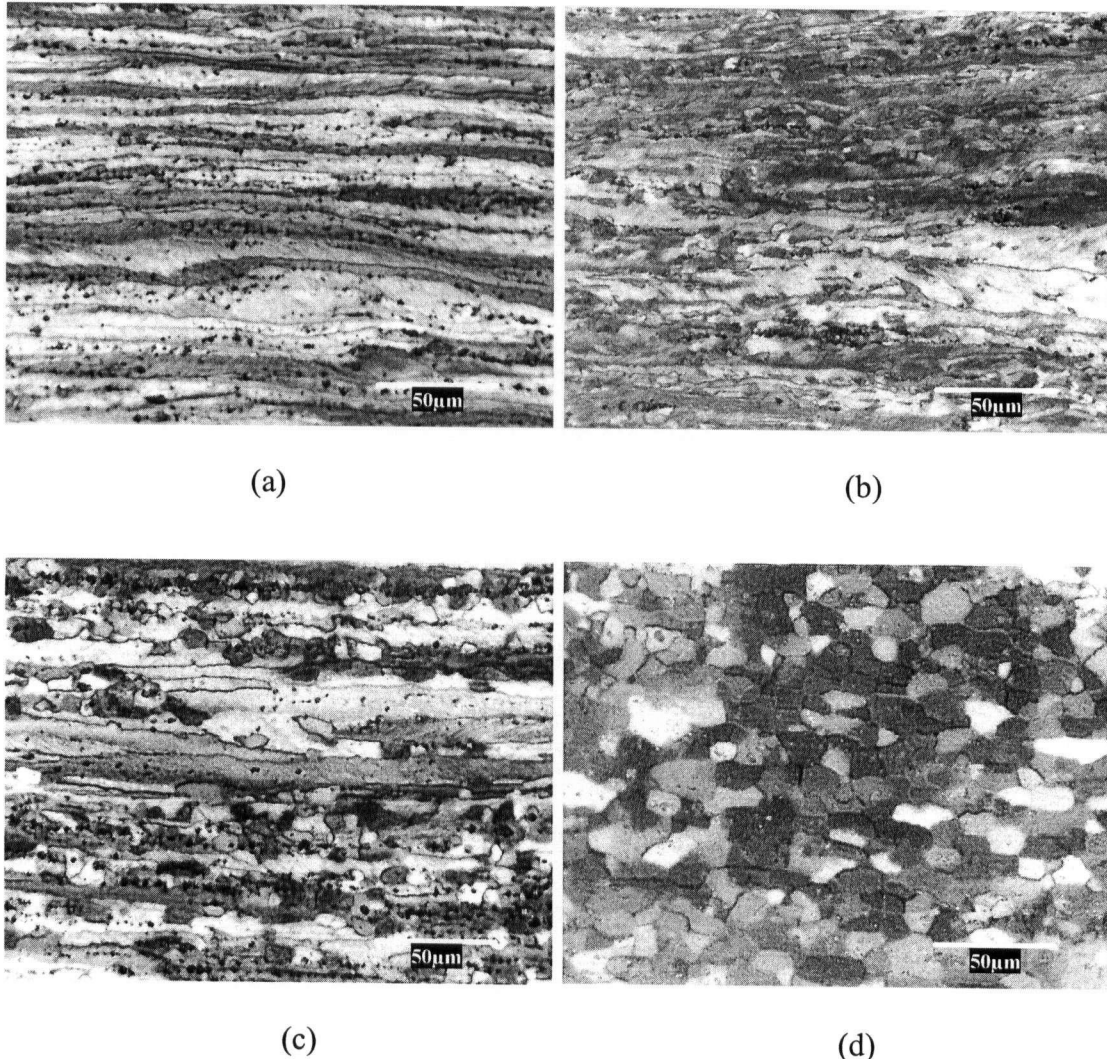


Figure 4.8 - Microstructure evolution of 80% cold rolled continuous cast material (starting material, recrystallized hot rolled material) during annealing at 300°C at various times: (a) 60s, (b) 300s, (c) 900s and (d) 7200s.

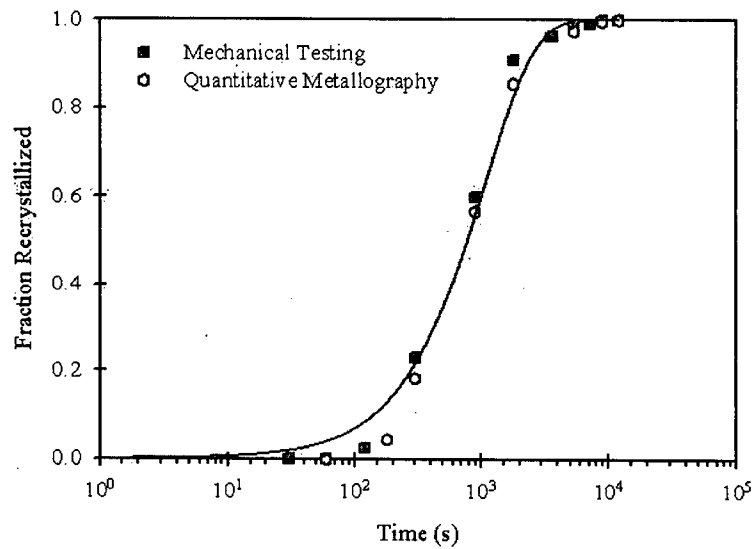


Figure 4.9 - Validation of isothermal recrystallization kinetics for 80% cold rolled continuous cast AA5754 at 300°C derived from mechanical testing by quantitative metallography results.

Note: Starting material fully recrystallized hot band.

Hence, after separating the recovery portion from the softening curve in Figure 4.7, the recrystallization kinetics for different temperature can be calculated as shown in Figure 4.10.

Using a similar procedure as outlined above and shown in Equation 4.1, isothermal recrystallization kinetics for ingot cast material was also derived from experimental data. Comparison of recrystallization kinetics for 80% cold rolled continuous and ingot cast material at 300°C and 325°C are shown in Figure 4.11 (a). As can be seen, the recrystallization kinetics for the continuously cast material are much slower than that of the ingot cast material (i.e. based on the plot the time required to achieve 50% recrystallization ($t_{0.5}$) for continuous and ingot cast material is 800s and 325s,

respectively at 300°C). This trend is consistent at both annealing temperatures, although at higher temperature the difference is slightly reduced (i.e. $t_{0.5}$ for continuous and ingot cast material is 65s and 40s respectively). As the amount of cold deformation is reduced the disparity in the recrystallization kinetics between the ingot and continuous cast material is also reduced. In fact at a cold reduction level of 40% the recrystallization kinetics are much closer at 300°C as shown in Figure 4.11 (b) (i.e. $t_{0.5}$ for continuous cast material is 3000s compared to 2525s for ingot cast material).

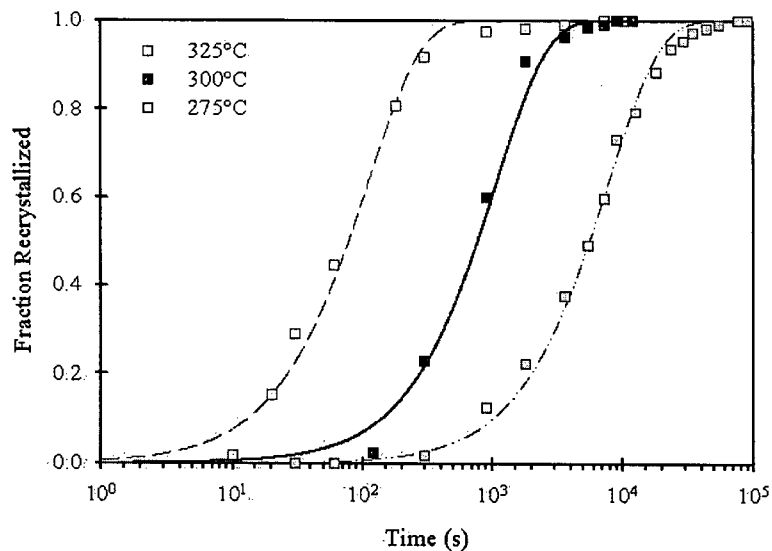
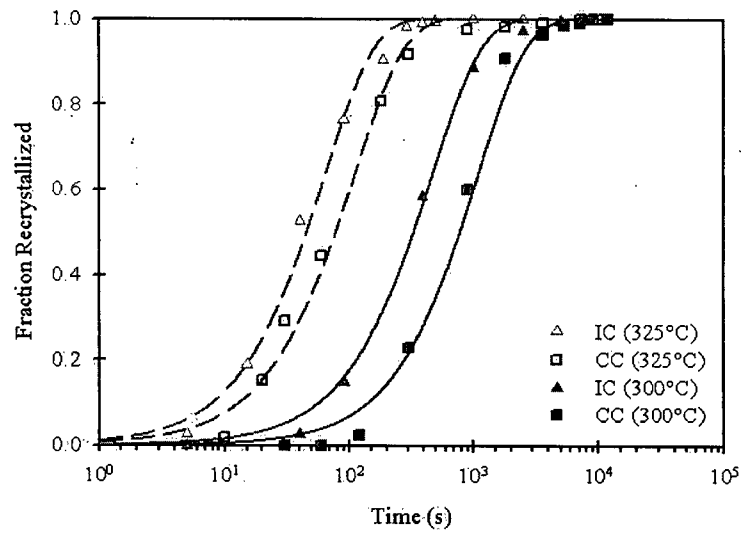
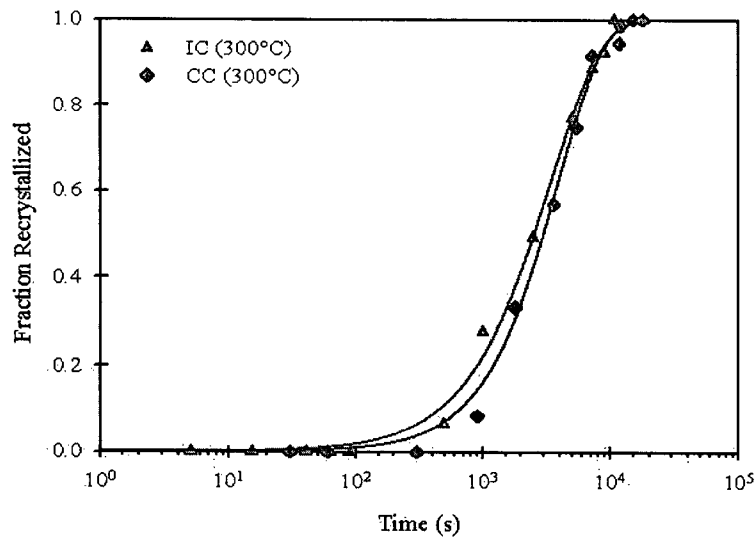


Figure 4.10 - Isothermal recrystallization kinetics of 80% cold rolled continuous cast AA57544.

Note: Starting material fully recrystallized hot band.



(a)



(b)

Figure 4.11 - Comparative isothermal recrystallization kinetics of (a) 80% cold rolled and (b) 40% cold rolled continuous and ingot cast AA5754.

Note: Starting material fully recrystallized hot band.

4.3.1.1 Effect of Direct Cold Rolling

The effect of direct cold reduction of continuous cast material from as-cast structure on the annealing behaviour was quantified. Continuous cast material was directly cold rolled from as-cast material by 80% and 90%. This section outlines the isothermal recovery and recrystallization kinetics of 80% directly cold rolled material and compares these results with the 80% cold rolled ingot and continuous cast material, produced from recrystallized hot rolled material.

As shown in Figure 4.12, the recovery kinetics are the slowest for the directly cold rolled material as compared to the other materials, even though the initial yield stresses are very similar as shown in Table 4.2.

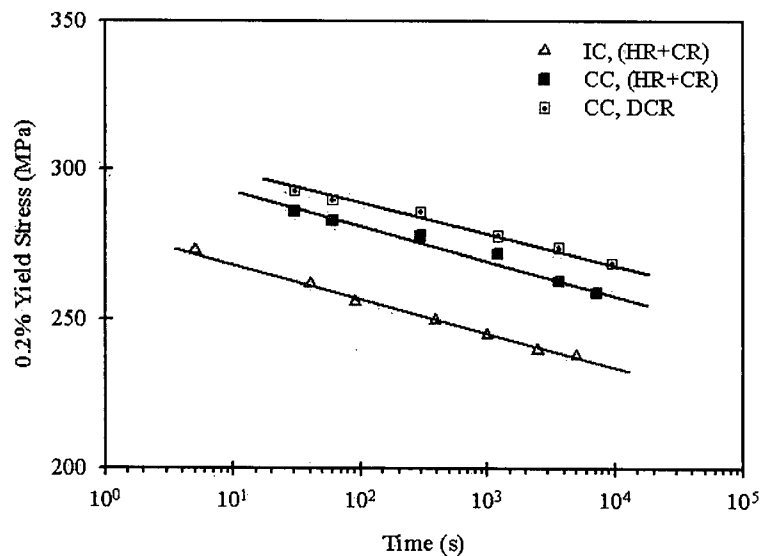


Figure 4.12 - Comparative isothermal recovery kinetics of 80% directly cold rolled (DCR) continuous cast AA5754 (starting material as-cast material) and 80% cold rolled continuous and ingot cast AA5754 (starting material, recrystallized hot rolled material) at 200°C.

As shown in Figure 4.13, a similar trend in recrystallization kinetics was observed when comparing the recrystallization kinetics of directly cold rolled continuous cast material to both ingot and continuous cast material that had undergone a hot rolling operation. Based on the Figure 4.13, the ingot cast material exhibits the fastest recrystallization kinetics compared to the continuous cast material. For example, the time to fifty percent recrystallization for the ingot cast material is approximately 325s, whereas it is approximately 800s and 1875s for the continuous cast material that had been hot rolled followed by cold rolling and directly cold rolled respectively.

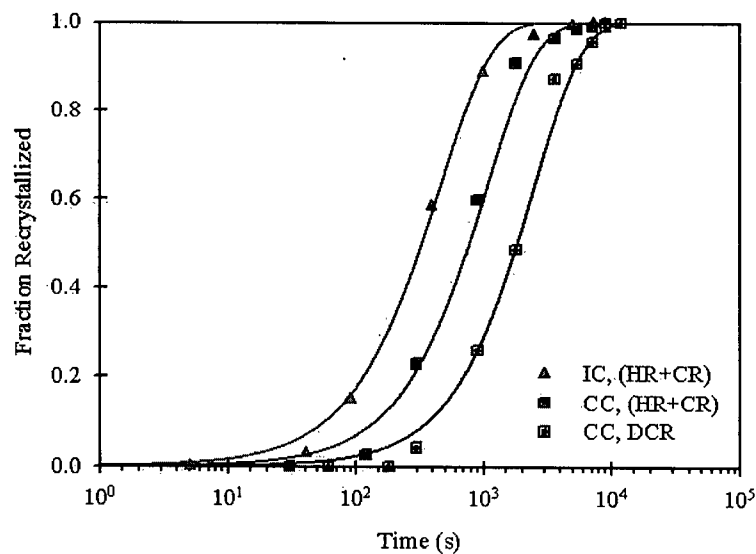


Figure 4.13 - Comparative isothermal recrystallization kinetics of 80% directly cold rolled continuous cast AA5754 (starting material, as-cast material) and 80% cold rolled continuous and ingot cast AA5754 (starting material, recrystallized hot rolled material) at 300°C.

4.4 Characterization of Fully Recrystallized Material

The fully recrystallized materials were studied at the end of the annealing treatment in terms of their mechanical properties, recrystallized grain size and texture.

4.4.1 Mechanical Properties

Table 4.5 shows the mechanical property data for all of the materials studied in the fully recrystallized state after various levels of cold deformation. As can be seen from Table 4.5, the final recrystallized strength increased with increased levels of cold deformation. Starting material (as-cast, unrecrystallized hot rolled and recrystallized hot rolled) has negligible effect on final mechanical property of the continuous cast material. It is clearly observed from Table 4.5 that for same level of cold deformation, the continuous cast material has a higher yield strength than that of ingot cast material, though the variation in final yield stress is within ~10% between the ingot and continuous cast material.

Table 4.5 – Average recrystallized yield stress of continuous and ingot cast AA5754 after various level of cold deformation. Material mentioned in first column in the bracket is the starting material for cold rolling. Error associated with the yield stress measurement was ± 5 MPa.

Material (starting material)	40% CR (MPa)	60% CR (MPa)	80% CR (MPa)	90% CR (MPa)
Ingot cast (Rx. HR)	94	102	112	-
Continuous cast (Rx. HR)	106	111	117	125
Continuous cast (UnRx. HR)	107	112	116	-
Continuous cast (as-cast)	-	-	118	127

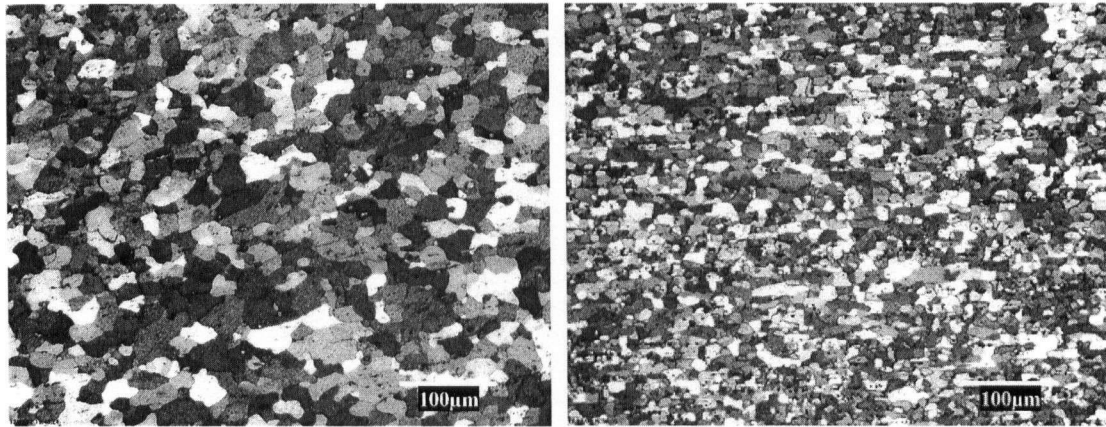
4.4.2 Grain Size Analysis

Recrystallized grain size measurements were done at quarter thickness for all the fully recrystallized materials for various levels of cold reduction according to the ASTM E112-88 standard (Jeffries' method). Figure 4.14 shows the fully recrystallized microstructure of 40% and 80% cold rolled continuous cast material rolled from recrystallized hot band. Figure 4.14 shows the equiaxed grain structure for both materials. The higher cold reduction produces much finer grain structure compared to the lower cold reduction as shown in Table 4.6. Both the materials exhibited gradual transformation from finer grain size near to surface to coarser grain size close to centre. The average grain size from surface to centre ranges from approximately 12 μm to 25 μm for recrystallized 40% cold rolled continuous cast material. Observations made in the current study are in good agreement with previous studies on ingot and continuous cast AA5754, which revealed that increasing cold deformation produces finer and more homogeneous recrystallized grain structure [Girard, 2002; Go, 2001].

Material which was directly cold rolled from as-cast material produced a finer average grain size after annealing as compared to continuous cast material, which had been rolled from recrystallized hot band as shown in Figure 4.15.

When comparing the recrystallized grain size of the continuous cast material to the ingot cast material for a given level of cold work, the ingot cast material exhibited a larger average grain size. Based on a visual inspection, it was observed that the recrystallized ingot cast materials exhibited a more equiaxed grain structure as compared to the

continuous cast material for any level of deformation. It can be seen from Figure 4.14 and Figure 4.15 that although most of the recrystallized grains in the continuous cast material are equiaxed in nature, some grains seem to be elongated to the rolling direction.

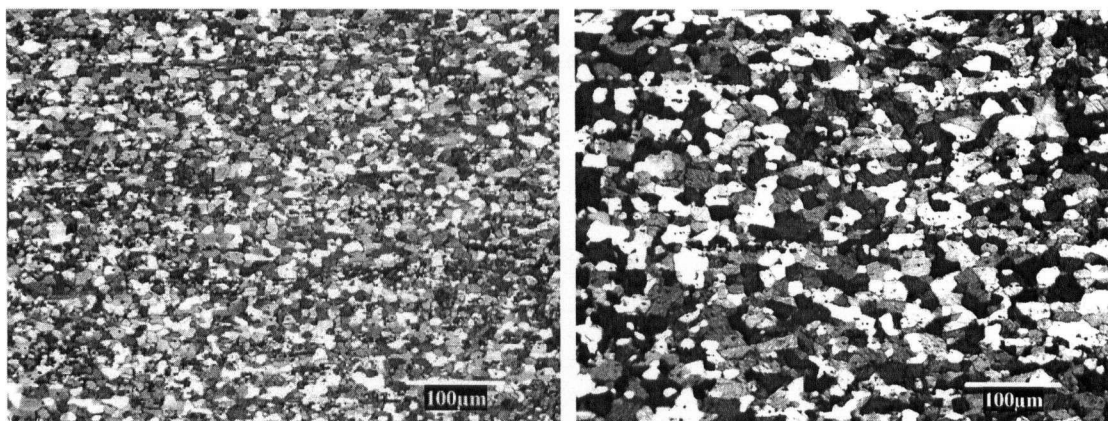


(a)

(b)

Figure 4.14 - Microstructure of (a) recrystallized 40% cold rolled and (b) recrystallized 80% cold rolled continuous cast AA5754.

Note: Starting material fully recrystallized hot band.



(a)

(b)

Figure 4.15 - Microstructure of (a) recrystallized 80% directly cold rolled continuous cast and (b) recrystallized 80% cold rolled ingot cast AA5754.

Table 4.6 gives the calculated average grain size at the quarter thickness location for recrystallized continuous and ingot cast materials at different levels of cold deformation.

Table 4.6 - Average grain size of recrystallized continuous and ingot cast AA5754. Material mentioned in the first column in bracket is the starting material for cold rolling. Error associated with the grain size measurement was $\pm 1 \mu\text{m}$.

Start Material Prior to Cold Work	Rx. 40% CR (μm)	Rx. 60% CR (μm)	Rx. 80% CR (μm)	Rx. 90% CR (μm)
Ingot cast (Rx. HR)	30.0	22.0	14.0	-
Continuous cast (Rx. HR)	19.5	16.0	11.5	-
Continuous cast (UnRx. HR)	18.0	15.0	12.0	-
Continuous cast (As-cast)	-	-	9.5	8.5

The final strength of the continuous and ingot cast AA5754 depends on the level of cold work, solution hardening by Mg atoms and final grain size of the material [Burger et al., 1995]. The relationship between the yield strength and recrystallized grain size was plotted as shown in Figure 4.16 and found to follow the Hall-Petch relationship given in Eq. 4.2, for AA5754 developed by Alcan [Burger et al., 1995].

$$\sigma_Y = \sigma_o + KD^{-1/2}, \quad \text{Eq. (4.2).}$$

where, σ_y is the yield stress (MPa), σ_o is the frictional stress (MPa) and D is the average grain size (m) and K is constant.

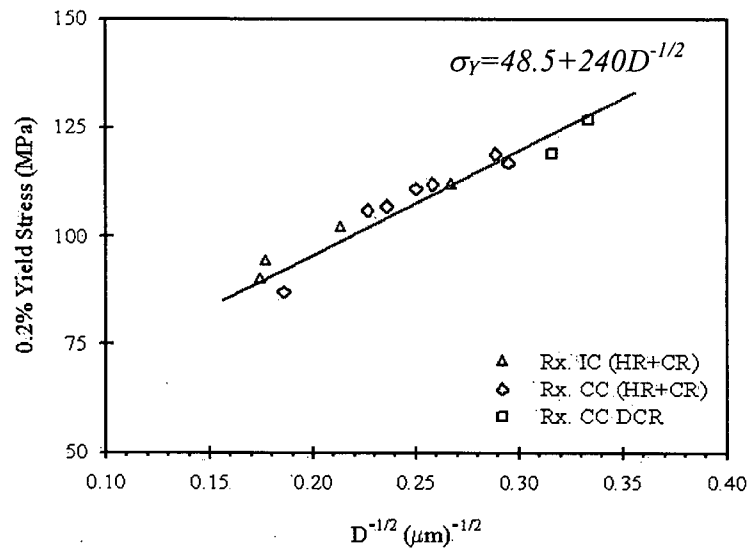


Figure 4.16 - Graph shows the relation between yield stresses vs. recrystallized grain size based on Hall-Petch Equation. The trend-line based on Alcan values for Frictional Stress (σ_0) and Hall-Petch constant (k) shows a good match with the experimental data.

4.4.3 Texture Analysis

The recrystallized continuous cast materials were subjected to micro-texture analysis and the results were compared with that of recrystallized ingot cast materials. For the analysis, the volume fraction of each texture component was calculated based on the area fraction derived by the 'HKL' software analysis. For the analysis, a component with up to a variation of 15° away from the ideal texture orientation was considered to be the ideal orientation. The texture results from this analysis can be used in terms of: 1) volume fractions, 2) texture component maps and 3) ODF's (orientation distribution functions).

Figure 4.17 shows the texture component map for the recrystallized 40% cold rolled continuous and ingot cast material. The corresponding ODFs' are shown in Figure 4.18. Based on the results presented in the Figure 4.17, it can be observed that both materials exhibit predominantly random texture. But, a closer inspection of Figure 4.18 indicates that the continuous cast material exhibited a slightly higher area fraction of the rolling texture components (Brass, Copper, S) compared to the ingot cast material. In addition, the cube texture component is stronger in the ingot cast material as compared to the continuous cast material. This observation is confirmed in Table 4.7, which shows the calculated volume fraction for each texture component shown in Figure 4.17 for continuous and ingot cast materials.

When direct cold rolling is applied to the continuous cast material, a lower volume of rolling texture components was found, as can be seen in the Figure 4.19. Figure 4.20 shows the corresponding ODF for the continuous and ingot cast material that was cold rolled 80% prior to annealing treatment. Texture analysis on the recrystallized 80% cold rolled ingot cast material produced quite similar recrystallized texture as was observed for the recrystallized 40% cold rolled ingot cast material. Close examination of Figures 4.18 and Figure 4.20, shows that a higher cold reduction resulted in the more random recrystallized texture for both continuous and ingot cast materials. Similar results have been reported by Azari [Azari et al., 2002] for continuous cast AA5754. Table 4.7 shows the volume fraction of texture components derived from texture analysis for recrystallized continuous and ingot cast for various amount of initial cold deformation.

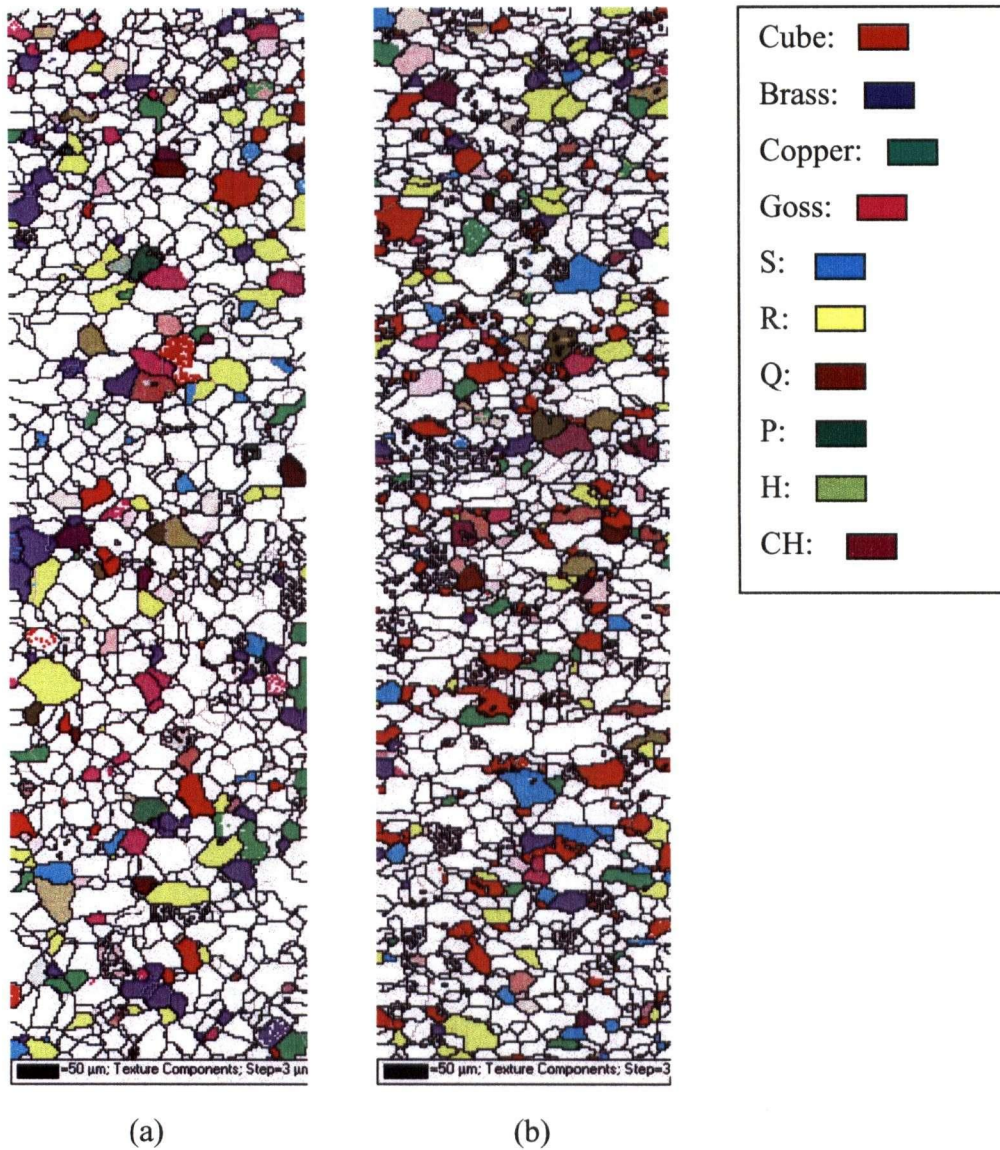
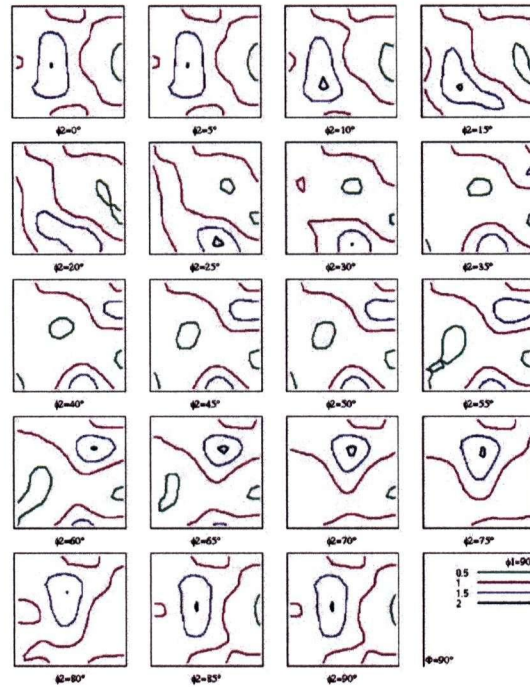
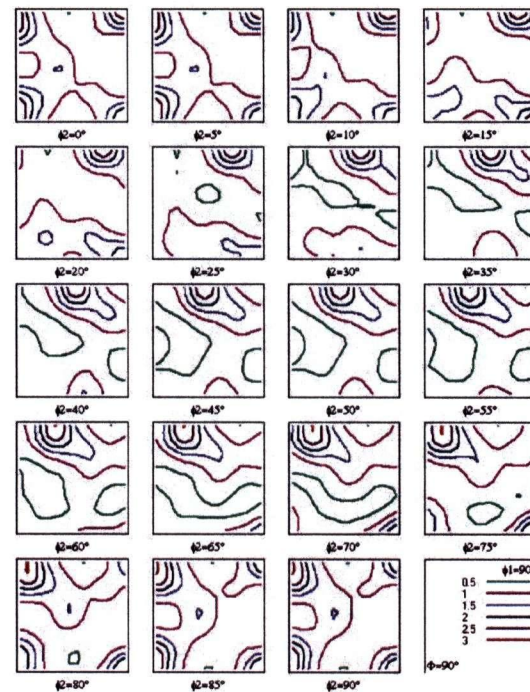


Figure 4.17 - Texture component map of (a) recrystallized 40% cold rolled continuous cast and (b) recrystallized 40% cold rolled ingot cast AA5754. Texture components are shown in different colours.



(a)



(b)

Figure 4.18 - Orientation Distribution Function (ODF) of (a) recrystallized 40% cold rolled continuous cast AA5754 and (b) recrystallized 40% cold rolled ingot cast AA5754.

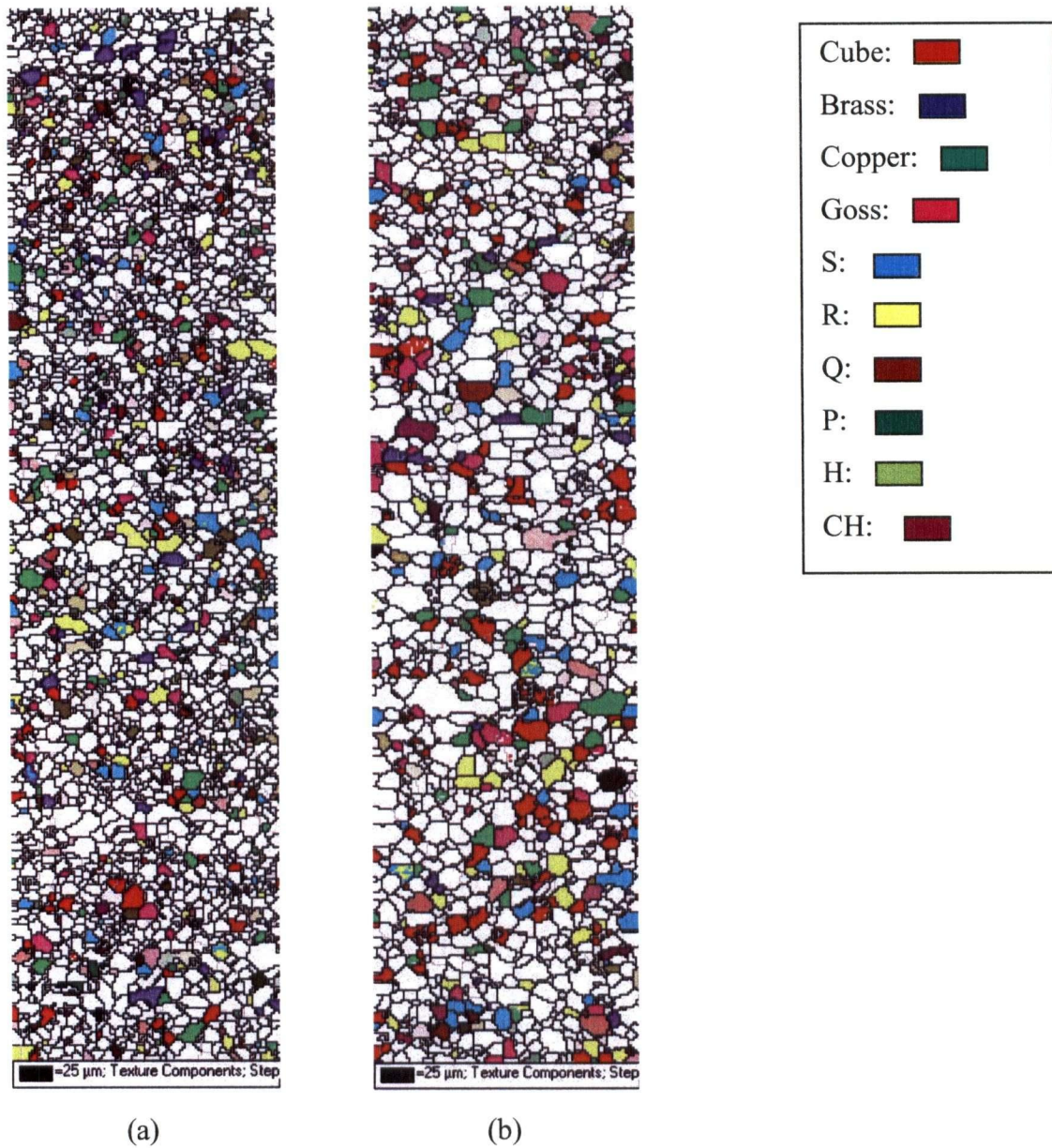
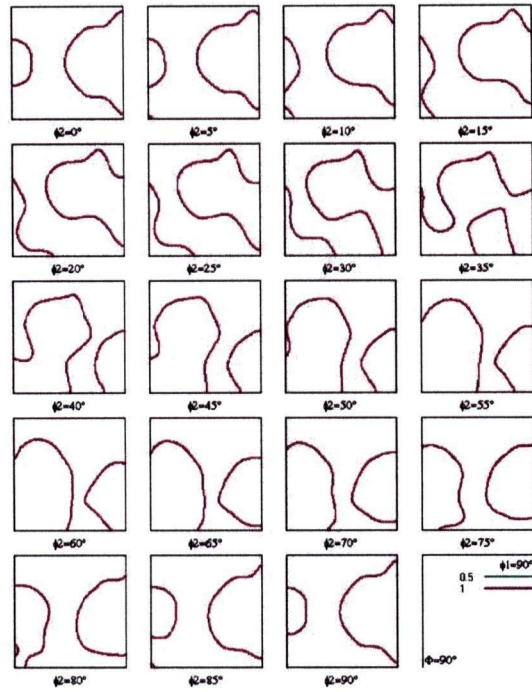
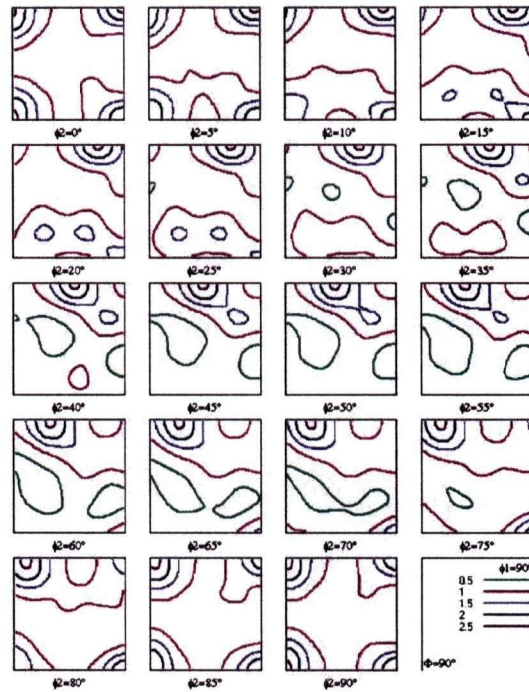


Figure 4.19 - Texture component map of (a) recrystallized 80% directly cold rolled continuous cast AA5754 and (b) recrystallized 80% cold rolled ingot cast AA5754.

Texture components are shown in different colours.



(a)



(b)

Figure 4.20 - Orientation Distribution Function (ODF) of (a) recrystallized 80% directly cold rolled continuous cast AA5754 and (b) recrystallized 80% cold rolled ingot cast AA5754.

Table 4.7 - Measured volume fraction of texture components (in %) for both the ingot cast and continuous cast AA5754 after 40% and 80% cold deformation and annealing at 325°C using an EBSD system.

Texture Component	CC material (Rx. 40%CR)	IC material (Rx. 40%CR)	CC material (Rx. 80%DCR)	IC material (Rx. 80%CR)
Cube	2.7	7.1	3	6.6
B	4.8	3.1	2.9	1.8
Cu	3.5	3.1	3	4
G	2.0	1.4	2.2	1.8
S	3.2	4.1	3	4.2
R	5.1	4.0	3.6	3.9
P	1.5	1.9	1.4	2.4
Q	2.4	2.8	2.7	2.9
H	1.9	1	2.7	1.7
CH	2.8	2.2	3.5	2.8

** C: Cube; B: Brass; Cu: Copper; G: Goss; R: Retained rolling..*

** Miller indices and Euler angles of each texture component is given in appendix A.*

4.5 Summary

Based on the results presented above, the softening kinetics of continuous and ingot cast materials are quite different during an annealing operation; even though both materials exhibited similar work hardening behaviour, i.e. a similar as-rolled yield strength. The difference in recrystallization kinetics between continuous and ingot cast material increases as the level of cold work in the material increases. The kinetics of the recrystallization process are dictated by nucleation and growth of strain free grains in the matrix hence one or both of these phenomena must be slower in the continuous cast

material. Since the continuous cast material exhibited finer recrystallized grain size after annealing, implying a higher number of nucleation sites relative to the ingot cast material, the difference in the kinetics is probably related to the growth rates of the recrystallized nuclei in these two materials.

Based on the microstructural observation presented above, the final recrystallized microstructures exhibited some differences between the continuous and ingot cast AA5754. Most obvious was the finer recrystallized grain size exhibited by the continuous cast material as compared to the ingot cast material. In terms of the grain structure it did not appear to be as homogeneous as the ingot cast material. Although both materials exhibited a random texture overall, the ingot cast material appeared to have almost three times more cube texture than the continuous cast material. This result was consistent for material which had been rolled at different levels of cold work as well as for the continuous cast material which was directly cold rolled after casting. Similar trend on recrystallized texture for continuous and ingot cast AA5182 and AA5052 has been reported by Slámová [Slámová et al., 2003].

5. Effect of Homogenization – Results and Discussion

As shown in the Chapter 4, material processing has a significant influence on the softening kinetics and final recrystallized microstructure in terms of the grain size and texture for continuous and ingot cast AA5754. To understand the reason for these differences in microstructure evolution during annealing of the cold rolled material, it is necessary to examine the differences in processing history experienced during each route. Aside from the as-cast microstructure, one of the main differences between ingot cast and continuous cast sheet material is the homogenization heat treatment, which is performed on the ingot cast material after casting but prior to hot rolling. In this process, the as-cast ingot is heated to $\sim 550^{\circ}\text{C}$ and held. The total time for this process is around 24-26 hours, which includes both the time to heat the ingot to temperature as well as the soak time. In contrast, the continuous cast material was taken directly for hot or cold reduction without any prior heat treatment or homogenization after casting. The main purpose of the homogenization treatment is to remove microsegregation in the as-cast material as well as preheat the material to the hot rolling temperature. During the homogenization process some of the microstructure changes which will occur in the as-cast structure include: coarsening and dissolution of the constituent particles, precipitation of dispersoids and a reduction of the solute in solid solution [Kyang et al., 1977]. Each of these can potentially affect the recovery and recrystallization behaviour of the material after cold rolling as well as the formability and final texture of the material. Therefore, the effect of the homogenization treatment on the continuous cast material was studied.

5.1 Changes in Resistivity

To understand the influence of a homogenization stage on the continuous cast material, as-cast continuous cast material was heat treated at 500°C and 530° for up to 30 hours. As outlined in the Chapter 3, resistivity values were calculated at different time intervals during the entire heat treatment cycle. Figure 5.1 shows the change in resistivity of the as-cast material over time during the heat treatment used to simulate a typical homogenization treatment.

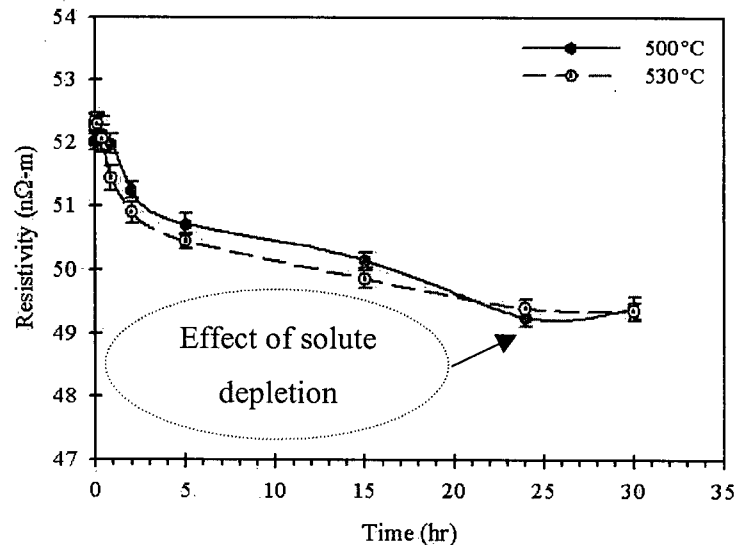


Figure 5.1 - Change in resistivity value of as-cast continuous cast AA5754 during homogenization at 500°C and 530°C for 30hrs.

As shown in Figure 5.1, there is a large change in the resistivity of the as-cast material after the heat treatment process is complete. The large change in resistivity value before and after the heat treatment can be attributed to solute depletion in the material as fine precipitates; as the solute level is reduced in the material, the resistivity decreases. Change in solute concentration results in changes in the electron scattering within the

material, which in turn changes the resistivity of the material based on Matthiessen's law as shown in Eq. 5.1 [Dugdale, 1977]:

$$\rho = \rho(T) + \sum \alpha C_i \quad \text{Eq. (5.1)}$$

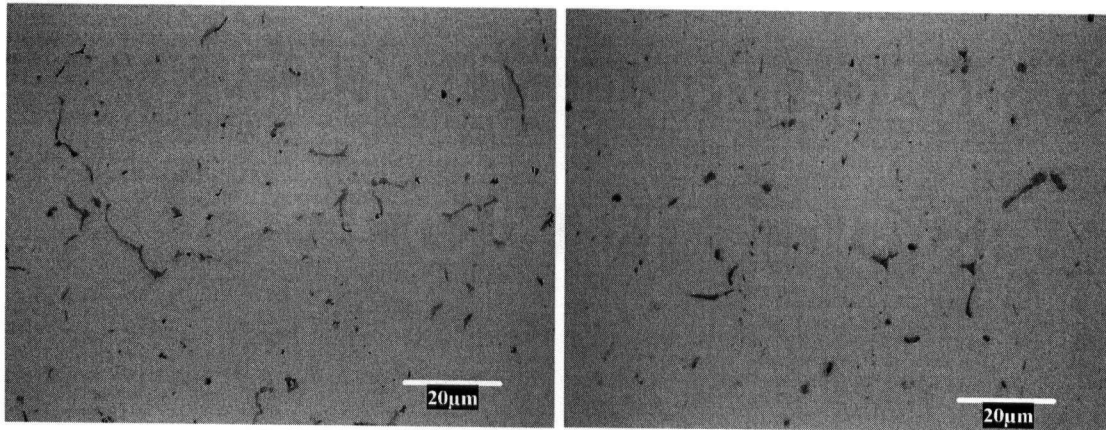
where ρ is the measured resistivity, $\rho(T)$ is the intrinsic resistivity (electron scattering by phonons) at that temperature, C_i is the concentration of solute and α is the Matthiessen's constant (specific resistivity), which depends on the alloying elements and the host material.

As can be seen in Figure 5.1, the resistivity value does not change appreciably after 24 hours and indicates that further time at this temperature does not significantly change the measured resistivity. It can also be observed that an increase in the homogenization temperature to 530°C accelerates the resistivity decrease, but the final resistivity value remains the same. As a result the heat treatment applied to the continuous as-cast material to simulate the homogenization process was 500°C for 24 hours.

5.2 Homogenized As-cast Material

The grain structure of the homogenized continuous as-cast material was studied and compared with the non-homogenized as-cast structure. The as-cast material before and after homogenization shows a similar microstructure in terms of the equiaxed grain structure with the grains being finer at the surface as shown in Figure 4.1 for the non-homogenized continuous as-cast material. The average grain size measured at quarter thickness of homogenized as-cast material is 64µm, which is close to the average grain size of non-homogenized as-cast material mentioned in Table 4.1. Figure 5.2 shows the

microstructure of these materials in the unetched condition showing second-phase particles. Very little change in the particle distribution after homogenization could be observed based on visual inspection.



(a)

(b)

Figure 5.2 - Microstructure of the continuous as-cast AA5754 in the unetched condition (a) before homogenization and (b) after homogenization.

5.3 Characterization of Cold Rolled Material

The homogenized as-cast material was directly cold rolled 80% so that a comparison to the 80% directly cold rolled material without a homogenization treatment prior to cold rolling could be made. Table 5.1 shows a comparison of some of the microstructure features of the homogenized and nonhomogenized material in terms of microstructure and mechanical properties. As can be seen both the as-cast grain size and yield strength after cold rolling are very similar.

Table 5.1 - Comparative as-cast grain size along with as-rolled yield stress (80% cold rolled) for continuous cast AA5754 before and after homogenization. Error associated with the grain size and yield stress measurement was $\pm 1 \mu\text{m}$ and $\pm 5 \text{Mpa}$ respectively.

Material	Average Grain Size (μm)	As-rolled Yield Stress (MPa)
Non-homogenized	60	352
Homogenized	64	343

5.3.1 Second-Phase Particles Distribution

Commercial AA5754 contains a large number of second-phase particles. Composition of the second-phase particles was studied for the ingot and continuous cast material using a Scanning Auger Microprobe (SAM). Deep etching on the RD-ND section reveals pits on the surface (due to over etching in some places) with large constituent particles and fine dispersoids between them (Figure 5.3). Qualitatively, little difference was observed between the 80% cold rolled ingot cast material and 80% directly cold rolled continuous cast material rolled from homogenized as-cast material in terms of the morphology of the second-phase particle distribution, which ranged in size from 100nm to 5 μm .

Larger particles with a size of approximately 750nm to 5 μm show the presence of Al, Fe and Mn, which is in good agreement with the composition of constituent particles [Al₆(Fe, Mn) or Al₃Fe] mentioned by some authors for Al-Mg-Mn alloys [Chen et al., 1989; Sanders et al., 1986, Karlík et al., 2002]. Some of the constituent particles were observed to be broken and present in clusters along the rolling direction. Figure 5.4 shows the SAM result on a big constituent particle present in 80% directly cold rolled

continuous cast material with a homogenization heat treatment. Most particles below 500nm in size, show the presence of Al, Mn, Fe, which is again in good agreement with the composition of fine dispersoids $[Al_6(Fe, Mn)]$ reported by R. K. Bolingbroke [Bolingbroke et al., 1992, Liu et al., 1998; Karlík et al., 2002]. Some particles around 800nm in size showed a weak signal of Mg and Si and can be considered as Mg_2Si particles (Figure 5.5).

Based on the results obtained from a qualitative SAM study of continuous and ingot cast material, both materials reveal little difference in the composition of the constituent and dispersoid particles. However a difference in size of both the constituent and dispersoid particles was observed with the size of the constituents ranging from 750nm to 5 μ m, where-as the size of dispersoids vary from 100nm to 500/600nm. Compositions are similar for both kinds of particles.

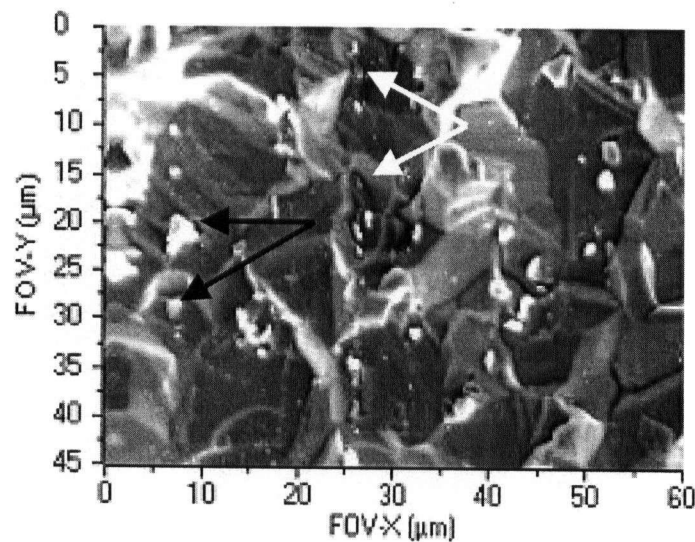


Figure 5.3 - Presence of big constituents (black arrows) and finer dispersoids (white arrows) in 80% direct cold rolled continuous cast material from homogenized as-cast AA5754.

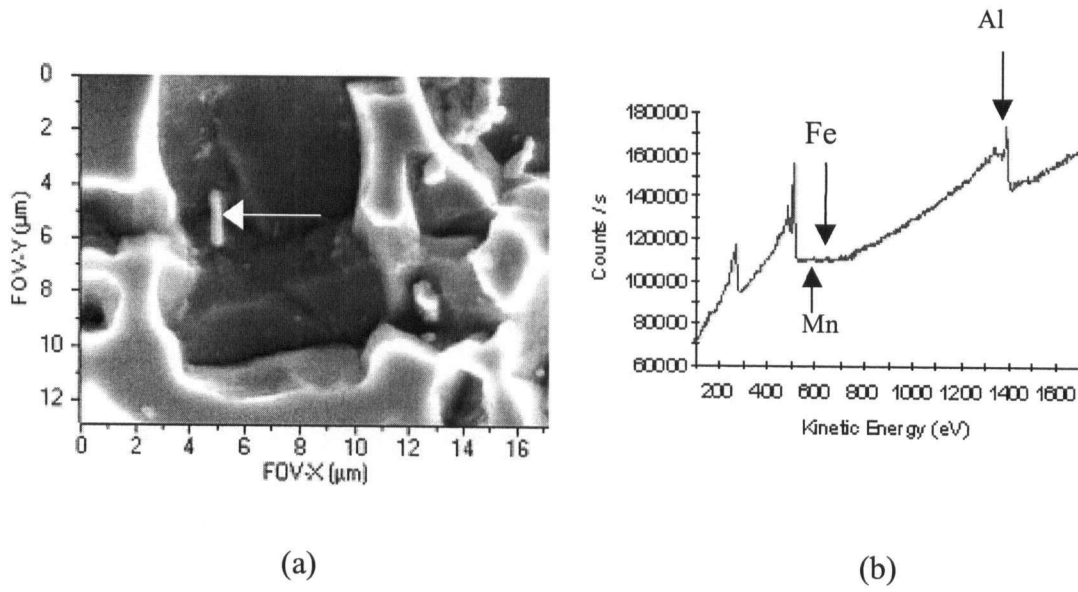


Figure 5.4 - (a) Constituents present (showed in white arrow) in homogenized 80% direct cold rolled continuous as-cast material, (b) corresponding SAM result reveals the presence of Fe, Mn and Al. Big spikes for kinetic energy present around 275ev and 500ev are for carbon and oxygen, which are always there as impurity signals.

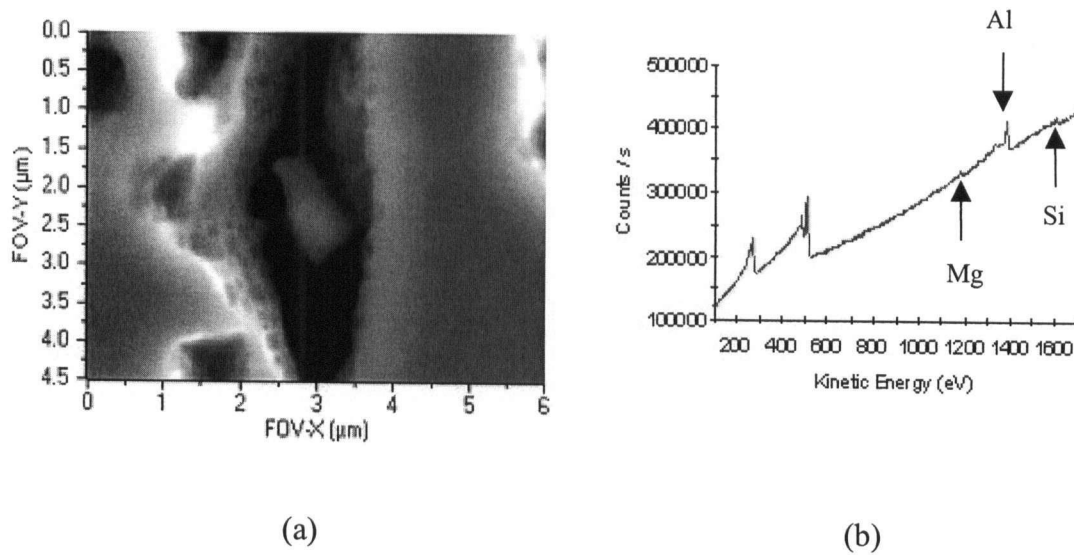


Figure 5.5 - (a) Particle from 80% direct cold rolled continuous cast non-homogenized material, (b) SAM result reveals the presence of Mg, Si signal, except Al . Again the two big spikes at around 275ev and 500ev are for carbon and oxygen, which are always present as impurities.

5.4 Isothermal Annealing

Isothermal annealing was done to the 80% directly cold rolled material to study the recovery and recrystallization kinetics of homogenized continuous cast material at 200°C and 300°C respectively. The effect of the homogenization treatment on recovery and recrystallization kinetics of continuous cast material was then compared with the recovery and recrystallization results presented in the previous chapter for 80% cold rolled continuous and ingot cast AA5754.

5.4.1 Comparative Recovery Kinetics

Figure 5.6 shows the comparative isothermal recovery kinetics at 200°C of 80% directly cold rolled continuous cast material both with and without a homogenisation heat treatment. As can be seen, even though the as-rolled yield strength is quite similar for both materials, the homogenized continuous cast material exhibits faster recovery behaviour compared to the non-homogenized continuous cast material.

Figure 5.7 compares these results with the previous results from the study and shows that the continuous cast material, which was homogenized and then cold rolled is the closest to the ingot cast material in terms of the recovery kinetics. The graph also indicates that the continuous cast material, which was hot rolled followed by cold rolling has the next fastest kinetics followed by the continuous cast material that was directly cold rolled without any pre-heat treatment.

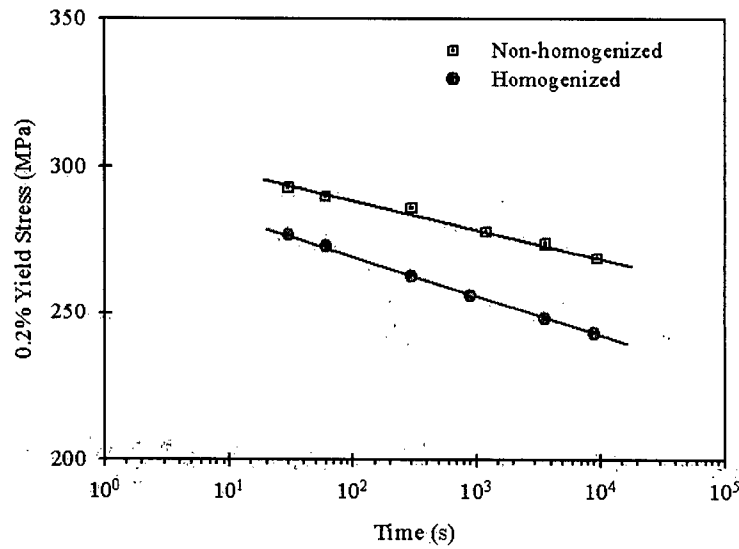


Figure 5.6 - Isothermal recovery kinetics for 80% directly cold rolled continuous cast AA5754 annealed at 200°C.

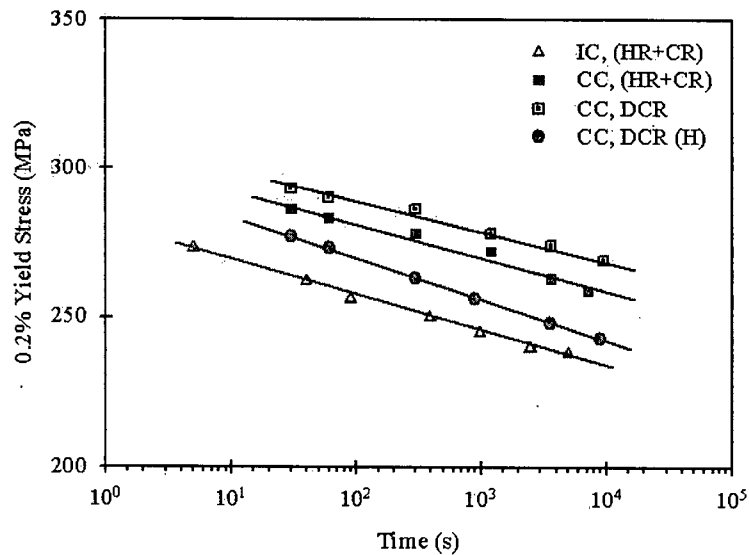


Figure 5.7 - Comparative isothermal recovery kinetics of 80% direct cold rolled continuous cast AA5754 (starting material, homogenized as-cast material), 80% directly cold rolled AA5754 (starting material, non-homogenized as-cast material) and 80% cold rolled continuous and ingot cast AA5754 (starting material, recrystallized hot rolled material) at 200°C.

5.4.2 Comparative Recrystallization Kinetics

As shown in Figure 5.8, similar to the recovery process, the recrystallization kinetics of the continuous cast material, which had been homogenized, was much faster than the material that had not been homogenized. Solute depletion during homogenization as fine dispersoids and hence the microstructural changes after homogenization results in faster recrystallization kinetics for 80% directly cold rolled continuous cast material.

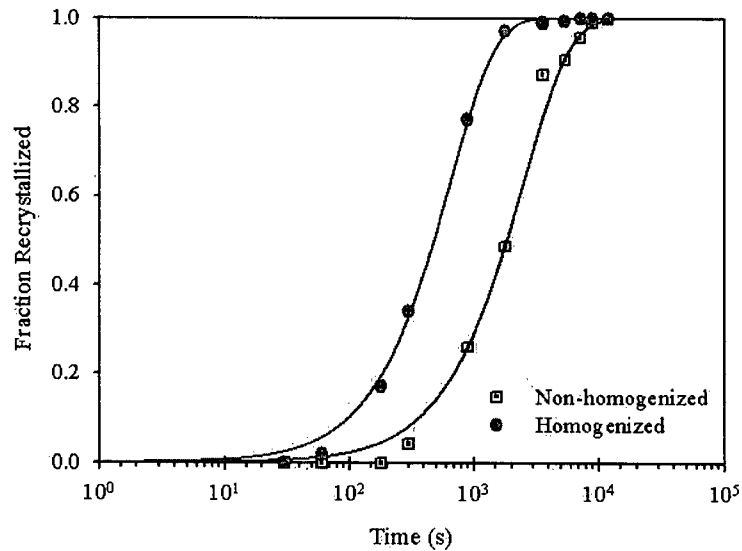


Figure 5.8 - Isothermal recrystallization kinetics for 80% directly cold rolled continuous cast AA5754 at 300°C.

As shown in Figure 5.9, when compared to the 80% cold rolled ingot and continuous cast material, the continuous cast material with the homogenization treatment is much closer to the recrystallization kinetics experienced by the ingot cast material. In fact the trends are very similar to what was seen in Figure 5.7 for the recovery kinetics. As shown in Figure 5.9, the time needed to obtain 50% recrystallization is approximately

325s for the ingot cast material as compared to around 480s for the continuous cast material with the homogenization treatment and 1875s for the continuous cast material without the homogenization heat treatment.

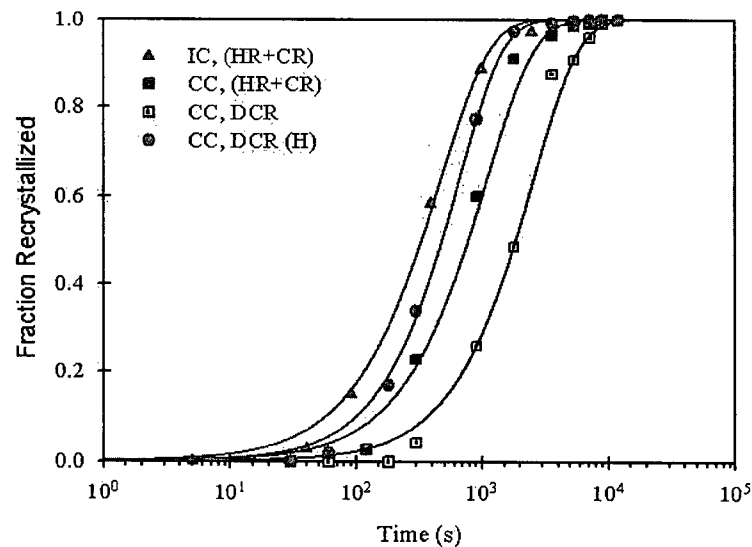


Figure 5.9 - Comparative isothermal recrystallization kinetics for 80% direct cold rolled continuous cast AA5754 (starting material, homogenized as-cast material), 80% direct cold rolled AA5754 (starting material, non-homogenized as-cast material) and 80% cold rolled continuous and ingot cast AA5754 (starting material, recrystallized hot rolled material) at 300°C.

To examine the possible precipitation of dispersoids during annealing of cold deformed non-homogenized continuous cast material, heat treatment was carried out at 300°C for 80% directly cold rolled material and undeformed non-homogenized as-cast material. The time chosen for the heat treatment was over 3 hours as this was the time taken for the 80% directly cold rolled material to completely recrystallize at this temperature. During the heat treatment, resistivity measurements were made on both materials at

various heat treatment times. Figure 5.10 shows the resistivity results for both materials at 300°C. As can be seen from Figure 5.10, resistivity changes significantly for 80% directly cold rolled continuous cast material, whereas the as-cast material shows little change. The change in resistivity for 80% directly cold rolled material can directly be attributed to the solute depletion as concurrent precipitation of fine dispersoids during the early stages of annealing.

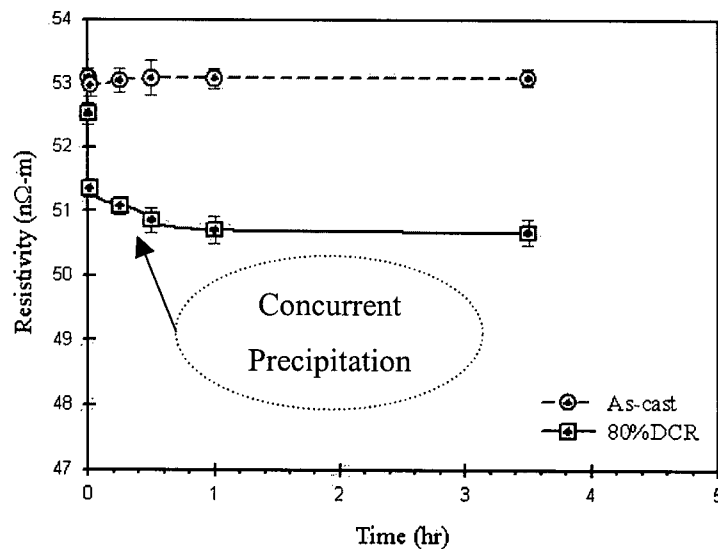


Figure 5.10 - Resistivity curve for continuous cast materials at 300°C.

The change in resistivity value observed for the 80% cold rolled material during the early stages of annealing at 300°C can be understood in terms of short circuit diffusion. The deformation process increases the dislocation density and grain boundary area. This increases the effective diffusion coefficient of the solute atoms by the significant contribution from grain boundary diffusion and dislocation core diffusion, thus accelerates the kinetics of precipitation during annealing of the cold deformed material.

In addition to the precipitation kinetics, spatial distribution of the precipitates is generally affected by this short circuit diffusion, i.e. precipitates primarily nucleate on the grain boundaries in the deformed structure.

5.4.3 Discussion of Recovery and Recrystallization

Some important points could be discussed based on the results shown in Figure 5.6-5.10.

Recovery: Both solutes and dispersoids can play an important role on dislocation movement and arrangement and hence on the recovery kinetics. Based on the recovery results presented in Figure 5.6 and Figure 5.7, it seems that solute supersaturation in the non-homogenized material may be responsible for the slower recovery behaviour. It has been observed that these solutes precipitate in a uniform distribution as fine dispersoids during homogenization [Liu et al. 1998; Slámová et al., 2003], which substantially reduces the effects of Mn and possible Fe on the recovery of the deformed state. It may also be possible for the precipitation to occur in parallel with recovery and can reduce the recovery rate for non-homogenized material. However, the low temperature studied here (i.e. 200°C) is probably too low for precipitation to occur; though this assumption requires careful verification.

Recrystallization: Figure 5.8 and Figure 5.9 show a strong solute drag or concurrent precipitation influence on the recovery and recrystallization kinetics for continuous cast material without homogenization. Both ingot and continuous cast material after

homogenization have complete precipitation of Fe and Mn rich dispersoids [Morris et al., 1998, 2000, 2003; Koizumi et al., 2000; Azari et al., 2002]. For the non-homogenized material, the situation is more complex. As the experimental result suggested that in addition to the solutes, parallel precipitation during the early stages of the annealing treatment could reduce the recrystallization kinetics of the cold rolled non-homogenized continuous cast material. In this case the precipitates are unlikely to be distributed uniformly and would form preferentially on the grain boundaries as the kinetics of the precipitation is controlled by the short circuit diffusion. These particles can then exerts a strong retarding pressure on the mobility of the grain boundary for the cold rolled non-homogenized continuous cast material, which is generally termed as Zener pinning pressure. Though present study cold not separate the effect of the solute and the parallel precipitates on the recrystallization behaviour of the non-homogenized material, a combination of these two factors could be responsible for retarding the recrystallization kinetics for non-homogenized continuous cast material. Precipitation of Fe and Mn rich dispersoids during annealing for Al-Mg and Al-Mg-Mn alloys (without prior pre-heat treatment) has also been reported by Koizumi and Tangen respectively [Koizumi et al., 2000; Tangen et al., 2002].

The continuous cast material, which was hot rolled and heat treated to ensure a fully recrystallized structure prior to cold rolling falls somewhere between the continuous cast material with the homogenization heat treatment and the non-homogenized material. Although no resistivity measurements were made of this material prior to cold rolling, both the hot rolling process and subsequent heat treatment of the material at

500°C for 30 minutes would cause some precipitates to come out of solution. Hence the softening kinetics and final recrystallized grain size fall between the continuous cast material with and without a homogenization heat treatment.

5.5 Characterization of Recrystallized Material

The mechanical properties and final recrystallized grain size were measured for the materials studied. Figure 5.11 shows the recrystallized microstructure for 80% directly cold rolled continuous cast material rolled from homogenized as-cast structure.

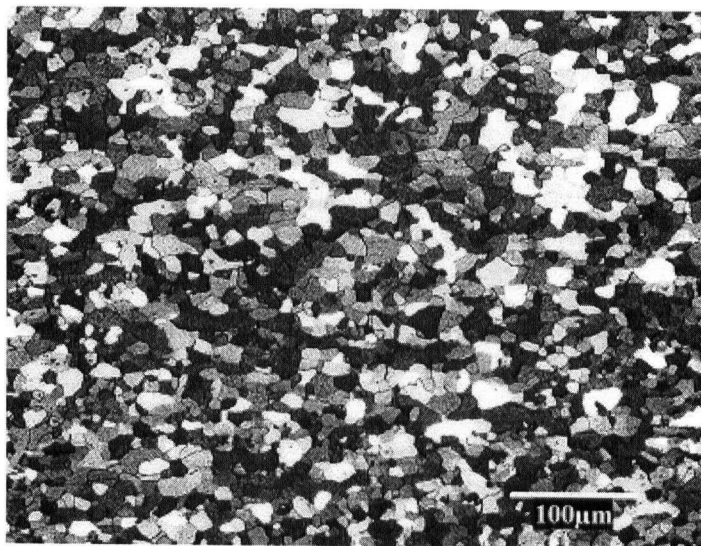


Figure 5.11 - Microstructure of recrystallized 80% directly cold rolled continuous cast AA5754 rolled from homogenized as-cast material.

Application of the homogenization treatment increases the average recrystallized grain size of continuous cast material to a negligible amount as shown in Table 5.2. But the recrystallized grain size remains finer compared to the same of the ingot cast material. Table 5.2 summarizes the effect of pre-heat treatment stage on the recrystallized grain

size and recrystallized yield stress for continuous cast material. The table also includes the recrystallized grain size and recrystallized yield stress for ingot cast material.

Table 5.2 – Comparative recrystallized grain size along with recrystallized yield stress for recrystallized 80% cold rolled continuous and ingot cast AA5754.

Material mentioned in the first column in bracket is the starting material for cold rolling. Error associated with the grain size and yield stress measurement was $\pm 1 \mu\text{m}$ and $\pm 5 \text{Mpa}$ respectively.

Material (starting material)	Rx. Grain Size (μm)	Rx. Yield Stress (MPa)
Ingot cast (Rx. HR)	14	112
Continuous cast (Rx. HR)	11.5	117
Continuous cast (Non-homogenized)	9.5	118
Continuous cast (Homogenized)	11	116

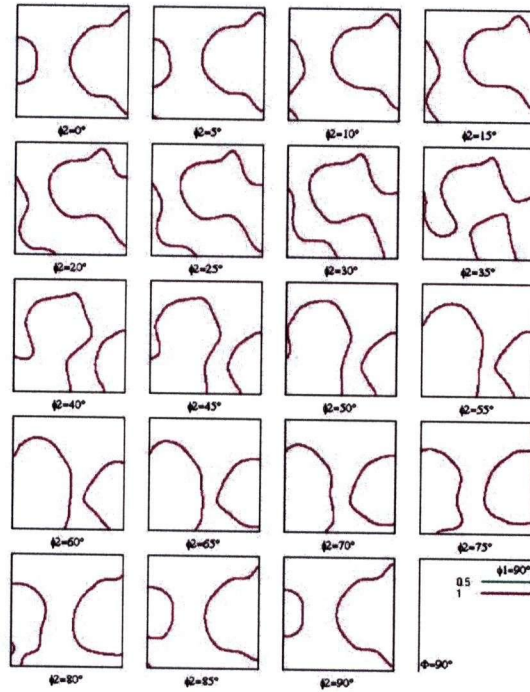
The relationship between, recrystallized yield stress and average grain size for recrystallized 80% directly cold rolled continuous cast material rolled from homogenized as-cast material was validated with the other results of continuous and ingot cast material shown in Figure 4.16 and the result shows a good match with the trendline presented in the Figure 4.16.

5.6 Texture Analysis

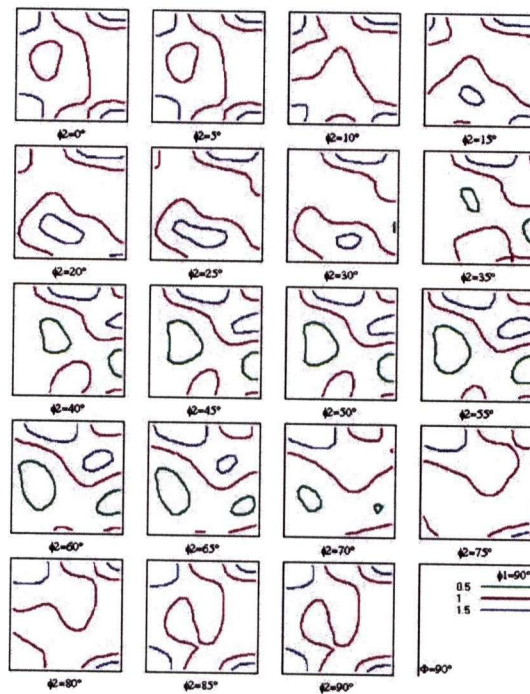
Texture analysis was done on the fully recrystallized material rolled from the continuous as-cast material, which had received a homogenization heat treatment. These

results were then compared with the results from the same material without the homogenization heat treatment and the ingot cast material. Figure 5.12 shows a comparison of the textures for the continuous cast materials with and without the homogenization treatment. Table 5.3 gives the volume fraction of the some important texture components for both the ingot cast and continuous cast AA5754 material. From the Table 5.3, it can be observed that though both textures are random in nature, there is a slight increase in the cube texture component for the continuous cast material that received the homogenization heat treatment. The corresponding ODF's for these materials are shown in Figure 5.13. The present study reveals that the overall texture of the recrystallized continuous cast material that had gone through homogenization treatment has many similarities with that of ingot cast material presented in Figure 4.20.

In summary, the texture measurements of the fully recrystallized material show quite random textures for each AA5754 sample. However, it is interesting to note that the Cube texture component follows a similar trend in that it is highest in the ingot cast material, and lowest in the continuous cast material without a homogenization treatment. Study of homogenization treatment on the recrystallized texture reveals that the homogenization stage slightly increases the Cube texture component of the recrystallized 80% direct cold rolled material.



(a)



(b)

Figure 5.13 - Orientation Distribution Function (ODF) of (a) recrystallized 80% directly cold rolled continuous cast AA5754 from non-homogenized as-cast and (b) recrystallized 80% cold rolled ingot cast AA5754 from homogenized as-cast material.

Table 5.3 – Measured volume fraction of texture components (in %) for both the ingot cast and continuous cast AA5754 after 80% cold deformation and annealing at 325°C using an EBSD system.

Texture Component	IC material	CC material (homogenized)	CC material (not homogenized)
Cube	6.6	4.9	3
B	1.8	2.7	2.9
Cu	4	3.5	3.0
Goss	1.8	2.4	2.2
S	4.2	3.1	3
R	3.9	3.4	3.6
P	2.4	1.6	1.4
Q	2.9	2.4	2.7
H	1.7	1.8	2.7
CH	2.8	3.0	3.5

** Miller indices and Euler angles of each texture component is given in appendix A.*

5.7 Summary

As shown, the homogenization treatment plays an important role in the subsequent recovery and recrystallization kinetics during annealing of the sheet material after cold rolling. It appears that the majority of the difference in the softening kinetics between the ingot cast and continuous cast material that was directly cold rolled is due to the contribution of solute drag and concurrent precipitation in parallel with softening, which impedes both the recovery and recrystallization process in the continuous cast material. The result of this is much slower recovery and recrystallization kinetics during the annealing process and a finer grain size after recrystallization due to the lower growth rates.

6. Summary and Conclusions

One of the main barriers faced by the aluminum industry in penetrating the automotive sheet market is ensuring that the cost of a sheet of aluminum is on par with steel. Towards this goal, the aluminum industry has focused their efforts towards alternative less expensive processing technologies, such as continuous casting to produce these sheet products. Continuous casting produces sheets of aluminum, which are then reduced via hot and/or cold rolling to the final cold-rolled sheet gauge followed by a continuous annealing operation. In contrast to the traditional DC or ingot casting process, continuous casting of aluminum eliminates the cost intensive intermediary stages of homogenization (or pre-heat treatment) and potentially hot rolling.

There are some obvious differences between the continuous casting and the ingot casting process routes for the production of sheet material. These include: the solidification rate experienced during casting which will influence the grain size as well as the size and distribution of the constituent particles, the absence of the homogenization stage in continuous casting and the amount of hot and cold deformation applied to the material after casting. These differences can ultimately affect the way in which the material responds to the annealing treatment as well as the final microstructure and properties of the sheet after this process is completed. Therefore, the goal of this research has been to understand the effect of industrial process route (continuous casting versus ingot casting) on the microstructure evolution during

continuous annealing for AA5754, a commercially significant aluminum alloy that has been slated for use in automotive sheet applications.

The research measured the recovery and recrystallization behaviour during the annealing process of continuous cast AA5754 and characterized the final recrystallized microstructure in terms of the grain size; yield strength and texture. These results were then compared to earlier results measured for AA5754, which had been ingot cast.

Based on the research conducted, a number of important conclusions can be made about the effect of processing route on the behaviour of AA5754 during isothermal annealing operation. Specifically these include:

- The as-cast structure of the continuously cast material was quite different from the ingot cast material and exhibited fine constituent particles which were not homogeneously distributed throughout the matrix but present in clusters. In addition the as-cast grain size was much finer for the continuously cast material as compared to the ingot cast material (50micron for continuous cast materials vs. 100-500micron for ingot cast material [Granger, 1986]).
- Processing route does not appear to significantly affect the work hardening behaviour of the material with the final yield strength of the material being similar for a similar level of cold work.

- The recovery and recrystallization behaviour of AA5754 during an annealing treatment differs greatly for material that had been ingot cast or continuously cast. Continuous cast material which was not homogenized after the casting operation prior to hot or cold deformation, exhibited slower softening kinetics compared to ingot cast material for the same amount of cold reduction. The slower softening behaviour observed for non-homogenized material can be explained by the presence of solute supersaturation and by the parallel precipitation during annealing operation. Both of these factors can exert a strong retarding force on the mobility of the grain boundary and thus impede the grain boundary motion of the material. Though the present study couldn't separate the individual contribution of each factor, but a combination of both the factors can be responsible for retarding the softening kinetics of non-homogenized material.
- Characterization of recrystallized continuous and ingot cast material shows some differences in the recrystallized grain size and shape, however recrystallized texture appeared to remain random for both materials. Comparing recrystallized grain size for both continuous and ingot cast material revealed that the average grain size decreases with increasing amount of cold work prior to annealing. In addition, the present study reveals that for any level of cold deformation the continuous cast material produced a finer grain structure compared to ingot cast material. Visually, the ingot cast material appeared to have a more homogenous and equiaxed grain

structure as compared to the continuous cast material and this may be due to the concurrent precipitation during annealing for non-homogenized continuous cast material.

- Though the texture study reveals a quite random texture for both continuous and ingot cast material, close observation for the texture of the recrystallized continuous cast material shows stronger presence of rolling texture components (Brass, Copper and S) compared to ingot cast material. On the other hand, the ingot cast material shows a higher Cube component in the recrystallized texture. Increased cold reduction yields more random texture after complete recrystallization for both continuous and ingot cast materials and hence texture present in recrystallized 80% cold rolled material is more random than recrystallized 40% cold rolled material. The present study indicates that application of homogenization treatment to the continuous cast material produced little change on the overall recrystallized texture.

6.1 Future Works

The present work has highlighted the effects of the processing routes experienced by AA5754 sheet on the softening kinetics during annealing and final microstructure. However, in order to obtain a better scientific understanding of the effect of processing route on this alloy the following future work should be considered:

- Quantitative knowledge of the second-phase particle size, distribution and chemistry in the material should be undertaken at each stage in the process so that the role these particles play in subsequent microstructure evolution can be more clearly delineated.
- TEM and SEM studies of the partially recovered and recrystallized materials for both continuous and ingot cast AA5754 should be conducted to understand the microstructure evolution during annealing and correlate the results with the change in mechanical properties during softening. Specifically knowledge of the relative importance of grain boundary nucleation and particle stimulated nucleation in both materials could help to explain the observed differences.
- Finally mathematical modeling of the softening kinetics including the role played by the particles both in terms of solute drag, Zener drag and particle stimulated nucleation would be very valuable.

References

- Altenpohl, D. G., (1998), Aluminum: Technology, Applications, and Environment, TMS, ed. Kaufman, G. J. and Das, S. K.
- Azari, H. N., Girard, S. X., Wilkinson, D. S. and Lloyd, D. J. (2002), *Effect of Thermomechanical Processing on the Evolution of Rolling and Recrystallization Textures in Twin-Belt Cast AA5754 Aluminum Alloy*, McMaster University, Hamilton (Canada), submitted to *Metallurgical and Materials Transactions A*.
- Bolingbroke, R. K., Creed, E., Marshall, G. J. and Ricks, R. A. (1993), *Aluminum Alloys for Packaging*, TMS, Warrendale (USA), 215.
- Burger, G. B., Gupta, A. K., Jeffrey, P. W. and Lloyd, D. J. (1995), *Materials Characterization*, **35**, 23.
- Carle, D. and Blount, G. (1999), *Materials and Design*, **20**, 267.
- Chan, H. M. and Humphreys, F. J. (1984), *Acta Met.*, **32**, 235.
- Chen, L. Morris, J. G. and Das, S. K. (1989), *Continuous Casting of Non-Ferrous Metals and Alloys*, TMS, Warrendale (USA), 269.
- Cheng, X. M. and Morris, J. G. (2002), *Materials Sc. And Engg.*, **A323**, 32.
- Cheng, X. M., Zhai, T. and Morris, J. G. (2001), *Materials Solutions Conference*, ASM, Indianapolis (USA), November, 361.
- Doherty, R. D., Fricke, W. G. and Rollett, A. D. (1986), *Conference Aluminum Technology*, 289.
- Doherty, R. D., Hughes, D. A, Humphreys, F. J., Jonas, J. J., Jensen, D. J., Kassner, M. E., King, W. E., McNelley, T. R., McQueen, H. J. and Rollett, A. D (1997), *Materials Sci Eng. A*, **238**, 219.
- Doherty, R. D. and Martic, J. W., (1962), *J. Inst. Met*, **91**, 332.
- Dugdale, J. S. (1977), *The Electrical Properties of Metals and Alloys*, Edward Arnold.
- Dündar, M. Birol, Y. and Akkurt, A. S. (2002), *Materials Sc. Forum*, **396-402**, 1647.
- Engler, O. (1998), *Acta Mater.*, **46**, 1555.

Friedman, P. A. and Sherman, A. M. (1998), *Proceeding of the Symposium on Automotive Alloys*, TMS, San Antonio, **32**, 147.

Gallerneault, M. and Lloyd, D. (2002), *Materials Sc. Forum (Switzerland)*, **396-402**, 95.

Gandhi, C. (1999), Masters thesis: *Effect of Homogenization on the Microstructural development in a D.C cast AA3104 Aluminum alloy used for Canbody stock*, University of British Columbia, Vancouver (Canada).

Girard, S. (2002), Masters thesis: *Effect of Thermomechanical processing on Texture development in a Twin-belt cast Automotive Aluminum alloys*, McMaster University, Hamilton (Canada).

Girard, S. X., Azari, H. N. and Wilkinson, D. S. (2002), *Effect of Thermomechanical Processing on Grain Structure Development in a Twin-Belt Cast Automotive Aluminum Alloy*, McMaster University, Hamilton (Canada).

Go, J. (2003), *Unpublished Research at University of British Columbia*, Vancouver (Canada).

Go, J. (2001), Masters thesis: *Recovery and Recrystallization behaviour of AA5754 and IF-Boron steel during Annealing*, University of British Columbia, Vancouver (Canada).

Gottstein, G. and Shvindlerman, L. S. (1992), *Scripta Metall. Mater.*, **27**, 1515.

Granger, D. A. (1989), *Aluminum Alloys- Contemporary Research and Applications*, **31**, 109.

Haga, T. and Suzuki, S. (2001), *JOM*, **113**, 291.

Haga, T., Nishiyama, T., Suzuki, S. (2003), *JOM*, **133**, 103.

Hayashi, H. and Nakagawa, T. (1994), *JOM*, **48**, 455.

Humphreys, F. J. (1977), *Acta Met.*, **25**, 1323.

Humphreys, F. J. and Hatherly, M. (1995), *Recrystallization and Related Annealing Phenomena*, Pergamon press.

Jensen, J. D. (1995), *Acta Metall. Mater.*, **43**, 4117.

Karlík, M., Slámová, M., Jnaeček, M. and Homola, P. (2002), *Kovove Materialy*, **40**, no. 5, 330.

- Katsukura, M. (2001), *Light Metal Age*, April, 70.
- Koizumi, M., Kohara, S. and Inagaki, H. (1997), *Zeitschrift für Metallkunde*, **88**, 576.
- Koizumi, M., Kohara, S., Inagaki, H. and Kohara, S. (1999), *National Research Council of Canada, Proceedings of the Twelfth International Conference on Textures of Materials (ICOTOM-12)*, **2**, 848.
- Koizumi, M., Kohara, S. and Inagaki, H. (2000), *Z. Metallkd.*, **91**, 460.
- Koizumi, M., Saitou, T., Okudaira, H. and Inagaki, H. (2000), *Zeitschrift für Metallkunde*, **91**, 717.
- Kyang, Y. and Morris, J. G. (1977), *Materials Sc. And Engg.*, 59.
- Li, D. and Ghosh, A. (2003), *Materials Sc. And Engg. A*, **352**, 279.
- Liu, W. C., Zhai, T. and Morris, J. G. (2003), *Materials Sc. And Engg.*, **A00**, 1.
- Liu, Y., Cheng, X. M., Liu, J. and Morris, J. G. (2000), *Materials Sc. Forum*, **331-337**, 191.
- Liu, Y., Liu, Y. L., Liao, G. and Morris, J. G. (1999), *Proceedings of the twelfth International Conference on Textures of Materials (ICOTOM-12)*, McGill University, Montreal (Canada), 1148.
- Liu, Y. L., Ding, S. and Morris, J. G. (1998), *Aluminum Alloys for Packaging*, TMS, **3**, 101.
- Liu, Y. L., Liu, Y. and Morris, J. G. (1998), *Hot Deformation of Aluminum Alloys*, TMS, **2**, 62.
- Lloyd, D. J. (1980), *Metall. Trans. A.*, **11A**, 1287.
- Lücke, K. (1974), *Canadian Met. Quart.*, **13**, 261.
- Mao, J. F., An, X. Y. and Lei, T. Q. (1990), *Mater. Chem. Phys.*, **25**, 297.
- Miller, W. S., Zhuang, L., Bottema, J., Wittebrood, A. J., De Smet, P., Haszler, A. and Vieregge, A. (2000), *Materials Sc. And Engineering*, **A280**, 37.
- Nes, E. (1995), *Acta Metall. Mater.*, **43**, 2189.
- Nes, E. and Embury, J. D. (1975), *Z. Metallke*, **66**, 589.

- Nes, E. and Slevolden, S. (1979), *Aluminum*, **55**, 319.
- Pennington, J. N. (1993), *Modern Metals*, July, 42F.
- Perryman, E. C. W. (1955), *Trans AIME*, **203**, 369.
- Petry, C. J. (1986), *Aluminum alloys- Their Physical and Mechanical Properties, International Conference, University of Virginia, Charlottesville (USA)*, **1**, 111.
- Petry, C. J. and Szczypiorski, W. (1987), *Light Metal Age*, **44**, No.7-8, 19-20, **22**, 24.
- Rabet, L., Ratchev, P., Verlinden, B. and Van Houtte, P. (1996), *Materials Sc. Forum*, **217-222**, 465.
- Randle, V., Engler, O. (2000), *Introduction to Texture Analysis: Macrotecture, microtexture and orientation mapping, Gordon and Beach Science Publishers Amsterdam, Netherlands*.
- Ryum, N. and Embury, J. D. (1982), *Scand. J. Metall.*, **11**, 51.
- Saitou, T. and Inagaki, H. (2001), *Zeitschrift für Metallkunde*, **92**, 1277.
- Samajdar, I., Rabet, L., Verlinden, B. and Van Houtte, P. (1998), *ISIJ International (Japan)*, **38**, 539.
- Samarasekera, I. V., Wells, M. A., Jin, D., Hlady, C. O., Brimacombe, J. K. and Hawbolt, E. B. (1995), *Materials Characterization*, **35**, 69.
- Sanders, R. E., Baumann, S. F. and Stumpf, H. C. (1986), *International Conference, University of Virginia, Charlottesville (USA)*, June, 1441.
- Sanders, R. E., Baumann, S. F. and Stumpf, H. C. (1989), *Aluminum Alloys- Contemporary Research and Applications*, **31**, 66.
- Schmidt, C. G. and Miller, A. K. (1982), *Acta. Met.*, **30**, 615.
- Schwartz, A. J., Kumar, M. and Adams, B. L. (2000), *Electron Backscatter Diffraction in Materials Science*.
- Slámová, M., Birol, Y., DüNDAR, M., Akkurt, A. S. and Janecek, M. (2002), *Materials Sc. Forum*, **396-402**, 711.
- Slámová, M., Karlík, M., Robaut, F., Sláma, P. and Véron, M. (2003), *Materials Characterization*, **49**, 231.

Spear, R. E. and Gardner, G. R. (1963), *Trans. American Foundrymen's Soc.*, **71**, 209.

Staley, J. T. and McBride, J. K. (1965), *Unpublished Research at Alcoa Laboratories (USA)*.

Stumpf, C. G. (1965-1971), *Unpublished research at Alcoa Laboratories (USA)*.

Tangen, S., Sjølstad, K., Nes, E., Furu, T. and Marthinsen, K. (2002), *Materials. Sc. Forum*, **396-402**, 469.

Verdier, M., Saeter, J. A., Janecek, M., Brechet, Y., Guyot, P., Duly, D., Nes, E. and Ørsund, R. (1996), *Materials Sc. Forum*, **217-222**, 435.

Appendix A

Euler angles and Miller indices of important texture components: -

Texture Component	Miller indices	Euler angles (°)		
		Φ_1	ϕ	Φ_2
Cube (C)	{001}<100>	0	0	0
Rotated Cube (C _{ND})	{100}<130>	12	0	0
Brass (B)	{011}<211>	35	45	90
Goss (G)	{011}<100>	0	45	90
Copper (Cu)	{112}<111>	90	35	45
S	{123}<634>	59	37	63
R	{124}<211>	57	29	63
P	{011}<122>	70	45	0
Q	{013}<231>	58	18	0
H	{001}<110>	0	45	0
CH	{001}<120>	27	0	0
Dillamore (D)	{4,4,11}<11,11,8>	90	27	45

Appendix B

Calculation of Resistivity from VERIMET M4900C

The Verimet M4900C conductivity meter is calibrated to read IACS (International Annealed Copper Standard) conductivity and according to calibration 100% IACS reads 58.0 MS/m. The measurement produced by conductivity meter was in %IACS and hence this IACS value was first converted to the conductivity value in MS/m. Final resistivity value (in $n\Omega\text{-m}$) was then derived by inverting the conductivity value in MS/m. As an example, for pure aluminum the Verimet M4900C generally shows an IACS value of 61.2, which up on conversion produces resistivity value of $2.81 \times 10^{-6} \Omega\text{-cm}$ (ideal resistivity of pure aluminum).

Appendix C

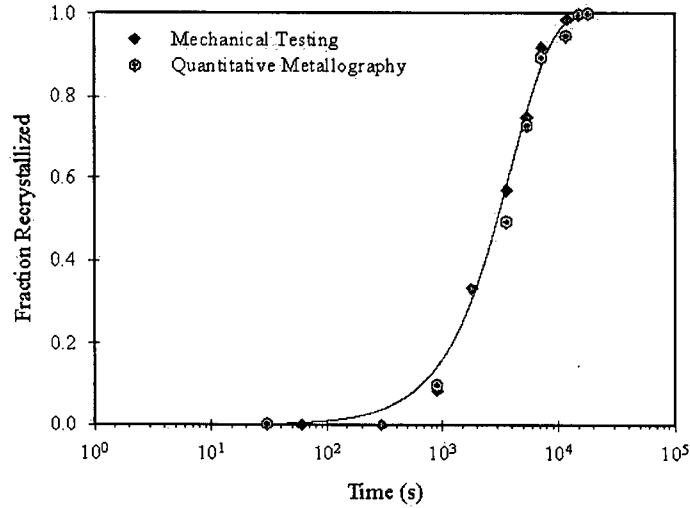


Figure C1. Validation of isothermal recrystallization kinetics for 40% cold rolled continuous cast AA5754 at 300°C derived from mechanical testing by quantitative metallography results.

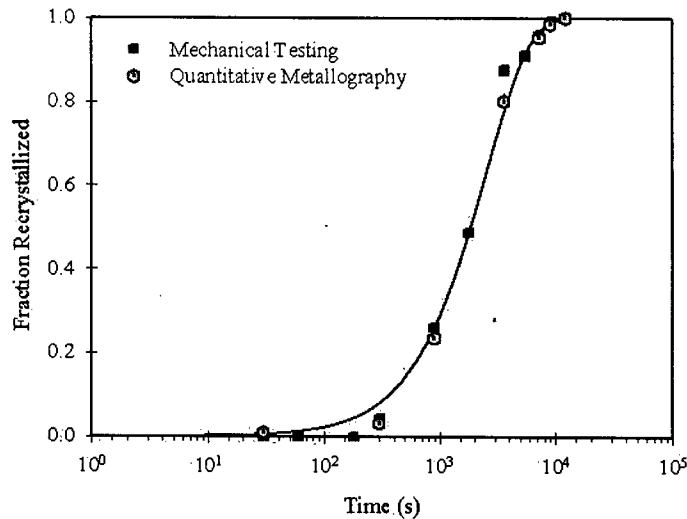


Figure C2. Validation of isothermal recrystallization kinetics for 80% directly cold rolled continuous cast AA5754 at 300°C derived from mechanical testing by quantitative metallography results.